UNIVERSITAT POLITÈCNICA DE VALÈNCIA

Title:

Real-time signal detection and classification algorithms for body-centered systems

Author:

Lara Traver Sebastià

Directors:

Narcís Cardona Marcet

Cristina Tarín Sauer

May 2012

Preface

The work of this thesis was mainly preformed at the Telecommunications and Multimedia Applications Technical Institude of the Technical University of Valencia.

I wish to thank Dr. Narcís Cardona and Dr. Cristina Tarín for their advice and continous support throughout the process I am also thankful to Dr. Juan Carlos Guerri, Dr. Leonardo Betancourt and Paula Martí for their collaboration. I also express my gratitude to all the members of the Telecommunications and Multimedia Applications Technical Institude with whom I had the pleasure to work.

This work is dedicated to my family and specially to my mother that always encouraged me to improve my education.

Abstract

The main objective for which body centered systems are being developed is to obtain and process biological signals in order to monitor and, in some cases even treat, a physical condition, either a disease or the athletic performance in the case of sports. Since the core of body-centered systems is sensing and processing, signal processing algorithms play a central role in the system's functioning. This thesis is focussed on those real-time algorithms that are needed to obtain the relevant information from the sensed signals. In the initial part, the types of sensors and algorithms are reviewed, after that, the thesis deals with two different applications and the related real-time signal processing algorithms are designed and implemented.

The first study case (Chapter 3) is glucose monitoring in diabetes patients. The objective was to detect therapeutically wrong measurements of Medtronic's Minimed CGMS using learning algorithms for pattern classification. The methodology used was the following: Patients were monitored using CGMS and simultaneously blood samples were taken in a clinical study. Gaussian SVM classifiers were tuned to detect wrong glucose estimations making use of monitor's electrical signal, the CGMS glucose estimation and the

real blood-glucose measure obtained from the blood samples. The results showed that the classifiers were indeed able to learn the data structure and an overall good detection of wrong measures was obtained in spite of the somewhat low sensitivity of the detector. The classifiers were able to detect the time intervals where the monitor's glucose profile shouldn't be trusted because of wrong measurements. This was illustrated with the detection of hypoglycaemic episodes missed by the CGMS. From this analysis it was concluded that detection of therapeutically wrong measurements given by the continuous glucose monitor Minimed CGMS is feasible through the use of SVM classifiers. For all patients, missed hypoglycaemic states were detected, as well as other therapeutically wrong measurements. The presence of False Positives did not alter the conclusions drawn out from the analysis of time profiles. This tool could thus support the clinician in the interpretation of continuous glucose monitor readings.

The second application of body centered systems, included in Chapter 4 is neural signal monitoring. Recent medical advances have demonstrated the benefits that such monitoring can bring to medicine and even to other areas as entertainment. That is why, nowadays, there are many research groups dedicated to develop wireless implantable brain monitors. In this work neural spike detection classification and compression algorithms have been implemented and evaluated together with wireless transmission techniques. Such combination will enable the implementation of the wireless brain monitors. A new method for adaptive threshold spike detection was applied

that successfully adapts to different input SNRs eliminating the need for manual threshold setting. For the classification algorithm, PCA pattern recognition techniques were used and a performance of 92% of correctly classified spikes was accomplished. Detection and classification were used together with a compression and resource management algorithm for efficient wireless transmission of neural signals. The frame-based algorithm was capable of adapting the compression of the 60 input channels according to: the neural activity present, the priority set to each channel and the bandwidth available at each processing frame. As a result, signals were compressed and multiplexed in a single transmission frame that fits in the available transmission bandwidth. The reconstruction algorithm at the receiving side was able to demultiplex and decode the received frame to reconstruct the neural spiking patterns. The conjunction of detection, sorting and compression algorithms produced a scheme for neural monitoring system that self-adapts to the signal conditions (adaptive threshold detector) and to the transmission bandwidth.

Finally, although the main topic of the thesis is signal processing, a chapter (Chapter 5) has been dedicated to wireless transmission technologies and more precisely to on-body UWB transmission. UWB was selected in this thesis as the most promising transmission technology for body-centered systems because of the combination of low-power, short-range and high data rates that characterize such technology. There are some additional considerations to be regarded. UWB allows only short distance communications with these high transmission rates, which is perfectly assumable for body area networks but

therefore it raises the need of a bridge between the close body field and the remote monitoring stations. In this work, the objective was to evaluate UWB for the particular application of real-time neural signal monitoring. As for the methodology, a channel measuring campaign was designed and performed in order to characterize the head-to-body channel. From such measures, model parameters were extracted. Additionally, and for performance evaluation, neural signals were transmitted through a UWB evaluation kit and the spiking characteristics of the received signals were compared to those of the transmitted signals for different experimental set-ups. The study concluded that for real-time neural signal monitoring, UWB seems to offer best transmission conditions in a near-body environment up to 2m. It allows high-fidelity signal transmission at extremely high data rates with low power consumption.

Resumen

El objetivo principal para el que se están desarrollando los sistemas de comunicaciones corporales es obtener y procesar señales biológicas que sirvan para monitorizar e incluso para tratar un determinada condición física, tanto si se trata de una enfermedad como si se trata del rendimiento de un deportista. Dado que el foco de estos sistemas está en la sensorización y en el procesado, los algoritmos de procesado de señal juegan un papel central en su funcionamiento. Esta tesis se centra en los algoritmos de procesado que se usan para obtener la información relevante a partir de las señales recogidas. En una primera parte, se revisan los tipos de sensores y algoritmos utilizados en este campo, para después centrarse en dos aplicaciones concretas para las cuales varios algoritmos de procesado son diseñados e implementados.

La primera de estas aplicaciones es la monitorización continua de pacientes con diabetes. En este caso, el objetivo era utilizar algoritmos de reconocimiento de patrones, en concreto “Support Vector Machines (SVM)” para detectar las medidas del monitor Minimed CGMS de Medtronic que resultan terapéuticamente erróneas. En el ensayo, un conjunto de pacientes fue monitorizado mediante el citado monitor mientras simultáneamente se

extrajeron muestras sanguíneas de las que se midió la glucosa en sangre. Los algoritmos de reconocimiento fueron entrenados para detectar los errores en la medida del Minimed CGMS con respecto a los valores correctos obtenidos mediante medidas en sangre. Los resultados mostraron que los clasificadores son realmente capaces de aprender la estructura de los datos y producir resultados de detección aceptables. Por tanto, son capaces de detectar los intervalos de tiempo en los que las medidas del CGMS no resultan fiables, especialmente esto se ilustró en la detección de los episodios de hipoglicemia que habían sido ignorados por el monitor continuo. En todos los pacientes monitorizados, el algoritmo de SVM fue capaz de detectar los estados de hipoglicemia ignorados por el monitor continuo. Aunque hay que señalar que esto fue a costa de algunos falsos positivos, los cuales no afectaron a las conclusiones que se pueden extraer de la serie temporal ya que ocurren de manera aislada. Esta herramienta permitiría pues apoyar la interpretación clínica de las medidas realizadas con este tipo de monitores en pacientes con diabetes.

La segunda aplicación que se incluye es la de la monitorización inalámbrica de señales neuronales. Avances recientes en este campo médico han demostrado que la monitorización neuronal puede traer avances muy importantes en el estudio del cerebro, en el tratamiento de algunas condiciones médicas como la tetraplegia e incluso en el campo del entretenimiento. Por este motivo, en la actualidad hay numerosos equipos de investigación que trabajan en desarrollar monitores neuronales inalámbricos.

En esta tesis, el objetivo fue implementar y evaluar algoritmos de detección, clasificación y compresión de señales neuronales junto con técnicas de transmisión inalámbricas para la monitorización inalámbrica de señales neuronales dado que esta combinación de técnicas es la que permitirá en un futuro que los monitores cerebrales inalámbricos sean una realidad. En concreto se ha desarrollado un detector de impulsos neuronales con umbral adaptativo a la relación señal a ruido, de modo que se elimina la necesidad de situar el umbral de forma manual. En cuanto a la clasificación se ha obtenido una tasa 92% en la clasificación correcta de los impulsos neuronales mediante clasificadores basados en PCA ("Principal Component Analysis"). Los citados algoritmos de detección y clasificación se han usado junto con un algoritmo de compresión y de gestión de recursos para la transmisión eficiente de las señales neuronales. El conjunto es capaz de adaptar la compresión de 60 canales de señales neuronales a la actividad que presentan las neuronas en cada momento de modo que el máximo de información pueda ser transmitido con el ancho de banda disponible. Como resultado se comprimen y multiplexan los 60 canales neuronales para acomodarlos al ancho de banda del canal disponible. En el extremo del receptor, el algoritmo de reconstrucción es capaz de reconstruir los patrones de impulsos neuronales de modo que las señales sigan siendo interpretables. El sistema completo se adapta automáticamente tanto a las señales entrantes como al ancho de banda proporcionado por el canal de comunicación.

Finalmente, aunque el tema principal de este trabajo es el procesado de señal, se ha incluido un capítulo dedicado a la transmisión inalámbrica, en concreto con la tecnología “Ultra-wide-band (UWB)” en el entorno del cuerpo humano. UWB fue seleccionada por permitir altas tasas de transmisión en el corto alcance, que es el caso de los sistemas que nos ocupan. En este trabajo se evalúa el uso de UWB en aplicaciones en el entorno del cuerpo humano (“BAN”, En concreto para la monitorización de señales neuronales). En cuanto a la metodología, se realizo una campaña de medidas para caracterizar el canal desde la cabeza a diferentes partes a lo largo del cuerpo humano. A partir de estas medidas se han obtenido los parámetros del modelo de canal. Adicionalmente, se realizó un experimento de transmisión de señales neuronales mediante un kit UWB y se evaluaron los efectos de la dicha transmisión mediante la comparación de los patrones de disparo de las señales antes y después de la transmisión. Los resultados muestran que UWB proporciona buenos resultados de transmisión a altas tasas de transmisión en distancias de hasta 2 metros.

Resum

L'objectiu fonamental per al qual actualment es desenvolupen sistemes de comunicacions corporals o BAN (del anglès "Body Area Networks") és per obtenir y processar senyals biomètrics i d'aquesta manera poder monitoritzar o inclús tractar una determinada condició física o mèdica. Donat que el focus en aquestos sistemes es troba en la sensorització i el processat, el algoritmes utilitzats en aquest processat tenen un paper central en el funcionament del sistema. Es per això que aquesta tesi es centra precísament en els algoritmes que permeten obtenir la informació rellevant a partir del senyals recollits. En una primera part, es revisen els tipus de sensors i algoritmes utilitzats en el camp de la tele-monitorització mèdica per a després centrar l'estudi en dues aplicacions concretes y en els algoritmes relacionats.

La primera d'aquestes aplicacions és la monitorització continua de pacients amb diabetis. L'objectiu fixat és la utilització de algoritmes de reconeixement de patrons i més concretament Màquines de Suport Vectorial o SVM (de l'anglès "Support Vector Machines"), per detectar les mesures realitzades per el monitor Minimed CGMS de Medtronic que resulten terapèuticament errònies. Metodològicament, es va monitoritzar amb el monitor CGMS Minimed un conjunt de pacients amb diapentes, dels quals, simultàniament es van

extraure mostres sanguínies de manera periòdica per a mesurar la glucosa en sang. Amb el conjunt de mesures del Minimed i les de glucosa en sang, es van realitzar el entrenament i el test dels algoritmes de reconeixement o classificadors. Els resultats mostraren que els classificadors tenen la capacitat de aprendre la estructura de les dades i produir resultats de detecció d'errors acceptables. Per tant, poden detectar els intervals de temps en els quals les mesures del CGMS Minimed no són fiables. Especialment açò es va mostrar en la capacitat de detecció dels episodis de hipoglucèmia que havien segut ignorats per el monitor continu. Cal assenyalar que aquesta capacitat de detecció es a costa de alguns falsos positius que globalment no afecten a la detecció dels períodes de hipoglucèmia ja que es produeixen de manera aïllada en el temps. Per tant aquesta ferramenta pot donar suport a la interpretació clínica de les mesures realitzades amb aquest tipus de monitors continus.

Per un altra banda, la segona aplicació considerada en aquest treball es la monitorització inalàmbrica de senyals neuronals. El recents estudis en aquest camp mèdic han demostrat que la monitorització neuronal pot propiciar avanços molt importants en l'estudi del cervell i també en el tractament de algunes condicions mèdiques com la tetraplegia o inclús en el camp de l'entreteniment. És per això que actualment hi ha nombrosos equips d'investigació que hi treballen en el desenvolupament de monitors neuronals inalàmbrics. En aquesta tesi, l'objectiu és implementar i avaluar algoritmes de detecció, classificació i compressió de senyals neuronals junt am tècniques de

transmissió per a la monitorització inalàmbrica i en temps reial de aquests senyals. Més concretament, s'ha desenvolupat, per una banda, un detector de impulsos neuronals amb llindar adaptatiu a la qualitat del senyal d'entrada, de manera que resulta innecessari situar el llindar de detecció de manera manual. Per un altra banda, s'han utilitzat classificadors basats en PCA (de l'anglès "Principal Component Anàlisi") per a la classificació de impulsos neuronals obtenint una taxa del 92% de classificacions correctes. Juntament amb la detecció i classificació del impulsos neuronals s'ha aplicat un esquema de compressió y gestió de recursos que permet la transmissió eficient dels patrons de impulsos per a la seua interpretació en el receptor. Aquest conjunt és capaç de adaptar la compressió de 60 canals d'entrada a, per una banda, la activitat neuronal del conjunt de canals, per altra banda a la prioritat assignada a cadascun dels canals i finalment també al ample de banda disponible en cada moment. Així, es comprimeixen i multiplexen 60 canals neuronals i s'acomoden al ample de banda del canal disponible. En l'extrem del receptor, el procés de reconstrucció, interpreta les dades rebudes de manera que es possible obtindre els patrons de impulsos i poder-los interpretar. El sistema s'adapta automàticament als senyals entrants i a les condicions de transmissió del canal de comunicació.

Finalment, tot i que el tema principal de la tesi és el processat de senyals, s'ha inclòs un capítol dedicat a la transmissió inalàmbrica, concretament a la tecnologia UWB (de l'anglès "Ultra-wide-band") per a la comunicació al voltant del cos humà. UWB es va seleccionar per què permet altes tasses de

transmissió en curtes distàncies. L'objectiu en aquest treball és avaluar l'ús d'UWB en sistemes "BAN" (comunicacions al voltant del cos humà), i més concretament en la monitorització de senyals neuronals. Pel que fa a la metodologia, s'ha realitzat una campanya de mesures del canal de UWB mesurat des de el cap a diverses posicions al llarg del cos. A partir d'aquestes mesures s'han obtingut els paràmetres que caracteritzen el canal. Addicionalment es va realitzar un experiment de transmissió reial de senyals neuronals a través d'un kit de avaluació d'UWB. A partir d'aquest experiment es van avaluar els efectes de la transmissió UWB sobre els senyals neuronals mitjançant la comparació dels patrons d'impulsos abans i després de la transmissió. Els resultats mostres que UWB proporciona una bona qualitat de transmissió a elevades taxes de transmissió fins a 2m de distancia.

Table of Contends

List of Figures

List of Tables

List of Symbols and Abbreviations

3D	Three Dimensional
3G	3rd generation mobile telecommunications
4G	4th generation mobile telecommunications
AAL	Ambient Assisted Living
AC	Alternate Current
ACL	Asynchronous Connection-Less
ADC	Analog to Digital Conversion
ADC	Analog to digital converter
AMR	Automated Meter Reading
AP	Action Potential
APDPs	Averaged Power Delay Profiles
AUC	Area-Under-the-Curve
BCC	Body Coupled Communications
BER	Bit Error Rate
Bluetooth LAP	Bluetooth LAN Access Profile
Bluetooth SPP	Bluetooth Serial Port Profile
Bluetooth's HDP	Bluetooth's Health Device Profile
BMI	Body-Mass Index
BW	Bandwidth
$CCDF_{exp}$	Complementary Cumulative Distribution Function
CDF	Cumulative Density Function
CDMA	Code division multiple access
CGMS	Continuous Glucose Monitoring System
CIR	Channel Impulse Response
CM	Channel Model
CMOS	Complementary Metal–Oxide–Semiconductor
CPU	Central Processing Unit
DFMM-DL	Dual-Fed Microstrip Monopole antenna with Dielectric Lens
dISIG/dt	derivative with respect to time of the sensor current
DNA	Deoxyribonucleic acid
DS	Direct Sequence
ECG	Electrocardiography
ECMA	European Computer Manufacturers Association
ECoG	Electrocorticography
EDR	Enhanced Data Rate
EEG	Electroencephalography
EGA	Error Grid Analysis
EMG	Electromyography
EMR	Emergency Medical Responders
ENSTA	École Nationale Supérieure de Techniques Avancées
ETSI	European Telecommunications Standards Institute
FCC	Federal Communications Commission
FDA	Food and Drug Administration
FDA	U.S. Food and Drug Administration

FDTD	Finite-Difference Time Domain
fMRI	Functional magnetic resonance imaging
FPR	False Positives Rate
f_s	sampling frequency
G_{CGMS}	glucose estimation given as output by Minimed CGMS
GHz	Gigahertz
GPRS	General Packet Radio Service
GPS	Global Positioning System
G_{RX}	Receiver Antenna Gain
GSM	Global System for Mobile Communications
GSR	Galvanic skin response
G_{TX}	Transmitter Antenna Gain
HbA1c	Glycosylated hemoglobin
HBC	Human Body Communications
HIS	Hospital Information System
HL7	Health Level Seven
HRM	Heart Rate Monitoring
Hz	Herz
I/O	Input / Output
IBVA	Interactive Brainwave Visual Analyzer
ICG	Impedance cardiography
IEEE	Institute of Electrical and Electronics Engineers
IEM	Ingestible Event Marker
IFFT	Inverse Fourier Transform
IP	Internet Protocol
ISI	Inter-Symbol Interference
ISIG	sensor current
ISM bands	Industrial, Scientific And Medical Bands
ISO	International Organization for Standardization
Kbps	Kilo bits per second
KKT	Karush-Kuhn-Tucker
LAN	Local Area Network
L_B	Losses Within Body Tissues
LDR	Low Data Rate
LED	Light Emitting Diodes
LFP	Local Field Potential
LFP	Local Field Potentials
L_{FS}	Free Space Loss
L_{OB}	On-Body Link's Losses
LOS	Line Of Sight
MAC	Medium Access Control
MAC	Medium Access Control
MANET	Mobile ad hoc network
Mbps	Mega bits per second
MCOT	Mobile Cardiac Outpatient Telemetry
MEA	Multielectrode Array
MEA	Multi-Electrode Array
MEG	Magnetoencephalography
MEMS	Microelectromechanical systems

m-health	Mobile Health
MLR	Multivariate Linear Regression
MMH	Maximum Margin Hyperplane
MPC	multi path component
MT	Monitor Transceiver
NB	Narrow Band
NEMS	Nanoelectromechanical systems
NEO	Nonlinear-Energy-Operator
OEP	Optoelectronic plethysmography
OFDM	Orthogonal Frequency Division Multiplexing
OFDM	Orthogonal Frequency Division Multiplexion
OSH	Optimum Separating Hyperplane
PAN	Personal Area Network
PC	Personal Computer
PC	Principal Component
PCA	Principal Component Analysis
PCA	Principal Components Analysis
PDA	Personal Digital Assistant
PDP	Power Delay Profile
PET	Positron emission tomography
PHY	Physical
PHY	Physical
PIR	Post-Isometric Relaxation
PL	Path Loss
PLS	Partial Least Squares
PPG	Photoplethysmography
P_{RX}	Received Power
PS	Personal Server
PT	Patient Transceiver
P_{TX}	Transmitter Output Power
QoS	Quality of Service
RF	Radio Frequency
RFID	Radio Frequency Identification
RM	Resource Management
RMS	Root Mean Square
ROC	Receiver Operating Curve
RTOS	Real Time Operating System
SAR	Specific Absorption Rate
SC	Signal Compression
SCO	Synchronous Connection Oriented
SDM	Speed and Distance Monitoring
SNR	Signal to Noise Ratios
SpO2	Saturation of peripheral oxygen
STH	Simple Threshold
SVM	Support Vector Machines
TCP	Transmission Control Protocol
TinyOS	Tiny Microthreading Operating System
TPR	True Positives Rate
UDP	User Datagram Protocol

USB	Universal Serial Bus
UWB	Ultra Wide Band
VCTR	registered voltage
VNA	Vector Network Analyzer
VNA	Vector Network Analyzer
WAN	Wide Area Network
WB	Wide Band
WBAN	Wireless Body Area Networks
WBSNs	Wireless Body Sensor Networks
WCDMA	Wide Band Code division multiple access
WSNs	Wireless Sensor Networks
ΔBW	bandwidth resolution
Δf	frequency step

Chapter 1

Introduction

1.1 Motivation

Body-centered communication systems have many applications in the biomedical, telemedicine and entertainment fields [15], [16], [17], [23], [24] and [25], where obviously wireless technology presents many advantages. Such systems are designed using the so-called Wireless Body Area Networks (WBANs), which are made up of a set of mobile and compact intercommunicating sensors, either wearable or implanted into the human body, which monitor vital body parameters and movements. In medical applications, these devices, communicating through wireless technologies, transmit data from the body to a central station, from where the data can be forwarded to a hospital, clinic or elsewhere [15]. In Figure 1. a basic scheme for a WBAN configuration is depicted.

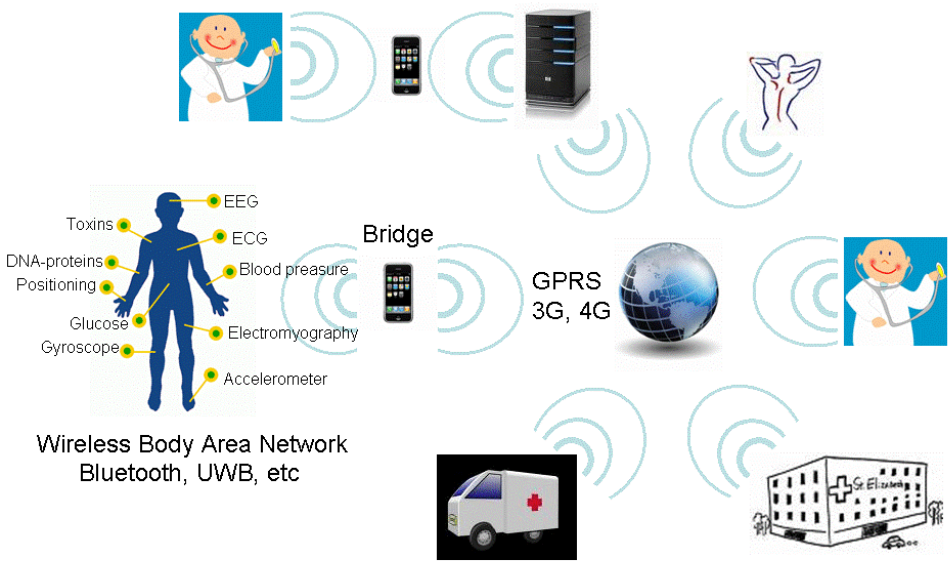

Figure 1. Schematic of a Wireless Body Area network for e-health application.

1.2 State of the art

WBAN applications in the healthcare domain are awaking interest in the medical community. For example in vital signs monitoring, in and outside the hospital, of patients suffering from chronic diseases such as diabetes, asthma and heart attacks [16]. Those diseases can present life-threatening episodes in which quick medical response is crucial. By means of a WBAN, alerts are sent to the hospital, even before the acute episode occurs thanks to the early detection of changes in vital parameters. Even in a step further from simple monitoring, a WBAN network on a diabetic patient could auto inject insulin through a pump, as soon as his insulin level declines. WBAN applications are of course not limited to the healthcare area but spread also in sports, military,

or security areas. However, they are out of the scope of this work which focuses in patient monitoring.

Wireless patient monitoring implies the use of sensors that produce signals with are digitized and wirelessly sent to a logging or processing system. Today's improved sensor technology, together with miniaturization of transmission and processing devices, allows the use of many sensors and in many locations on the body and also inside the body, which, in turn, results in a considerable data rate to be transmitted over the wireless link [17], [18], [19].

A wide range of wireless transmission technologies are used in WBAN for communicating such amounts of data: Bluetooth, Zigbee, UWB, IEEE 802.11, IEEE 802.15.6, Near-Field Communications, etc. As a consequence WBAN systems are heterogeneous and do not use the same technology, they are not interoperable and the industry has not yet adopted a standard in this field. This has an effect in commercialization of WBAN products since the economy of scale has not yet been reached. For this reason, in the future, it would be desirable for WBAN systems to ensure seamless data transfer across standards, to promote information exchange and to allow plug and play device interaction.

In the present, wireless sensor units are usually composed of the sensor itself, connected to a transmission unit by a small cable, as in the example of Figure 2. Still further miniaturization and integration of both sensor and transmitter in a single unit is expected. Sensors used in WBAN need to be low

on complexity, small in form factor, light in weight, power efficient, easy to use and reconfigurable.

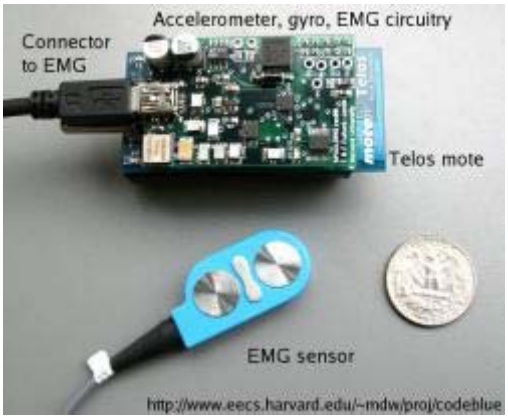

Figure 2. EMG sensor integrated in a Telos mote platform for vital sign monitoring.

Security is also an important issue in WBAN for patient monitoring. WBAN transmission has to be secure and accurate to make sure that the patient's data is only derived from each patient's dedicated WBAN system and is not mixed up with other patient's data. Further, the data generated from WBAN should have secure and limited access. People might consider the WBAN technology as a potential threat to freedom, if the applications go beyond 'secure' medical usage. Social acceptance would be key to this technology finding a wider application.

Apart from the exposed issues, in order to design practical WBAN systems, body interaction in electromagnetic propagation properties impose further study and development. The propagation along or through the body must be characterized. It becomes fundamental to characterize the body proximity

effects on the channel characteristics as path loss, maximum link distance, delay spread, etc. ([26] - [29]).

1.3 Objectives

The main objective of the proposed thesis is to design and evaluate a wireless telemetry system for **real-time monitoring of biomedical signals** and more specifically, neural signals.

To accomplish that, several minor objectives are implied:

- Design a compression and reconstruction method for wireless transmission of neural signals.
- A real-time resource management algorithm so that adequate source compression is applied to each channel in order to fit them into the available bandwidth.
- Evaluate the performance of the algorithm using dynamically changing bandwidth and neural recordings with different neural activity characteristics.
- Obtain a model of the UWB channel for the specific application of neural signal monitoring where the propagation occurs from the transmitter located on the head to the receiver that can be in different parts along the body.

- Apart from the main objective, a different medical application will be studied consisting in applying pattern recognition techniques in error detection in subcutaneous continuous blood-glucose monitors.

For the design of the neural signal compression, reconstruction and resource management methods a set of real recordings have been obtained and are be used. The method is designed for real time operation, this is, signals are divided in frames and each frame is processed at a time. Matlab™ and Simulink™ are used for the implementation. The results show how compression and reconstruction affect to the spike detection and classification algorithms which are the basic techniques for neural signal processing. This demonstrates the feasibility of a system for wireless transmission of compressed signals without affecting their main characteristics.

A wireless neural signal transmission demonstrator is implemented using Bluetooth and 3G. Also real UWB transmission is used for neural signals and the effects of transmission distance and power is studied.

In the on-body statistical channel modellization, frequency measurements from 1GHz to 12GHz are made in an anechoic chamber using a vector network analyzer (VNA), the S-parameter S_{21} is measured in the complex frequency domain. Two antennas are connected to the VNA by means of suitable low attenuation cables. A calibration procedure is implemented so that measurements are not affected by cable attenuation and frequency response. Measures are taken for male and female subjects and finally channel parameters are extracted form the measures to obtain the channel model.

In medical applications, also signal processing techniques are necessary in the process of sensing, compressing, transmitting and reconstructing the signals to be interpreted by the medical community. In this thesis two types of medical applications are considered where signal processing is involved:

- Neural signals telemetry [19], [20], [21], [22].
- Blood-glucose monitoring [30], [31], [33].

1.4 Main contributions

The main scientific contributions of this dissertation are:

- Implementation of neural signal processing algorithms (detection, sorting, compression, reconstruction) [2], [3].
- Implementation of a neural signal transmission demonstrator using Bluetooth and 3G [7].
- Simulation of the whole real-time system for neural signal telemetry including resource management to adapt compression to different transmission capacities [1], [3].
- Study on-body UWB propagation properties: [8]-[12].
- Evaluation of distance and power effects on UWB transmission of neural signals [4].

- Evaluation of Support Vector Machines (SVM) techniques in the detection of incorrect measurements in existing blood glucose monitors [13].

1.5 Thesis' structure

Chapter 2 contains a review of wireless sensor technologies for body-centered systems from the types of sensors to the current medical systems available in the market. In Chapter 3 SVM is evaluated as a support decision tool for error detection in commercial continuous blood glucose monitoring devices. Chapter 4 deals with the main real-time signal monitoring applications of this thesis consisting on the implementation of the algorithms for neural-signal monitoring and the implementation of a prototype for detection, compression and Bluetooth transmission of a set of pre-recorded neural signals. Evaluation of UWB transmission is also included. Continuing with UWB, Chapter 5 contains a study of the transmission properties of the on-body UWB channel. Finally Chapter 6 draws the main conclusions of this work as a whole.

Chapter 2

Body-centered systems

2.1 Introduction

Biomedicine, sensor technology and wireless communication are fields the combination of which will bring continuous, 24 by 7 human body monitoring in the future. However, though the needed innovations are either already developed or will be soon, commercial products won't make it to the market until years of testing have proven their safety. That is why in recent years, Wireless Body Area Networks (WBAN) have received increased consideration due to their widespread applicability the mentioned fields of health monitoring and telemedicine. Improved sensor technology together with miniaturization of transmission and processing devices have increased the scope of potential applications. Chronic patients need to be monitored and, of course, they much more prefer to be able to remain away from hospitals and medical centers and, therefore, patient parameters, measured by a set of sensors, need to be sent to the medical centre over some communication network. In the medical centre, data are evaluated by clinicians and eventually added to the patient's historical files. Monitoring of patients in medical centers has been done over many decades through cabled systems. Cables are a handicap since they may

fall off, tangle up with each other and make mobility difficult for patients and clinicians. Furthermore, they are a problem when a patient who needs continuous monitoring, moves around or is moved.

Mobile devices are the key allowing this new way to treat patients since they allow ubiquitous access to data, provide Internet connection and serve as documentation systems. With the help of mobile devices the health system is also more transparent and accessible to patients. In the future doctors might call patients before having a heart attack, responding to an alarm sent out by monitoring systems. Also real-time monitoring of blood's chemical concentrations could enable tailoring of medicine dosages to patient's body chemistry and metabolism. The huge amounts of data that would be accumulated from hundreds of thousands of continuously monitored persons would allow further advances in research which are not possible nowadays.

However, in spite of the many advantages, wireless body monitoring is not yet common practice. The reason being that most of the interesting signals to be monitored require the sensor to be implanted inside the body, and this is not an easy problem to overcome. Extracting blood samples periodically only works for periodic monitoring. It does not provide continuous access to bodily fluids. The possible infections caused by implants and degradation they suffer from moisture, enzymes, and the immune system complicate their use. Future advances in biocompatible materials are expected to gradually alleviate this scenario allowing safer and longer monitoring through implanted sensors.

This chapter is a general introduction to body-centered systems and intends to serve as a topic umbrella for the following parts of the thesis. Here we will review in a general manner the types of biomedical sensors used in body-centered systems together with the related signal processing techniques used to deal with the obtained signals. Wireless technologies and communications topologies for data transmission will also be covered and finally a large but obviously non-exhaustive list of existing applications and products will be presented.

2.2 Biomedical sensors

2.2.1 Physiological Signals

Many biological processes are subject to be measured. Measuring a process produces a physiological signal which gives an idea of what is happening in the underlying mechanism. Basically there are six types of signals: mechanical, thermal, magnetic, electric, chemical, and radiation. The devices that convert one type of signal into another are called transducers and more precisely, when signals are converted to electrical signals, the devices are called sensors. Most measurement systems use sensors because electric signals provide many advantages as signal amplification, availability of a large number of signal conditioning circuits and displays and also the fact that electrical signals are easily transmitted and converted into digital signals and radio signals. A variety of physiological signals are subject to be acquired with the available sensor technologies such as: Electrocardiogram signal (ECG), body temperature, blood pressure, body acceleration and many others.

In a basic classification, sensors can be separated into active or passive types. Active sensors are those that obtain power from an external source while passive sensors obtain the output power from the input signal. On the other hand physiological signals can be classified according to their physical nature into:

- Electrical signals: caused by changes in potential in cells generating an electric field which fluctuates and in this process it is to emit bioelectric signal.
- Mechanical Signals: They are related to motion, displacement, pressure and flow of the physiological system.
- Magnetic signals that originate from magnetic fields generated by various organs like heart, brain and lungs while functioning.
- Chemical signals: they are obtained by chemical measurement from the living tissues or analysis of the samples obtained from the body.
- Impedance Signals: measurement of skin impedance helps in finding the state of skin and functioning of various physiological systems.
- Optical Signals: These signals are produced by the optical variations by the functioning of the physiological system.
- Acoustic Signals: These are sounds created by the flow of blood and air.

Nowadays, in telemedicine and health monitoring many types of sensors are used. Among the more common are: Electrocardiography (ECG),

Electroencephalography (EEG) and Electromyography (EMG) sensors, blood-glucose meters and pulse-oximeters. Others are only starting to find their applications and are mainly used in medical research such as neural multi-electrode sensors and motion sensors. Miniaturization has not yet reached the level of development to allow the majority of sensors to incorporate the transmission device in a single-packet. As a consequence, usually in this type of systems a small cable connects the sensor with the transceiver unit while from this unit to the monitoring device a wireless link is used.

2.2.2 Electrocardiology (ECG) sensors

ECG monitors attach up to 10 sensors to the body. Each sensor consists of an electrode recording the electrical activity in a different section of the heart. An ECG is used to measure the electrical activity of the heart [34]. The cardiac signal, typically 5 mV peak to peak, is an AC signal with a bandwidth of 0.05 Hz to 100. The ECG signal is characterized by six peaks and valleys labeled with successive letters of the alphabet P, Q, R, S, T, and U (Figure 3).

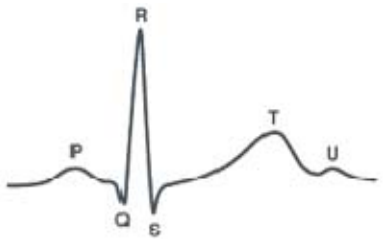

Figure 3. Typical ECG waveform

From an ECG, an expert can extract: the rate and regularity of heartbeats, the position of the various chambers, the existence of any damage to the heart and the effects of drugs and devices used to regulate the heart. Many types of

ECG equipment exist in the market for hospital and portable use. There is an effort as well to produce wireless ECGs, however, commercial wireless ECGs replace the cables between the patient and the monitoring device, but the ECG sensors are still connected to the transmission device through cables.

Alternative heart activity recording approaches exist such as:

- Stethoscope function: mechanical work of the heart muscle movement conducted through tissue.
- Impedance cardiography (ICG): impedance change due to blood volume and velocity change in aorta
- Blood saturation: measurement of the amount of oxygen attached to the hemoglobin cell in the circulatory system (SPO2) using light reflection (this is done with a sensor placed around a finger)
- Mechanical work of the heart sensed through tissue/body motion (e.g. sensors integrated in mattress).

2.2.3 Electromyography (EMG) sensors

EMG is the technique to evaluate the recording of electrical activity produced by skeletal muscles cells, when electrically or neurologically activated [35]. Muscle potentials range 50μV to 30mV and the signal spectrum lies in the 7Hz to 500Hz band. The device used in electromyography is called electromyograph and has applications in diagnose of neuromuscular diseases and also the more innovative control of prosthetic devices among others [36].

Wireless EMGs have already started to be available in the market mainly using 802.15.4 technology. Examples are listed in section 2.6.2.

2.2.4 Electroencephalography (EEG) sensors

It is a non-invasive technique that measures the electrical brain activity by placing electrodes on the head at convenient positions to obtain the most relevant information from the recorded signals. It measures the electric fluctuations resulting from ionic current flows within the neurons of the brain [37]. EEG is widely used in epilepsy diagnosis [38], [39]. Examples of wireless EEG products are listed in section 2.6.2.

2.2.5 Electrocorticography (ECoG) sensors

In ECoG, the electrodes are placed on the motor cortex surface of a spinal cord injury patient. Therefore, they measure the electrical activity of the brain taken from beneath the skull in a similar way to non-invasive electroencephalography, but the electrodes are embedded in a thin plastic pad that is placed on the cortex, beneath the dura mater [40].

ECoG has been intensively used in epilepsy research, diagnostic and treatment [38], [41] and [42]. Today's research starts to produce wireless ECoG prototypes that are hopefully going to be on the market soon [43] and [44].

2.2.6 Neural Multi Electrode Array (MEA) sensors

Implanted MEAs are used to obtain in-vivo recordings of neurons activity [45]. These implanted sensors are used in the types of applications where a very high spatial resolution is needed, i.e. when it is needed to register the activity of a single neuron or of a small group of neurons. Because placing a MEA in or on the brain requires an invasive technique, other types of neuronal activity monitoring unless spatial resolution is strictly needed.

2.2.7 Magnetoencephalography (MEG) sensors

MEG is a non-invasive technique to measure the electromagnetic fields created by the electrical currents in the brain cells [46]. With MEG it is possible to locate the sources of the currents and thus construct maps of brain activity. MEG sensors are based on superconducting detectors capable of registering the weak magnetic fields created by the neural activity. MEG has the advantage of high spatial (millimeter range) and temporal resolution (in the order of milliseconds). The single drawback being the huge volume of the equipment needed to fight against interference from the environment which would otherwise hide the weak magnetic signals.

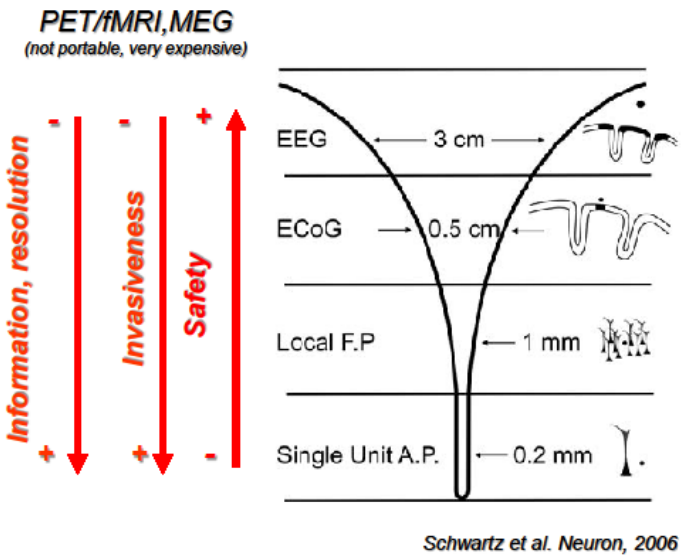

Figure 4. Comparison of existing brain activity recording technologies.

2.2.8 Blood-glucose sensors

They measure glucose concentration in a person's blood. Implantable and non-invasive sensors for continuous blood glucose monitoring have been researched for over a decade, however diabetic patients can not yet rely solely on these types of monitors but need to calibrate them periodically (several times during one day). The research activity in glucose sensors is quite high nowadays mainly focused on implantable biosensors [47], [48] although also researchers in Japan [49] and others [50], [51], are developing non-invasive optical glucose sensors.

2.2.9 Pulse oximeters

Pulse oximeters or saturation monitors measure the oxygen saturation in the arterial blood (SpO2) and the pulse by analyzing the absorption of light from a couple of Light Emitting Diodes (LEDs) after it has passed through or been

reflected from the skin [52]. For many years the measurement location was small parts of the body where light could be passed through as fingers, ear lobes or toes, however with the development of sensors capable of measuring oxygen saturation from reflected light, measures can be made from any part of the body.

2.2.10 Optoelectronic plethysmography (OEP)

This type of sensors measure respiration parameters using external optical sensors that can follow the chest wall surface motion. In OEP, a number of small reflectors are placed on the thorax surface while infrared cameras follow the displacement of the reflectors during respiration. In this way it is possible to follow thorax volume changes in the process [53].

2.2.11 Biosensors

A biosensor is a sensor which combines a physical or chemical part with a biological part, i.e., enzymes, antibodies, biological molecules, such as DNA single strand, proteins or a biological system, such as membrane, a tissue, a cellular or microorganism culture, etc. The biosensor is thus constituted by the molecular recognition element and the transducer material and it takes advantage of the natural sensitivity and specificity of the biological processes. Research interest in biosensors is considerable nowadays because of the large amount of applications in medical diagnostic health care and environmental sciences [54].

2.2.12 Implantable sensor Technologies

Revolutionary changes in Micro and Nano–Electro-Mechanical Systems (MEMSs and NEMSs) enable embedded and implanted biomedical sensors. MEMSs or NEMSs are very small, micro or nano scale respectively, mechanical devices driven by electricity. They usually consist of a central unit that processes data, and one or several micro/nano sensors. Latest generations of MEMS include the sensor, analog amplification, analog-to-digital converter and digital intelligence with memory cells for calibration and temperature compensation.

In some medical applications the sensor needs to be implanted in the body [55] as for example probes that measure blood flow [56], Microelectrode Arrays to measure neural signals [57] (This application is covered in detail the chapter 4 of this thesis).

The challenges in the design of those devices are biocompatibility, and energy supply for the implanted device. Biocompatibility is not in the scope of this work. Neither is battery design for energy supply, however, when discussing processing and transmission technologies, the power consumption is taken into account as one of the main restrictions.

2.3 Signal processing in body-centered systems

2.3.1 General signal processing techniques

Physical sensors detect and convert natural physical quantities into analog signals. Medical signal processing techniques can sometimes be performed on

raw, analog signals, however, advanced, frequency-domain methods are performed in the digital domain. Also, digital signals are much more efficient when it comes to storing and transmitting them over networks or utilizing automated feature-extraction and recognition. The first step in signal processing is sampling the signal to convert it into a time series, since computers cannot handle or store continuous data. Sampling is followed by quantization through Analog to Digital Conversion (ADC), signal conditioning, which may itself include level adjustment, frequency filtering, feature extraction and data compression. In the case of real-time monitoring, buffering and finally wireless transmission are needed. Current trends are toward integration of all these functions into a single-chip solution. These chips are usually called motes [58].

It needs to be noted that in the sampling process original signal reconstruction can be achieved as far as the sampling frequency is at least double the signal bandwidth; this requirement is known as the Shannon theorem [59] and, in theory, it is the decisive requirement for the sampling process. On the other hand in the quantization process, the range of values should be both compact and efficient.

When the application requires real-time sensing, the samples of the monitored process are taken and processed at the time they are produced and therefore delay and latency issues must be considered. In real time operation, there is no data storing for later processing but data are obtained and processed in a continuous stream. Monitoring systems are usually real-time

systems since they require immediate reaction at the events being monitored and the requirement that the average processing time per sample is no greater than the sampling period has to be met. Real time processing usually requires that the data are divided in frames. A frame is a set of one or multiple channel samples that are first stored in a memory buffer and then processed. The duration of the frame processing needs to be always smaller than the frame acquisition time to avoid buffer overload and it also defines the processing delay of the application, the longer the frame the longer the delay. Real-time requirements, minimum and maximum sampling rates, minimum and maximum resolution and number of channels are the main characteristics to be taken into account when defining the processing and storage requirements.

As a summary, Table 1 (partly taken from [60] and further extended) presents the characteristics of common physiological signals.

Physiological parameter	Type of sensing device	location	Sampling rate (Hz) (min–max)	Precision (bits) (min–max)	Channels (min–max)	Data rate (kbps)
ECG (per channel)	Electrodes	Chest	(100–1000)	(12–24)	(1–3)	1.2 – 72
EMG	Electrodes	Muscles	(125–1000)	(12–24)	(1–8)	1.5 – 192
EEG	Electrodes	Head	(125–1000)	(12–24)	(1–8)	1.5 – 192
MEA	Electrodes	Head	(15000 - 50000)	(10-12)	(1-128)	150 – 76800
PPG	Photodiode	Ear or finger	(100–1000)	(12–16)	1	1.2 – 16
Blood pressure	Pressure cuff	Arm or finger	(100–1000)	(12–24)	1	1.2 – 24
Respiration	Elastic chest belt/electrodes	Chest	(25–100)	(8–16)	1	0.2 – 1.6
Blood glucose	Chemical	Skin	<0.01	(8–16)	1	<0.00016
GSR	Electrodes	Fingers	(50–250)	(8–16)	1	0.4 – 4
Skin temperature	Thermistor probe	Wrist/arm	< 1/60	(16–24)	1	< 0.0004
Localization	GPS receiver	Personal server (PS)	(0.01–10)	(80–120)	1	0.0008 – 1.2
Gait	Inertial gyroscope	Chest	(25–100)	(16–32)	(1–3)	0.4 – 9.6
Activity	Accelerometers	Chest, extremities	(25–100)	(12–24)	3	0.9 – 7.2
Steps	Mechanical foot switch	Shoe insole	(2–100)	(1–16)	(1–8)	0.002 – 12.8
Humidity	—	Attached to PS	< 1/60	(12–16)	1	< 0.0003
Light	—	Attached to PS	< 1/60	(12–16)	1	< 0.0003
Ambient temperature	—	Attached to PS	< 1/60	(12–16)	1	< 0.0003
Atmospheric pressure	—	Attached to PS	< 1/60	(12–16)	1	< 0.0003
Ambient noise		Attached to PS	< 1/60	(12–24)	1	< 0.0003

Table 1 Physiological signals: sampling rates, precision typical for wearable health monitoring applications, and likely locations of deployment

After basic sampling, digital conversion and conditioning, typically signals are sent as data to a processing remote server, where, in order to obtain relevant information several signal processing techniques can be used. As it is

known, sensors provide with a readout signal which is related to the underlying physical or chemical process. One of the main goals of signal processing in biomedicine is to compensate for the possible effects of measuring devices and noise on the measured signal. Additionally signal processing often aims at identifying and separating desired and unwanted components of a signal and finally also uncover the nature of underlying process responsible for generating the signal.

Signals derived from biological processes are often not well represented by simple deterministic signals. Real-world biomedical signals usually include large stochastic components; they also may be fractal or chaotic. Often we ignore the properties of their sources and are unable to know a priori what the character of the signal will be. Therefore we must first recognize the range of possible signal types and be able to determine the most appropriate type of analysis for the signal of interest. Unfortunately, this choice is not always clear. It is of special importance also being able to recognize whether the selected analysis method is appropriate and to determine the best way to process the signal depending on the objectives.

The main issues to take into account in signal processing for body-centered systems are:

- choosing a class of signal model
- selecting a specific form of the model, i.e., statistical versus deterministic etc.
- evaluating indicators of adequacy of the model

A general review of signal processing for biomedical signals is way too wide to be covered here. Signal enhancement techniques are well covered in many signal processing books. Here we will have a limited review of the decision support techniques that will be used in the following chapters. As a general fact, signal processing techniques can be separated in two steps, first signal enhancement or pre-processing that separates the captured information from noise and prepares it for the second step consisting of specialized processing, classification, and recognition algorithms.

Signal enhancement may include:

- Sampling
- Analog to Digital Conversion (ADC)
- Level adjustment
- Frequency filtering
- Noise reduction

After signal enhancement specialized algorithms which are tailored to the type of signal and type of application are used and may include:

- Feature extraction
- Computing features as variance, mean or range
- Data compression
- Buffering
- Wireless transmission. This is the topic covered in section 2.4.

- Decision support techniques:
    - Detection. The earliest efforts to formalize medical decision making involved the application of statistical decision methods (ROC, Receiver Operating Curves) in radiographic interpretation. Since then, detection algorithms have been applied in many fields.
    - Pattern recognition: Automatic diagnosis is possible in many cases through pattern recognition algorithms that sort symptoms into diagnostic categories. Pattern recognition develops and applies algorithms that recognize patterns in data. Those algorithms involve techniques as Principal Component Analysis (PCA), Partial Least Squares (PLS) and Multivariate Linear Regression (MLR), Support Vector Machines (SVM), neural networks, etc.

Signal enhancement techniques are well covered in many signal processing books [60], [61], [62] and [63]. Here we will have a limited review of the decision support techniques that will be used in the following chapters.

A pattern is any item whose important characteristics form a set of descriptors (usually numerical) that characterize the object. Each pattern (object) has associated with it a property value. A property is an attribute of a pattern that is difficult, expensive, or time-consuming to measure, or not even directly measurable. The descriptors capture some important characteristics of the pattern, and then a mathematical function (e.g., machine learning

algorithm) can generate a mapping between the descriptor space and the property, classifying therefore the patterns according to the resulting property.

Lets see the pattern recognition problem in mathematical notation: An n-dimensional pattern (object) x has n coordinates, $x=(x_1, x_2,\ldots, x_n)$, where each x_i is a real number, $x_i \in \mathcal{R}$ for i = 1, 2, …, n. Each pattern x_j belongs to a class $y_j \in \{-1, +1\}$. T is a training set of m patterns together with their classes, $T=\{(x_1, y_1), (x_2, y_2), \ldots, (x_m, y_m)\}$. S is the dot product space in which the patterns x are embedded, $x_1, x_2, \ldots, x_m \in S$. Any hyperplane in the space S can be written as

$$\left\{x \in S \middle| w \cdot x + b = 0\right\}, \quad w \in S, b \in R \tag{2-1}$$

The dot product w•x is defined by:

$$w \cdot x = \sum_{i=1}^{n} w_i x_i \tag{2-2}$$

A training set of patterns is linearly separable if there exists at least one linear classifier defined by the pair (w, b) which correctly classifies all training patterns (Figure 5). This linear classifier is represented by the hyperplane H (w•x+b=0) and defines a region for class +1 patterns (w•x+b>0) and another region for class -1 patterns (w•x+b<0).

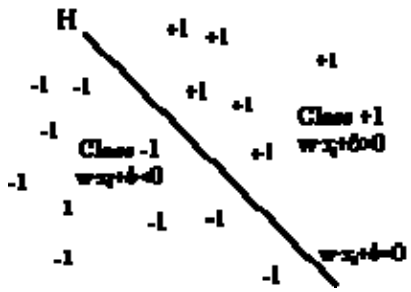

Figure 5. Linear classifier defined by the hyperplane H (w•x+b=0).

After training, the classifier is ready to predict the class membership for new patterns, different from those used in training. The class of a pattern x_k is determined with the equation:

$$class(x_k) = y_k = \begin{cases} +1 & \text{if} \quad w \cdot x_k + b > 0 \\ -1 & \text{if} \quad w \cdot x_k + b < 0 \end{cases} \tag{2-3}$$

equivalent to:

$$y_k (w \cdot x_k + b) - 1 \geq 0 \tag{2-4}$$

Therefore, the classification of new patterns depends only on the sign of the expression w•x+b.

In general, for each linearly separable training set, one can find an infinite number of hyperplanes that discriminate the two classes of patterns. An optimum hyperplane is obtained that has a maximum margin (separation between the two classes), and with the separation hyperplane being equidistant from the two classes.

2.3.2 Support Vector Machines (SVM)

Support vector machines (SVM) are a group of supervised learning methods that can be applied to classification or regression. SVM models were originally defined for the classification of linearly separable classes of objects and later extended for the non-linearly separable case. For any particular set of two-class objects, an SVM finds the unique hyperplane having the maximum margin ($2/\|w\|$, see Figure 6).

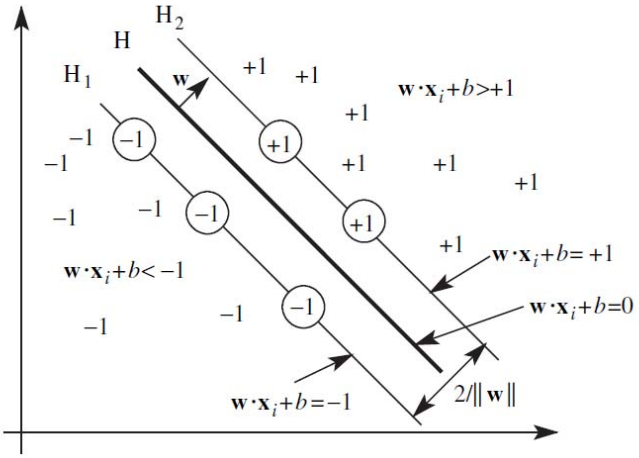

Figure 6. Separating hyperplane H.

In Figure 6, the hyperplane H_1 defines the border with class +1 objects, whereas the hyperplane H_2 defines the border with class -1 objects. Two objects from class +1 define the hyperplane H_1, and three objects from class -1 define the hyperplane H_2. These objects, represented inside circles, are called support vectors. A special characteristic of SVM is that the solution to a classification problem is represented by the support vectors that determine the maximum margin hyperplane. Given that the margin equals $2/\|w\|$, maximizing the margins is equivalent as minimizing $\|w\|^2/2$, thus the problem of finding the optimum H can be described by equation (2-5).

$$\begin{aligned} &\text{minimize} \quad f(x)=\frac{\|w\|^2}{2} \text{ with the constraints:} \\ &g_i(x)=y_i(w\cdot x_i+b)-1\geq 0, \quad i=1,\cdots,m \end{aligned} \tag{2-5}$$

Based on the use of a Lagrangian function, equation (2-6) is transformed into its dual formulation showed in equation (2-7).

$$\begin{aligned} &L_P(w,b,\Lambda)=f(x)-\sum_{i=1}^{m}\lambda_i g_i(x) \\ &\min_{w,b}\max_{\lambda_i}\{L_P(w,b,\Lambda)\} \quad \equiv \quad \min_{w,b}\max_{\lambda_i}\left\{f(x)-\sum_{i=1}^{m}\lambda_i g_i(x)\right\} \end{aligned} \tag{2-6}$$

$\Lambda=(\lambda_1,\lambda_2,\cdots,\lambda_m)$ is the set of Lagrange multipliers of the training (calibration) patterns, $\lambda_i \geq 0$.

$$\begin{aligned} L_P(w,b,\Lambda)&=f(x)-\sum_{i=1}^{m}\lambda_i g_i(x)=\frac{1}{2}\|w\|^2-\sum_{i=1}^{m}\lambda_i\left(y_i(w\cdot x_i+b)-1\right) \\ &=\frac{1}{2}\|w\|^2-\sum_{i=1}^{m}\lambda_i\left(y_i(w\cdot x_i+b)\right)+\sum_{i=0}^{m}\lambda_i \\ &=\frac{1}{2}\|w\|^2-\sum_{i=0}^{m}\lambda_i y_i w\cdot x_i-\sum_{i=1}^{m}\lambda_i y_i b+\sum_{i=1}^{m}\lambda_i \end{aligned} \tag{2-7}$$

The Lagrangian function L_P must be minimized with respect to w and b, and maximized with respect to λ_i, subject to the constraints $\lambda_i \geq 0$ (equation (2-8)).

$$\min_{w,b}\max_{\Lambda}\left\{\frac{1}{2}\|w\|^2-\sum_{i=0}^{m}\lambda_i y_i w\cdot x_i-\sum_{i=0}^{m}\lambda_i y_i b+\sum_{i=0}^{m}\lambda_i\right\},\ \lambda_i\geq 0 \tag{2-8}$$

This is equivalent to maximize L_P subject to the constraints that the gradient of L_P with respect to w and b is zero, and subject to the constraints $\lambda_i \geq 0$. By the Karush-Kuhn-Tucker (KKT) conditions [64], [65], we obtain:

$$\begin{aligned} &\frac{\partial L_{p(w,b,\Lambda)}}{\partial w}=\left(\frac{\partial L_P}{\partial w_1},\frac{\partial L_P}{\partial w_1},\cdots,\frac{\partial L_P}{\partial w_n}\right); \\ &\|w\|^2=w\cdot w \Rightarrow \frac{\partial L_{p(w,b,\Lambda)}}{\partial w}=w-\sum_{i=1}^{m}\lambda_i y_i x_i=0 \\ &\frac{\partial L_{p(w,b,\Lambda)}}{\partial b}=\sum_{i=1}^{m}\lambda_i y_i=0 \\ &\frac{\partial L_{p(w,b,\Lambda)}}{\partial \lambda_i}=g(x)=0 \\ &\lambda_i\geq 0 \end{aligned} \tag{2-9}$$

$$\lambda_i g_i(x)=\lambda_i\left[y_i(w\cdot x_i+b)-1\right]=0,\quad i=1,\cdots,m \tag{2-10}$$

$$y_i(w\cdot x_i+b)-1\geq 0,\quad i=1,\cdots,m \tag{2-11}$$

When we introduced the Lagrange function we assigned a Lagrange multiplier λ_i to each training pattern via the constraints $g_i(x)$ (see equation (2-5)). The training patterns from the SVM solution that have $\lambda_i > 0$ represent the support vectors. The training patterns that have $\lambda_i = 0$ are not important in obtaining the SVM model, and they can be removed from training without any effect on the SVM solution. As we will see below, any SVM model is completely defined by the set of support vectors and the corresponding Lagrange multipliers. The vector w that defines the optimum separating hyperplane (OSH) is obtained from the first condition in equation (2-9).

$$w = \sum_{i=1}^{m} \lambda_i y_i x_i \tag{2-12}$$

From equation (2-10) and equation (2-12) and given that $\lambda_j > 0$ for the support vectors, b can be obtained by averaging the b values obtained for all support vector patterns:

$$\sum_{i=1}^{m} \lambda_i y_i x_i \cdot x_j + b = y_j \quad \Rightarrow \quad b = y_j - \sum_{i=1}^{m} \lambda_i y_i x_i \cdot x_j \tag{2-13}$$

Once w and b are determined any new pattern can be classified as:

$$class(x_k) = \begin{cases} +1 \text{ if } w \cdot x_k + b > 0 \\ -1 \text{ if } w \cdot x_k + b < 0 \end{cases} \tag{2-14}$$

However, equation (2-12) offers the possibility to predict new patterns without computing the vector w explicitly. In this case, we will use for classification the support vectors from the training set and the corresponding values of the Lagrange multipliers λ_i :

$$class(x_k) = sign\left(\sum_{i=1}^{m} \lambda_i y_i x_i \cdot x_k + b\right) \tag{2-15}$$

Patterns that are not support vectors ($\lambda_i = 0$) do not influence the classification of new patterns.

Extension to nonlinear case

In the case that the sampled vectors can not be linearly separated, a non-linear transformation can be used to map the set of input vectors into a new space of higher dimensionality. If the function performing the mapping is nonlinear and the target space dimension is high enough, probably the transformed set of vectors will be linearly separable in the new hyperspace. Once in the new hyperspace SVM can be used to obtain the optimum hyperplane that separates the training set.

In mathematical notation, vectors are mapped in the $\mathcal{H}$ space using a function:

$$\Phi: \mathbb{R}^n \to \mathrm{H},\ x \to \Phi(x) = \left[\Phi_1(x), \Phi_2(x), \Phi_3(x), \cdots, \Phi_L(x)\right] \tag{2-16}$$

where Φ_i are chosen functions. Because of the high dimension of the hyperspace $\mathcal{H}$, the separation algorithm becomes computationally complex. In order to reduce the complexity, a kernel function K is selected such that, the dot product: $\Phi(x_i) \cdot \Phi(x_j)$ is directly computed as $K(x_i, x_j) = \Phi(x_i)\Phi(x_j)$. In this way the nonlinear function Φ does not need to be used in the learning process.

There is no theoretical tool to predict which kernel will give the best results for a given dataset, experimenting with different kernels is the only way to identify the best function. Like all other multivariate algorithms, SVM can over fit the data used in training, a problem that is more likely to happen when complex kernels are used to generate the SVM model. Minimum complexity should guide the selection of the kernel function.

In Chapter 3, SVM are evaluated in predicting the accurateness of the measures and clinical security of continuous blood glucose meters.

2.3.3 Principal Component Analysis (PCA)

PCA is applied in the analysis of multivariate data, and the main idea behind this technique is that of reducing the complexity of the analysis by lowering the dimensionality, i.e., the number of variables of the signal while keeping as much as possible the variation (variability usually holds information) in the data set. It is a way for optimizing a trade-off between information and complexity for a given problem. Dimension reduction is accomplished by linearly transforming the data set into a hyper-space, the basis of which is a new set of uncorrelated variables, the principal components (PCs), and which are ordered so that the first few retain most of the variation present in all of the original variables. At that point by selecting only the first part of the variables, the dimensionality is reduced while keeping much of the variation in the original data.

Given a vector x of p random variables, if p is rather large, identifying patterns by looking at the p variances and all of the $\frac{1}{2}p(p-1)$ correlations or

covariances can become complex. An alternative approach is to look for a few *k*<<*p* derived variables that preserve most of the information given by these variances and correlations or covariances.

The covariance matrix Σ is the matrix whose *(i, j)th* element is the covariance between the *ith* and *jth* elements of vector *x* when $i \neq j$, and the variance of the *jth* element of *x* when *i* = *j*. In practical applications Σ is unknown, and we only have a set of observations of the real process, in this case, an approximation is taken by replacing Σ by a sample covariance matrix *S*.

It turns out that for *k = 1, 2, ..., p*, the *kth* PC is given by $z_k = \alpha_k' \cdot x$ where α_k is an eigenvector of Σ corresponding to its kth largest eigenvalue λ_k. Furthermore, if α_k is chosen to have unit length ($\alpha_k' \cdot \alpha_k = 1$), then $var(z_k) = \lambda_k$, where $\mathrm{var}(z_k)$ denotes the variance of z_k.

To derive the form of the PCs, consider first $z_1 = \alpha_1' \cdot x$; the vector α_1 maximizes $var(\alpha_1' \cdot x) = \alpha_1' \cdot \Sigma \cdot \alpha_1$. It is clear that, as it stands, the maximum will not be achieved for finite α_1 so a normalization constraint must be imposed. The constraint used in the derivation is $\alpha_1' \cdot \alpha_1 = 1$,

To maximize $\alpha_1' \cdot \Sigma \cdot \alpha_1$ subject to $\alpha_1' \cdot \alpha_1 = 1$, the standard approach is to use the technique of Lagrange multipliers. Maximize

$$\alpha_1' \cdot \Sigma \cdot \alpha_1 - \lambda\left(\alpha_1' \cdot \alpha_1 - 1\right), \tag{2-17}$$

where λ is a Lagrange multiplier. Differentiation with respect to α_1 gives

$$\Sigma \cdot \alpha_1 - \lambda \cdot \alpha_1 = 0 \quad \Rightarrow \quad (\Sigma - \lambda \cdot I_p) \cdot \alpha_1 = 0\,, \tag{2-18}$$

where I_p is the (*pxp*) identity matrix. Thus, λ is an eigenvalue of Σ and α_1 is the corresponding eigenvector. To decide which of the p eigenvectors gives $\alpha_1 \cdot x$ with maximum variance, note that the quantity to be maximized is $\alpha_1' \cdot \Sigma \cdot \alpha_1 = \alpha_1' \cdot \lambda \cdot \alpha_1 = \lambda \cdot \alpha_1' \cdot \alpha_1 = \lambda$, so λ must be as large as possible. Thus, α_1 is the eigenvector corresponding to the largest eigenvalue of Σ, and $var(\alpha_1' \cdot x) = \alpha_1' \cdot \Sigma \cdot \alpha_1 = \lambda_1$, the largest eigenvalue. In general, the kth PC of x is $\alpha_k \cdot x$ and $var(\alpha_k' \cdot x) = \alpha_k' \cdot \Sigma \cdot \alpha_k = \lambda_k$, where λ_k is the kth largest eigenvalue of Σ, and α_k is the corresponding eigenvector.

As stated above, it can be shown that for the third, fourth, . . . , *p*th PCs, the vectors of coefficients $\alpha_1, \alpha_2, \alpha_3, ..., \alpha_p$ are the eigenvectors of Σ corresponding to $\lambda_1, \lambda_2, \lambda_3, ..., \lambda_p$, the first, second, and third largest, . . . , and the smallest eigenvalue, respectively. Furthermore, $var(\alpha_k' \cdot x) = \lambda_k$ for $k = 1, 2, ..., p$.

As a conclusion to this process, the PCs are defined by an orthonormal linear transformation of x,

$$z = A' \cdot x\,, \tag{2-19}$$

where *z* is the vector whose kth element, z_k $k = 1, 2, ..., p$, is the *k*th PC, *A* is the orthogonal matrix whose *k*th column, α_k, is the *k*th eigenvector of Σ.

Once the PCs are obtained from the data set, depending on the application, a subset of the first of those PCs is to be selected to simplify the problem. With

the reduced subset of PCs pattern recognition techniques can more easily be applied. Because of this capacity in simplifying problems PCA is widely used in signal analysis. In this thesis, in chapter 4, a PCA application to neural signal spikes sorting is presented.

2.4 Wireless transmission in body-centered systems

Wireless biomedical sensing is important in telemedicine and in medical research. For the first field, it is often beneficial for patients to mobilize for a better recovering; moreover it is very uncomfortable to remain wired to a bed for a long time. Additionally attaching, releasing and re-attaching cables for patient transportation can be very time-consuming [66]. Secondly, in the research field, experiments may also need a freely moving subject which is impossible with the use of cables. Actually, not only in the health monitoring domain but in general, applications in which wireless devices have to run on battery power for very long periods and still be able to participate in ad-hoc wireless networks, have given birth to a new class of networks, known as Wireless Sensor Networks (WSNs).

2.4.1 Wireless Body Sensor Networks (WBSN)

When sensors are located around or in the body, the requirements and characteristics become different to the ones in general environments, to signify such particularities, those networks are called Wireless Body Sensor Networks,

(WBSNs)[1] and are emerging as promising enabling technologies to implement mobile health (m-health). A WBSN is a self-organizing network at the human body scale, which consists of multiple small, self-powered and hardware-constrained sensors placed on, or eventually implanted into, the human body. In fact, a patient's health parameters can be collected by a WBSN, thus monitoring vital body physiological states and movements.

In Figure 7 a basic scheme for a WBSN configuration is depicted. In WBSN, the information is transmitted through wireless technologies from the body to a central station, from where it can be forwarded to a hospital, clinic or elsewhere. The sensors in/on the body are usually referred to as nodes and the central device is called bridge, hub or coordinator.

[1] WBSNs are also called WBANs and we treat both indistinctive.

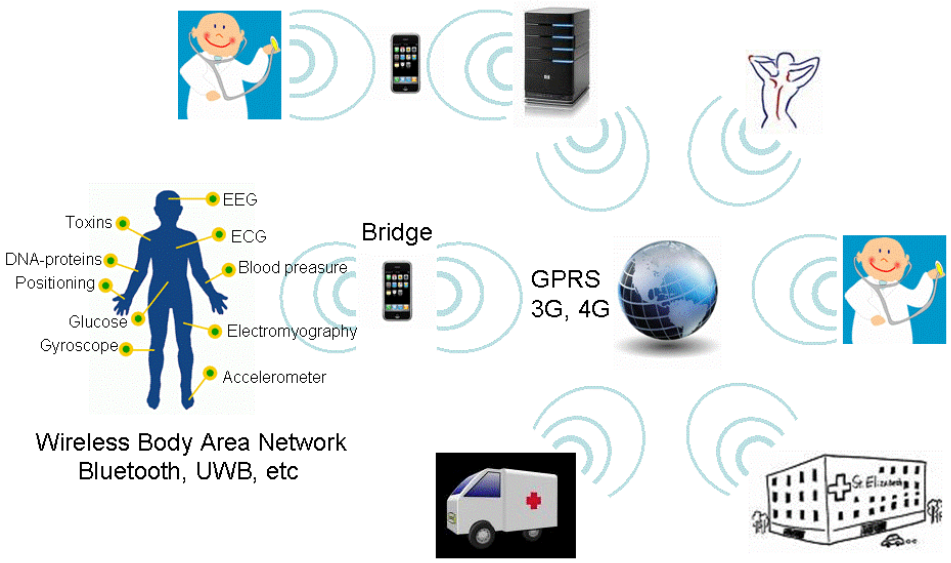

Figure 7. Schematic of a Wireless Body Area network for e-health application.

A WBSN for health monitoring may also feature active devices for control of the user's physiological state. For example, some WBSN nodes may be responsible for drug delivery. These sensor nodes are strategically placed on the human body. The exact location and attachment of the sensor nodes on the human body depend on the sensor type, size, and weight. Sensors can be worn as stand-alone devices or can be built into jewelry, applied as tiny patches on the skin, hidden in the user's clothes or shoes, or even implanted in the user's body. Each node in the WBSN is typically capable of sensing, sampling, processing, and wirelessly communicating one or more physiological signals. The exact number and type of physiological signals to be measured, processed, and reported depends on end-user application and may include a subset of the following physiological sensors:

- An ECG sensor for monitoring heart activity
- An EMG sensor for monitoring muscle activity
- An EEG or ECoG sensor for monitoring brain electrical activity
- A PPG sensor for monitoring pulse and blood oxygen saturation
- A cuff-based pressure sensor for monitoring blood pressure
- A resistive or piezoelectric chest belt sensor for monitoring respiration
- A galvanic skin response (GSR) sensor for monitoring autonomous nervous system arousal
- A blood glucose level sensor
- A thermistor for monitoring body temperature

In addition to these sensors, a WBSN for health monitoring may include sensors that can help determine the user's location, position or even activity level using sensors as:

- A localization (GPS) sensor.
- A tilt sensor for monitoring trunk position
- A gyroscope-based sensor for gait-phase detection.
- Accelerometer-based motion sensors on extremities to estimate activity level

- A sensor to count steps and/or delineate phases and distribution of forces during individual steps

Also ambient conditions can have an effect on the user's physiological state or even on the accuracy of the sensors. For that reason, WSNs can integrate ambient sensors that help in the interpretation of the body parameters.

Challenges or limiting factors in biomedical sensors are:

- Power consumption or battery life
- Latency of the measures. Constant delay between measures is required in many real-time monitoring applications. WBSN nodes must have enough storage resources for temporary data buffers to accommodate for lost messages and intermittent communication. The size of these buffers is determined by allowed event latency and available memory capacity. Event latency requirements define the maximum propagation delay from the moment an event has been detected on a WBSN node until the moment the personal server application has received that event.
- Capacity of the wireless link.

2.4.2 System architecture

The most common system architecture for a WBSN has three blocks:

- The data acquisition block: responsible for sensing and collecting information concerning health conditions, i.e. set of sensors.

- The data distribution block is responsible for distributing relevant data for analysis, i.e., the coordinator or bridge.
- The processing and control block is responsible for processing, interpreting summarized data, and making appropriate controls or responses. Usually this task is performed by a processor unit connected to the network through the coordinator of by a remote server connected through the coordinator and an access point and some kind of LAN.

In reality, the functions of a block are usually carried out by groups of components simultaneously at different topological levels.

Figure 7 shows a typical and practical architecture for a health monitoring system. At the lowest level topologically, a group of sensors operate within a confined area (e.g., over the body of a person) and form a wireless body area network (BAN so that they can rely on one another to relay sensed information to a more powerful sensor, which then relays the information to a local server.

One of the main problems for telemonitoring systems to become more widespread is the lack of interoperability among the different solutions. As exposed in the general system architecture, medical devices at home or in other non-clinical Environments are connected with some kind of gateway, possibly a smartphone or home PC application to a remote monitoring service, which in turn needs to interact with other systems containing patient information like electronic health records systems, chronic disease management systems, etc. Thus, it is essential for these systems to

interoperate with existing healthcare IT. In this direction, several interoperability and standardization efforts are being made as the ISO/IEEE 11073 or the Continua Alliance.

ISO/IEEE 11073 standard [67] defines a common framework for real-time plug-and-play interoperability for citizen-related medical, healthcare and wellness devices that facilitates efficient exchange of data, acquired at the point-of-care, in all care environments. The standard aims at: creating an abstract transport-independent model of personal health data, defining the transfer syntax required to establish logical connections between systems and providing presentation capabilities and services needed to perform communication tasks. It is targeted at personal health and fitness devices (such as glucose monitors, pulse oximeters, weighing scales, medication dispensers and activity monitors) and at continuing and acute care devices (such as pulse oximeters, ventilators and infusion pumps). They comprise a family of standards that can be layered together to provide connectivity optimized for the specific devices being interfaced. The standard is:

- "Real-time", meaning that data from multiple devices can be retrieved, time correlated, and displayed or processed in fractions of a second.
- "Plug-and-play" meaning that all a user has to do is make the connection – the systems automatically detect, configure, and communicate without any other human interaction.

- "Efficient exchange of care device data" meaning that information that is captured at the point-of-care (e.g., personal vital signs data) can be archived, retrieved, and processed by many different types of applications without extensive software and equipment support, and without needless loss of information.

Continua [68] is an industry alliance of over 230 organizations with a mission of establishing a system of interoperable personal health solutions. For doing that, Continua Alliance designs guidelines for building interoperable sensors and telemonitoring platforms. As other interoperability alliances, Continua's objective is for the general public to identify its logo with interoperability across telehealth products. Thus Continua works with several standardization bodies, including ISO, ETSI, European AAL Association and HL7.

2.4.3 Transmission technologies

Although wireless telemetry has been available for a few decades, wireless intelligent sensors capable of real-time signal processing have been developed only recently. Apart from other difficulties as biocompatibility and miniaturization, also the interaction of the body in terms of network and electromagnetic propagation properties shall be studied. The propagation along (external) or through (implants) the body must be characterized and will be decisive in selecting the physical (PHY) and medium access control (MAC) layers to be used. According to this, there are two possible types of links in a WBSN, the through body and along body links for implants and on-body

devices respectively. Any general WBSN has to take into account these two types of electromagnetic propagation.

For the human body, the most relevant transmission characteristics are transmission power and transmission frequency. It becomes fundamental to know the absorption of energy within the body and to study the effects through the Specific Absorption Rate (SAR). Besides, other determining WBAN characteristics are: maximum link distance, interferences with other equipments, path loss, delay spread, and other dispersion related characteristics.

In the case of implanted devices, the radio frequency (RF) module must consume very little power so that it can last on battery power for years.

The general link budget formula for an implant's and for the on-body device wireless links are equation (2-20) and (2-21) respectively:

$$P_{RX} = P_{TX} + G_{TX} + L_{FS} + L_B + G_{RX} \tag{2-20}$$

$$P_{RX} = P_{TX} + G_{TX} + L_{OB} + G_{RX} \tag{2-21}$$

where P_{RX} is received power (dBm); P_{TX}, transmitter output power (dBm); G_{TX}, transmitter antenna gain (dBi); L_{FS}, free space loss or path loss. (dBm); L_B, losses within body tissues (dBm); L_{OB}, losses of the on-body link and G_{RX}, receiver antenna gain (dBi). A sensitive receiver permits communication over a longer range. However, it may consume more power and hence decrease battery lifetime. Therefore, an optimal wireless medical system design should

balance the need for a longer communication range against the desired longevity of the implanted device.

Different transmission techniques can be chosen to implement WBAN. Many external devices use the band in 2.45-GHz as Bluetooth, ZigBee or 802.11. Also UltraWideBand (UWB) has been proposed. For the implants case, non-RF transmission technologies are more suitable. Here is a summary list of both RF and non-RF technologies:

1. ZigBee technology [69] should be considered if sensors are to be very small and need to communicate over a very short distance, batteries have to last for a long time (a few months), and low data transmission rates are adequate. ZigBee operates in the industrial, scientific and medical (ISM) radio bands, builds upon the physical layer and medium access control defined in IEEE standard 802.15.4 [70] and data transmission rates vary from 20 to 250 kbps. IEEE 802.15.4 was not designed to support WBANs but for general WSN. The ZigBee network layer natively supports both star and tree typical networks, and generic mesh networks. Every network must have one coordinator device, tasked with its creation, the control of its parameters and basic maintenance. Evaluation of the standard for WBSN conducted in [71] points out that although it can provide QoS, the technology is not scalable in terms of power consumption and although it acts as a quick (and easy) implementation it can not be used as a single solution for all WBAN applications.

2. UWB technology is applicable at high data rates over extremely short distances via small sensors. UWB operates at very low radiated power density by employing very large bandwidths. Two technologies competed for reaching the IEEE UWB standard: Direct Sequence UWB and Multi-Band Orthogonal Frequency Division multiplexing (OFDM) UWB. However, after several years of deadlock, the IEEE 802.15.3a task group was dissolved in 2006 due to lack of agreement. Direct Sequence UWB, which was promoted by the ZigBee Alliance, has been approved by the IEEE 802.15.4a standardization body as a suitable radio technology to enable low-cost and low-power devices for low data rate (LDR) applications within ad hoc sensor networks, while Multi-Band OFDM UWB was adopted by the WiMedia Alliance which published ECMA-368 [72].

3. Bluetooth technology [73] is used as a wire replacement and a bridge between sensor devices and more powerful control. Bluetooth devices can often serve as local servers to coordinate and control wireless sensors, as shown in Figure 7, where the mobile device is collecting the information from the body sensors and forwarding it to a remote server. However it does not support (or only very limited) multi-hop communication. It has a complex protocol stack and high energy consumption compared to IEEE 802.15.4.

4. IEEE 802.11 [74] technology is normally deployed as a bridge between sensors and the wired and wireless Internet. It requires more power and is not often used in mobile wireless sensors.

5. IEEE 802.15.6 [75]. The standardization group is currently actively working towards providing an international standard for a short range (i.e. about human body range), low power and highly reliable wireless communication for use in close proximity to, or inside, a human body. The current IEEE 802.15.6 standard defines three PHY layers, i.e., Narrowband (NB), Ultra wideband (UWB), and Human Body Communications (HBC) layers. The selection of each PHY depends on the application requirements. On the top of it, the standard defines a sophisticated MAC protocol that controls access to the channel.

6. Non-RF communication: it has been shown possible to use Body-Coupled Communication (BCC) to transfer data from an implant to an external link [76]. The advantage of BCC is that it requires less power than traditional radio for providing the same BER (Bit Error Rate). Additionally, as no power is radiated away from the body, it does not create interference and also it is more secure since it can not be intercepted. These radios work at low frequencies (ranging from 10 kHz to 10 MHz). High variations of the transmission attenuation have been observed at different locations of the body. As a BCC is restricted to a person's body, the BCC can be used to discover and identify sensor nodes on the same body and for waking up RF radios from low-power sleep mode.

7. Mobile cellular technologies (GSM, GPRS, CDMA2000, and WCDMA) are needed to connect devices over WANs. They are often used to connect

local servers to global servers that oversee the overall aspects of an application over the mobile Internet.

Chapter 5 of this thesis includes a study of on-body UWB transmission and also an evaluation of the performance of an UWB system for the application presented in Chapter 4, i.e., real-time neural signal monitoring. On the other hand, a section in Chapter 4 describes a prototype for the compression-transmission-reconstruction of neural signals using Bluetooth and 3G.

2.4.4 Communication topologies

Star, tree and mesh are the basic topologies for WSN which can be seen in Figure 9 [77]. The single-hop star topology is the most straightforward and most commonly proposed topology for WBSN. However, studies of on-body electromagnetic propagation (see Chapter 5) show that it is not always possible to assume single-hop communication along the body. In a one-hop star, frame exchanges may occur directly only between nodes and the hub. In a two-hop extended star, the hub and a node may optionally exchange frames via a relay capable node. Mesh topologies are more complex to design an optimized and have not been widely used in WBSNs.

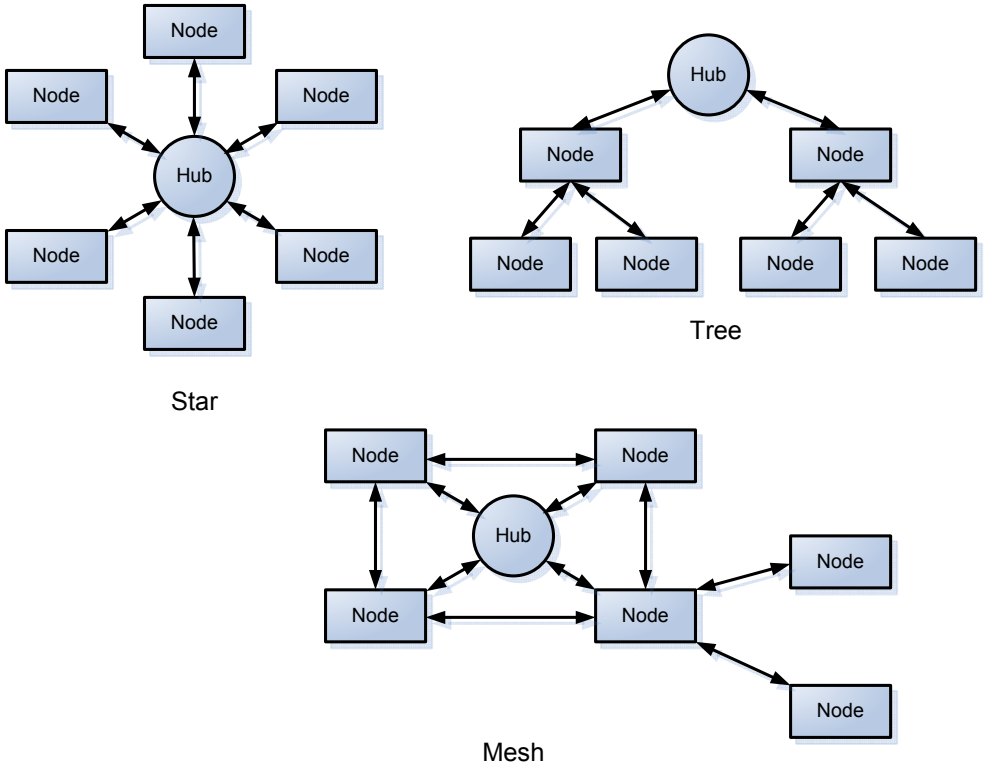

Figure 8. WSN basic topologies.

Energy consumption can be divided into three domains: sensing, (wireless) communication and data processing. The wireless communication is likely to be the most power consuming. As the design of effective network architectures is a key issue to achieve energy-efficient, low-latency WBSNs, the 2-hop extended star architecture has recently been promoted by the IEEE 802.15.6 task group (TG6) as ideal candidates for WBSNs (see Figure 9).

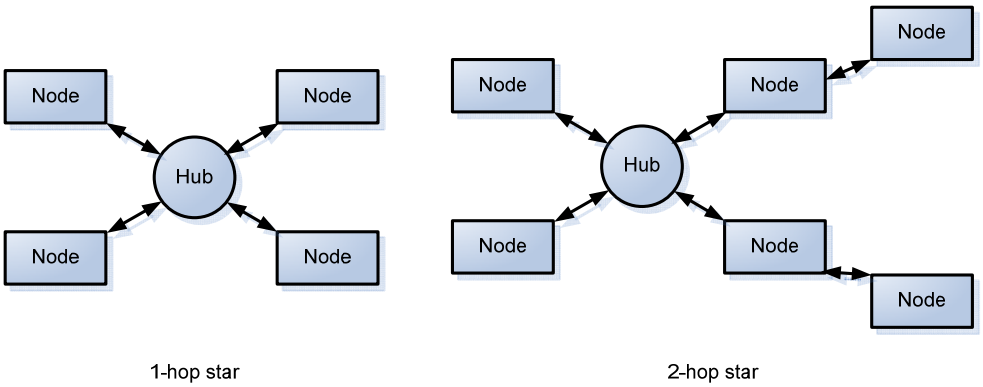

Figure 9. 802.15.6 topologies.

2.5 Applications of body-centered systems

WBANs can be used from fitness/exercise monitoring to control of patients with chronic or impeding medical conditions in hospitals and ambulatory settings and to early detection of disease, or emergency care. Although this thesis covers health applications only, here are the most common areas of WBSN applicability:

- Remote health/fitness monitoring and telemedicine: health and motion information are monitored in real-time, and delivered to nearby diagnosis or storage devices, through which data can be forwarded to off-site doctors for further processing.
- Localization in Emergency.
- Military, sports training and rehabilitation: For example, motion sensors can be worn at both hands and elbows, for accurate feature extraction of sports players' movements.

- Interactive gaming: Body sensors enable game players to perform actual body movements, such as boxing and shooting, that can be fed back to the corresponding gaming console, thereby enhancing their entertainment experiences.
- Personal information sharing: Private or business information can be stored in body sensors for many daily life applications such as shopping and information exchange.
- Secure authentication: This application involves resorting to both physiological and behavioral biometrics schemes, such as facial patterns, finger prints and iris recognition.

Two specific applications are considered in detail in this thesis, first Chapter 3 deals with blood-glucose monitoring and secondly in Chapter 4 covers neural signal processing is covered.

2.6 Commercial products

In this section a list of commercially available products has been included. The list is not exhaustive since it would be too long and also because new products appear everyday so any attempt to keep an updated list would be unattainable, however from the following one can have an idea of the vast number of opportunities in the WBSNs field.

2.6.1 Diabetes Control

1. The company Echo Therapeutics, Inc. is developing a non-invasive, wireless, transdermal continuous glucose monitoring system called

Symphony™ tCGM and at the same time the Prelude™ SkinPrep System for trans-dermal drug delivery [78].

2. DexCom [79] and Medtronic [80], among others, currently offer systems based on subcutaneous sensors that can be worn for up to 72 hours before replacement is needed. DexCom also has reported results for patients with surgically implanted long-term glucose level sensors..

3. Medtronic MiniMed is an example of efforts to develop an artificial pancreas for diabetes patients. Medtronic offers two products [81], first, the Guardian® REAL-Time Continuous Glucose Monitoring System that uses the wireless MiniLink REAL-Time Transmitter for monitoring and, second, the MiniMed Paradigm® Revel™ System which includes glucose monitoring and insulin delivery.

4. SMSI® Glucose Sensor [82] is another example of an implantable sensor that is currently under development.

5. GlucoTrack® [83], by Integrity Applications, uses three independent technologies that are operated simultaneously: ultrasonic, electromagnetic and thermal to non-invasively measure glucose levels in the blood. It is in clinical trials phase so not yet available for commercialization.

6. Abbot's FreeStyle Navigator® CGM [84] is yet another continuous monitor using wireless non-invasive sensors.

2.6.2 Brain and Muscle Activity

In the field of brain and muscle activity sensors, some commercial wireless products have started to appear:

1. Enobio Wireless Brain Monitoring from Starlab [85] which allows wireless recording of EEG, ECG and EOG (Electrooculogram – Eye movement).

Figure 10. Enobio's image taken from the product's site [85].

2. Also the company NeuroFocus has announced, in March 2011, a dry (no need to use any conductive product) wireless EEG system called Mynd™ [86].

3. Advanced Brain Monitoring Inc with the b-alert range of products [87] offer ECG, EOG, EMG or respiration wireless real-time monitoring up to 10-meters. Additionally an on-board accelerometer quantifies head movement & position.

4. Brain Products also has a range of EEG and EMG products [88] to perform monitoring and Brain Computer Interface applications.

5. Neurosky [89] is yet another company developing wearable EEG recording devices as MindSet and MindWave for education entertainment and research applications.

6. Medtronic has developed the Activa Therapy Deep Brain Stimulator [90], an implantable, multi-programmable system that delivers electrical stimulation to selected areas of the brain. Such stimulation can block the brain signals associated with dystonia, Parkinson's disease, and essential tremor.

7. Brainfingers [91] hardware and software by Brain Actuated Technologies Inc. allows a person to control a computer totally hands-free.

8. Bio.Switch MCTOS WX from Technos Japan, Ltd [92] is described as a simple switch that is controlled by bioelectrical activity measured at the forehead. This hardware can be operated by muscle twitch, eye movement (EOG), eye blink (EMG), and mental activity (EEG). The Bio.Switch combines these systems in a single input system, or switch. It can be used to enhance communication between patients and caregivers by relaying the needs and intentions of severely disabled individuals, providing vital support to people with special needs.

9. The IBVA (Interactive Brainwave Visual Analyzer) from IBVA Technologies, Inc. [93] – measures EEG from the anterior of the frontal lobes called the pre frontal cortex. The EEG is translated into 3D coordinates using its amplitude and frequency, grouped into the standard bandwidths known as Delta, Theta, Alpha, Beta, Gamma and Eye movement. IBVA simultaneously displays left and right sides of the prefrontal cortex. It reads real time data and provides wireless

transmission to the receiver plugged into the computer of choice were the IBVA software plots the corresponding diagram.

10. BTS Bioengineering [94] offers wireless EMG products: BTS FREEEMG 300 (16 miniaturized probes with active electrodes), BTS POCKETEMG (for 16 electromyograph channels acquisition, visualization, and a first level of processing), BTS EMG-Analyzer (software solution for EMG signal analysis), BTS EMGenius (software to acquire, elaborate and report electromyography and footswitch signals).

11. Brainquiry PET EEG 2.0 Neurofeedback equipment [95] measures EEG or EMG or ECG with active electrodes and sends data to a PC, laptop or PDA remotely through a Bluetooth link.

12. BrainGate™ Neural Interface System [96] is a prototype used in research for computer cursor control. BrainGate's technology is used in the Neuroport (Blackrock Microsystems) [97], which is a sophisticated multichannel system for recording and analyzing human brain and peripheral-nerve electrical activity from up to 256 electrodes. The system captures, processes, and analyzes (in real time) action potentials (spikes), field potentials, and other physiological signals as well as experiment state events. The front-end is compatible with individual stiff-wire electrodes, microelectrode and microwire arrays, planar silicon probes, subdural ECoG grids, and epidural and scalp EEG electrodes.

13. Ripple LCC offers two products, the Grapevine Neural Interface and the Epoch Wireless EEG [98]. The Grapevine Neural Interface records and

processes up to 512 channels of microelectrode, LFP, ECoG, EEG, and EMG signals for real-time experiments. On the other hand, the Epoch collects long-term wireless EEG continuously for up to one year from behaving laboratory animals.

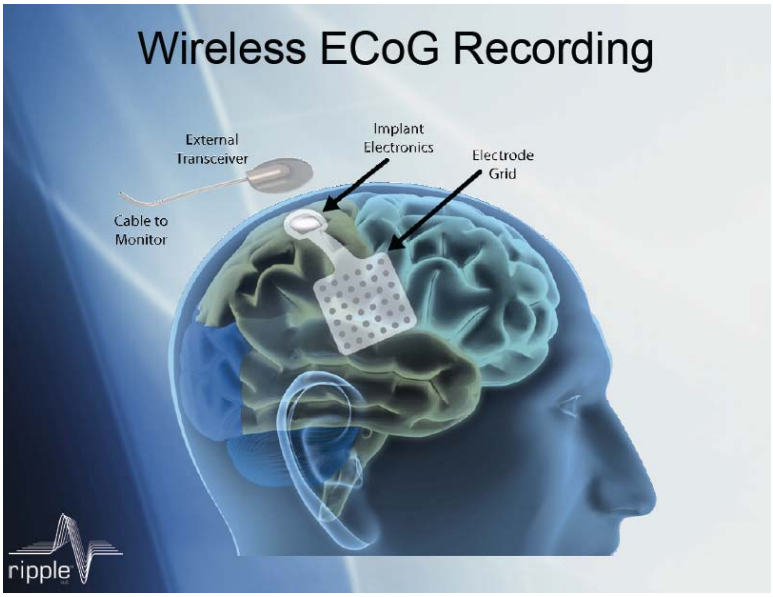

Figure 11. Ripple's wireless ECoG recording system

14. Emotiv [99] is an EEG acquisition and processing wireless headset. It uses a set of 14 saline sensors to detect EEG signals and wirelessly send them to a PC. A gyroscope generates optimal positional information for cursor and camera controls. It can be used for disabled patients (controlling a wheelchair, mind keyboard) or in gaming.

Besides the exposed commercial products, also a set of prototypes are currently under research and will probably bring future products as for example the Neurophone [100] that uses EEG to mentally control and dial a number in a mobile phone.

2.6.3 Cardiopulmonary Monitoring

1. CardioNet MCOT™ [101] (MCOT stands for Mobile Cardiac Outpatient Telemetry). It monitors heart activity, non-invasively, during patient's normal daily activities, for up to 21 days, and detects, records, and transmits event data automatically to the prescribing physician. The system comprises a sensor, a monitor, and a base. Patients wear three leads attached to a lightweight sensor worn on a neck strap or belt clip that continuously transmit two channels of ECG data to the monitor. The monitor analyzes the patient's ECG in real time. When the monitor identifies an abnormal rhythm, the data are automatically sent via cell phone or land line to the CardioNet Monitoring Centre for review by a certified monitoring technician.

2. Medtronic Reveal Plus [102] records subcutaneous ECG for up to 14 months. It can store 42 minutes of data and it is activated either by the patient or automatically on heart rate limits surpassing. It is indicated for patients with clinical syndromes or situations at increased risk of cardiac arrhythmias, patients who experience transient symptoms that may suggest a cardiac arrhythmia.

3. LifeSync Wireless ECG system [103]. It includes a patient transceiver ("PT") and a monitor transceiver ("MT"). The disposable LeadWear® product is applied to a patient's torso with standard ECG electrodes. The PT plugs into the LeadWear® product and is worn in an armband or placed in a patient's hospital gown pocket. The PT transmits ECG and

respiration data to the MT. The MT is connected to lead wires that are attached to virtually any patient monitor. The MT receives the signal from the PT up to thirty feet or more away. In 2003 the LifeSync System was cleared by the FDA and complied with the FCC Part 15 regulations for RF devices.

4. CardioMEMS EndoSure MEMS [104], an implantable blood pressure sensor that uses wireless and MEMS technology.

5. Avant® 4000 Wireless Tabletop Pulse Oximeter by Nonin [105] provides oximetry without the constraints of cables. It uses Bluetooth® wireless technology for reliable and secure transfer of patient data. 120 hours of battery life and 33 hours of memory. Onyx® II, Model 9560 fingertip pulse oximeter is designed for interoperability and is compatible with emerging open standards such as Bluetooth's Health Device Profile (HDP), IEEE11073 and Continua.

6. CareCenter MD [106] is a wireless diagnostic workstation with both PC ECG and PC stress test modalities.

2.6.4 Gastrointestinal Monitoring

1. Several vendors have developed wireless capsule cameras to be ingested disposable imaging capsule is swallowed by a patient and passes through the gastrointestinal tract while wirelessly transmitting images to a receiver that provide images of the gastrointestinal tube. Examples of those capsules are: PillCam Platform (from Given Imaging),

EndoCapsule (from Olympus), Sayaka (from RF System), MiroCam (from IntroMedic), Capsule Endoscopy (From SynMed), [107]-[111].

2.6.5 Integrated sensor Systems

1. TeleMedic Systems has developed telemonitoring system VitalLink [112]. The VitalLink receives data from a variety of medical sensors non-invasive blood pressure, temperature, 6 or 12-lead ECG and SpO2. ECG and SpO2 from different manufactures, the resulting real-time telemedicine data is sent over the VitalNet (wireless Bluetooth or 802.11b to 3G/GPRS/GSM or wired connections such as RS-232, USB or Ethernet) to medical professionals. The VitalLink system is being used in medical emergencies on aircrafts or ships. It provides patient screening in medical practices and general health monitoring in hyperbaric chambers.

2. CareTrends developed Med Surg careTrends™ [113], a software system to communicate vital signs data from wirelessly enabled, legacy point-of-care medical devices. This healthcare software automates the transfer of clinical data from bedside and mobile devices to EMR or Hospital Information System (HIS).

3. ClevelandMedical Devices Inc. markets CrystalMonitor [114] as a lightweight programmable wireless physiological monitor, capable of viewing and recording electroencephalography (EEG), ECG, electromyography (EMG), electro-oculography (EOG), pulse oximetry oxygen saturation (SpO2), and other signals. Collected data are

wirelessly transferred to a personal computer (PC) up to 50 feet away, using the 2.4 GHz Industry, Science, and Medicine (ISM) band. The device can operate continuously for up to 12 hours on two AA batteries.

4. Equivital Limited has developed the Equivital™ [115] system for continuous monitoring and storage of physiological life signs. The system allows real-time or off-line analysis of the data and incorporates the sensors for monitoring heart rate, respiratory rate, user's motion and position, temperature, and G shocks caused by falls and heavy impacts. It also provides a rudimentary cognitive response from the user to assess the user's consciousness and awareness. The 3G wireless cellular data system can be used for direct transmission of all patient data (video, medical images, ECG signals, etc.).

5. GE Healthcare offers a wireless extension to their patient monitoring system [116].

6. Welch Allyn also provides a wireless extension to their telemetry systems in their Acuity® system [117].

7. Proteus Biomedical's Raisin system [118] is a platform for body monitoring, which measures when and if a patient takes his medication, and also measures how various vital signs, such as heart rate, respond to the medication. As it is explained in Proteus' website: Proteus ingestible event markers (IEMs) are tiny, digestible sensors made from food ingredients, which are activated by stomach fluids after swallowing. Once activated, the IEM creates an ultra-low-power, private, digital

signal detected by a microelectronic recorder configured as either a small bandage style skin-patch or a tiny device inserted under the skin. The detector date- and time-stamps, decodes, and records information such as type of drug, dose, and place of manufacture, and also measures and reports physiologic parameters such as heart rate, activity, and respiratory rate. Detector data can be combined at the server-level with other telemetered parameters such as blood pressure, weight, blood glucose, and patient-generated feedback. The development of the Raisin™ System is currently in its clinical trials phase.

8. Toumaz Sensium [119] provides ultra low power monitoring of ECG, temperature, blood glucose and oxygen levels. It can also interface to 3 axis accelerometers, pressure sensors and includes a temperature sensor on chip. Data are streamed using a wireless data link over a short range (~5m) to a USB adapter or data logger.

2.6.6 Sensor motes

1. A sensor mote is a concept defined in the field of WSN. It is a node of the WSN that integrates the devices to: take sensor measurements, make routing decisions and manage power consumption. The Tiny Microthreading Operating System (TinyOS) is a basic framework and development environment for WSNs motes developed at UC Berkeley that aims at setting a standard for pervasive monitoring.

2. Based on the TinyOS "mote" hardware platform, the Harvard Sensor Networks Lab, in its CodeBlue project ([120], [58]), has developed a range of wireless medical sensors: as for example a wireless pulse oximeter and wireless two-lead ECG. These devices collect heart rate (HR), oxygen saturation (SpO2), and ECG data and relay it over a short-range (100m) wireless network to any number of receiving devices, including PDAs, laptops, or ambulance-based terminals. The data can be displayed in real time and integrated into the developing pre-hospital patient care record. The sensor devices themselves can be programmed to process the vital sign data, for example, to raise an alert condition when vital signs fall outside of normal parameters. Any adverse change in patient status can then be signaled to a nearby emergency unit. These vital sign sensors consist of a low-power microcontroller (Atmel Atmega128L or TI MSP430) and a low-power digital spread-spectrum radio (Chipcon CC2420, compliant with IEEE 802.15.4, 2.4 GHz, approximate range 100 meters, data rate about 80 Kbps). The devices have a small amount of memory (4-10 KB) and can be programmed (using the TinyOS operating system) to sample, transmit, filter, or process vital sign data. These devices are powered by 2 AA batteries with a lifetime of up to several months if programmed appropriately.

3. Also at the Harvard sensors Lab they are developing the Mercury system, which is designed to support high-resolution motion studies of patients being treated for neuro-motor conditions such as Parkinson's disease, stroke, and epilepsy [121].

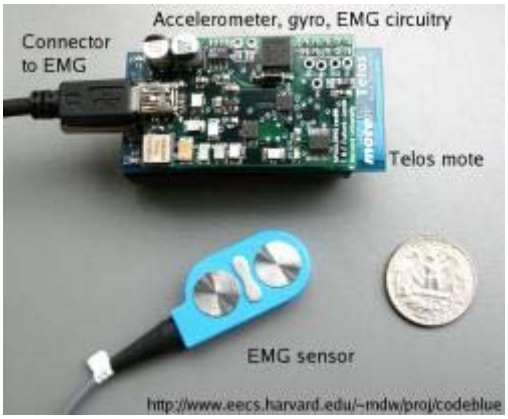

Figure 12. EMG sensor integrated in a Telos mote platform for vital sign monitoring.

A non-exhaustive list of existing motes is presented here:

1. TelosB [122] appeared as the result of the research carried out at UC Berkeley [123]. It uses an 802.15.4 radio for wireless communication to a base station for physical activity and health monitoring research.

2. Shimmer mote [124] is small wireless wearable sensor platform that can record and transmit physiological and kinematics' data in real-time. Shimmer incorporates wireless ECG, EMG, GSR, Accelerometer, Gyro, PIR, Tilt and Vibration sensors. Additionally it is an extensible platform: its firmware is open-source, it offers compatibility with a wide variety of sensor and system technologies (raw data can be sent through Bluetooth, 802.15.4 radio, or stored locally to a microSD card) and it can be connected to self designed or third party sensors.

3. MICAz / MICA2 motes [125], [126]. The MICA Mote platform is used for enabling low-power, wireless sensor networks available in

2.4GHz and 868/916 MHz. The MICAz Mote offers a 2.4 GHz, IEEE/ZigBee 802.15.4, board and the MICA2 is an 868/916 MHz Multi-channel radio transceiver used for low-power wireless sensor networks. The MICA Mote platforms are fully compatible with the MoteWorks Software Platform, a standards-based platform for the development of wireless sensor network [127].

4. The IRIS [128] is a 2.4 GHz Mote is an evolution of the MICA motes. It provides up to three times improved radio range and twice the program memory over previous generations of MICA Motes.

5. The Cricket Mote (MEMSIC) [129] is a location aware version of the MICA2. The Cricket Mote includes all of the standard MICA2 hardware and an ultrasound transmitter and receiver. This device uses the combination of RF and ultrasound technologies to establish differential time of arrival and hence linear range estimates.

6. IntelMote2 (iMote2) has been developed at Intel Research as part of Platform X [130]. It is built around the low-power PXA271 XScale CPU and also integrates an IEEE 802.15.4 compliant radio. The design is modular and stackable with interface connectors for expansion boards on both the top and bottom sides, providing a standard set of I/O signals as well as additional high-speed interfaces for application specific I/O.

7. The Mulle platform [131] is a sensor node aimed at ad-hoc sensor networking and ambient intelligence systems. Both Bluetooth and

Zigbee versions of the Mule are available. The Bluetooth-based one uses standardized profiles (LAP, SPP and PAN) and TCP/IP to communicate. This approach enables users all over the world to access sensor data from a Mulle in real time. The newest Mulle, version v5.2, comes with a IEEE 802.15.4 (Zigbee) transceiver. TinyOS, the world's de-facto operating system for sensor nodes, is now also supported on the Mulle.

8. ZigBits [132] are compact 802.15.4/ZigBee modules by Meshmetrics for wireless sensor network solutions.

9. LOTUS [129], by MEMSIC, is an advanced wireless node platform developed around the low power ARM7 Cortex M3 CPU and incorporates the best of IRIS, TelosB and Imote2 onto a single board. LOTUS is built on a modular and stackable design, incorporating connectors for expansion boards. LOTUS is factory configured to run RTOS (Real Time Operating System). Several other options are also available for LOTUS, including MEMSIC Kiel, RTOS, IAR Systems, Free RTOS, MoteRunner™ and TinyOS. The 51pin expansion connector supports Analog Inputs, Digital I/O, I2C, SPI and UART interfaces enabling ease of connection to a variety of external peripherals.

10. The BTnode [133] is a wireless communication and computing platform based on a Bluetooth radio, a second low-power radio and a microcontroller. It serves as a demonstration and prototyping

platform for research in mobile and ad-hoc connected networks (MANETs) and distributed sensor networks (WSNs). The low-power radio is the same as used on the Berkeley Mica2 Motes, making the BTnode rev3 a twin, both of the Mote and the old BTnode. Both radios can be operated simultaneously or be independently powered off completely when not in use, considerably reducing the idle power consumption of the device.

11. ANT™ [134] is a proprietary WSN 2.4GHz protocol and embedded system solution by ANT Wireless (a division of Dynastream Innovations Inc.) for ultra-low power networking applications: Wrist-mounted instrumentation, Heart Rate Monitoring (HRM), Speed and Distance Monitoring (SDM), Bike computers, Medical instrumentation, Industrial sensors, Low data-rate communications, Active RFID, Location-based services, Utilities wireless Automated Meter Reading (AMR), Smart toys, Automotive instruments. ANT™ has been designed to simplify network development and optimize network operational efficiency and is suited for any kind of low data rate sensor network topologies - from peer- to-peer or star, to practical mesh. ANT-powered network. The ANT WSN protocol has been intentionally engineered for simplicity and efficiency which results in an ultra-low power consumption (nodes can operate for years on coin cells). Additionally it offers the possibility to trade-off data rate against power consumption, and support for broadcast, burst and acknowledged transactions up to a net data rate of 20

Kbit/s. The protocol also features bi-directional communications and adaptive isochronous channels.

12. MeshScape from Millennial Net utilizes standard IEEE 802.15.4 unlicensed radio band or other types of radios including 433MHz, 900MHz and 2.4 GHz ISM bands with data rates up to 250 kbps and up to 750 feet range.

Name	OS support	Wireless standard	Data rate (kbps)	Outdoor range (m)
BTNode	TinyOS	Bluetooth v1.2	720	–
iMote	TinyOS	Bluetooth	720	30
iMote2	TinyOS or .NET	IEEE 802.15.4	250	30
IRIS	TinyOS	IEEE 802.15.4	250	300
MICAz	TinyOS	IEEE 802.15.4	250	75–100
Mica2	TinyOS	IEEE 802.15.4	38,4	>100
Mulle	TCP/IP or TinyOS	Bluetooth or IEEE 802.15.4	–	>10
Telos	TinyOS	IEEE 802.15.4	250	75–100
ZigBit	ZDK	IEEE 802.15.4	250	3.7
LOTUS	RTOS, Kiel, RTOS, IAR Systems, Free RTOS, MoteRunner™ and TinyOS	IEEE 802.15.4	250	100
Shimmer	TinyOS	Bluetooth, IEEE 802.15.4	–	>10
ANT	proprietary	proprietary	20	
MeshScape	proprietary	IEEE 802.15.4 and others in the ISM band	250	220

Table 2. Summary of existing sensor motes (obtained from [135]).

Additionally a software framework called SPINE (open-source Signal Processing in Node Environment) has been developed to be used with the motes. It enables efficient implementations of signal processing algorithms for analysis and classification of sensor data through libraries of processing and utility functions and protocols. SPINE currently includes: a library of features computing parameters of the sensor data such as variance, mean or range of the sensor data an over-the-air protocol that allows the coordinator of a WSN to dynamically request the computation of specific features to the sensor nodes and obtain the result a set of utility functions such as a circular buffer and a sorting algorithm The node side of the framework is developed in TinyOS environment, while the server side is in Java language.

Sensor motes based on UWB 802.15.4a are currently under development but commercial products are not yet available. Development examples are:

1. IMEC that made the first UWB transmitter that is compliant to the new standard [136], [137] which they plan to use in wireless autonomous transducer systems used in healthcare, lifestyle and process automation applications.

2. DecaWave with its 802.15.4a compliant UWB sensor chip called ScenSor [138], a single chip Wireless Transceiver using Ultra Wideband radio technology, compliant with the IEEE802.15.4a standard and implemented using CMOS wafer technology.

Chapter 3

Glucose monitoring

3.1 Introduction

With more than 284 million affected people worldwide in 2010 [140], diabetes mellitus is one of the most widespread diseases and causes 3.8 million deaths per year, similar to HIV/AIDS. Type 1 diabetes is characterized by the autoimmune destruction of the beta cells of the pancreas. Beta cells produce insulin, which is essential for the uptake of glucose in the muscles and storage in the liver. In practice, the common treatment for type 1 diabetes consists of one slow acting insulin analogue injection per day to ensure a basal insulin concentration and several single shots (one for each meal) of a fast acting insulin analogue. To get a feedback of the glucose control, several daily finger stick blood glucose concentration measurements should be made as well, and following insulin injections are adjusted according to these measurements.

Since the 1980s, insulin delivery can also be achieved by continuous subcutaneous insulin infusion from a portable pump. Most recently, research is focused in linking insulin infusion to continuous glucose monitoring systems to

get the so-called ”artificial pancreas”. Although great effort has been given to this topic in the last years, there is still no wearable commercial system allowing closed-loop glucose controlled insulin delivery. One of the limiting factors is the fact that up to now, only few continuous measurement devices are approved by the FDA (U.S. Food and Drug Administration), and none of them is approved as a substitute of standard glucose testing via strip measurements. The lack of accuracy of the continuous glucose measurement devices, especially in the hypoglycemic range, is being the most limiting factor in the clinical use of closed-loop glucose control.

The ability to detect therapeutically incorrect measurements of a continuous glucose monitor, from the information supplied by the monitor itself, is of utmost importance in clinical applications, since it allows an adequate interpretation of continuous glucose profiles in clinical practice, the detection of missed hypoglycemic states by the continuous glucose monitor, and other important discrepancies among monitor’s readings and actual glycaemia [30].

In [31], the detection of therapeutically incorrect measurements of Minimed CGMS Gold (Medtronic, Northridge CA) was addressed by means of Support Vector Machines (SVM), a powerful technique for pattern classification used in many applications [32]. The readings provided by the monitor were classified according to Clarke’s Error Grid Analysis (EGA). In this work, the methodology is extended to Consensus EGA and CG-EGA, to classify measurements in ”therapeutically dangerous” versus ”therapeutically safe” measurements, and results are compared. While Clarke and Consensus EGA only take into

account the glucose level error, CG-EGA considers additionally the glucose trend and it is specifically designed for continuous glucose monitors. Furthermore, validation through a permutation technique is introduced, besides cross validation.

3.2 Experimental Setup

3.2.1 Clinical study

For the clinical study 22 patients with Type 1 Diabetes were selected. Their mean age is 27 years with a standard deviation of 5 years and they have a mean body-mass index (BMI) of 24.4 with a standard deviation of 2.9. 40% of the patients are female and thus, 60% are male. All of them have had a long term diabetes evolution and have not achieved optimum metabolic control presenting an HbA1c value larger than 6.5%. In order to obtain the experiment's data set, the patients have been monitored during 3 days using Medtronic's Minimed CGMS Gold monitor. During the first monitoring day, the patients stayed at the hospital for 12 hours and for the following 2 days they remained at home. On the third day monitor's data were downloaded to a computer. During the stay at the hospital, blood samples were extracted:

- every 15 minutes during 2 hours after meals
- every 30 minutes otherwise

From those blood samples, plasma glucose level was measured in duplicate using the glucose oxidase method with a Glucose Analyzer II (Beckman Instruments, Brea, CA), which has a variation coefficient below 2%. During the

whole clinical study, the patients maintained their habitual insulin dosage, including amounts and administration sites, and their usual food ingestion. Although meals preparation was supervised by nutrition experts in order to gain exact information about their exact composition and nutrients content. Additionally, in order to assure proper usage of the glucose monitor, especially during the home period, the selected patients were trained and instructed in its use and their knowledge regarding the functionalities and usage of the monitor was asserted by clinicians.

Patient number 5 met exclusion criteria defined in the protocol (anemic state was detected) and was withdrawn. Patient number 6 was also disregarded due to the fact that the introduction of an erroneous calibration point was detected. As a consequence the valuable data of the clinical study originates from 20 patients.

3.2.2 Data conditioning

For each of the 20 patients that successfully finished the experiment, 40 plasma glucose readings were obtained. 6 measurements were dismissed due to measurement problems, resulting in a total of 794 samples:

- 97 samples in the hypoglycemic range (<=70 mg/dL)
- 352 in hyperglycemic range (>180 mg/dL)
- 345 in euglycemic range

As for the interpolation and synchronization a cubic method was used, obtaining all in all 2281 valid data pairs, e. g. (CGMS, plasma glucose) pairs.

As an example, the data conditioning procedure's results corresponding to patient nr. 12 are shown in Figure 13

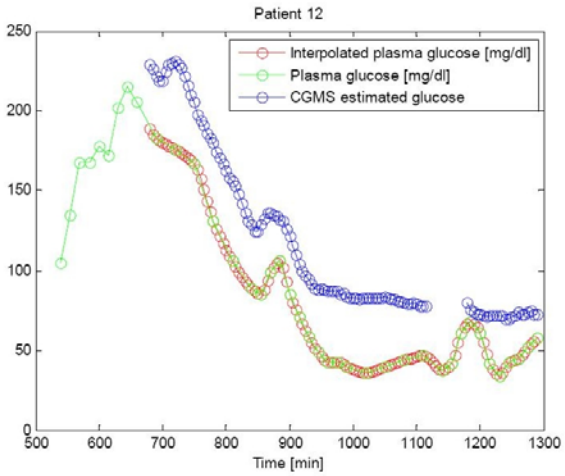

Figure 13. Synchronization of CGMS and plasma glucose value pairs by cubic interpolation for patient nr. 12. Blue circles correspond to CGMS measurements every 5 minutes; green circles to plasma measurements every 15 minutes during 2 hours after a meal and every 30 minutes otherwise; red circles correspond to interpolated plasma glucose values synchronized with CGMS measurements. A gap in the data supplied by the monitor happened between minutes 1120 and 1175.

3.3 Error Grid Analysis. Detection of potentially dangerous CGMS measurements.

As mentioned above, the objective in this work is to find an automated mechanism to detect therapeutically dangerous CGMS measurements. The ground truth for training and testing the detector being the set of (CGMS, plasma glucose) data pairs. Errors in the CGMS measurements with respect to the plasma glucose have different significance in terms of therapeutic criteria depending the position of the (CGMS, plasma glucose) space [141]. Ideal measurements would be in the diagonal. Based on that and in order to measure accuracy, several grid-based methods have appeared that go farther

than classical methods as correlation or regression. The definition of a grid of regions in the (CGMS, plasma glucose) space is called Error Grid Analysis (EGA) and several grid definitions have been previously used: Clarke's EGA, Consensus EGA and CGEGA (including measurement and process time lags).

3.3.1 Clarke's Error Grid Analysis

The Clarke EGA [142] was developed to quantify clinical accuracy of patient estimates of their current blood glucose as compared to the blood glucose value obtained in their meter. Eventually, the EGA became accepted as one of the gold standards for determining the accuracy of blood glucose meters.

The grid breaks down the space defined by reference glucose meter (x-axis) and an evaluated glucose meter (y-axis) into five regions. Region A are those values within 20% of the reference sensor, Region B contains points that are outside of 20% but would not lead to inappropriate treatment, Region C are those points leading to unnecessary treatment, Region D are those points indicating a potentially dangerous failure to detect hypoglycemia or hyperglycemias, and Region E are those points that would confuse treatment of hypoglycemia for hyperglycemias and vice-versa.

3.3.2 Consensus Error Grid Analysis

The Consensus EGA (also known as the Clarke's EGA [143]) was developed as a new tool for evaluating the accuracy of a blood glucose meter and in recent times, it has been used increasingly by blood glucose meter

manufacturers in their clinical studies. The new EGA was constructed to reflect the opinion of a large number of clinical diabetes experts.

In Figure 14 the complete data is classified following Clarke EGA (top) and Consensus EGA (bottom). As it can be observed, in both cases the number of data points located in therapeutically dangerous regions C+D+E is small (less than 10%).

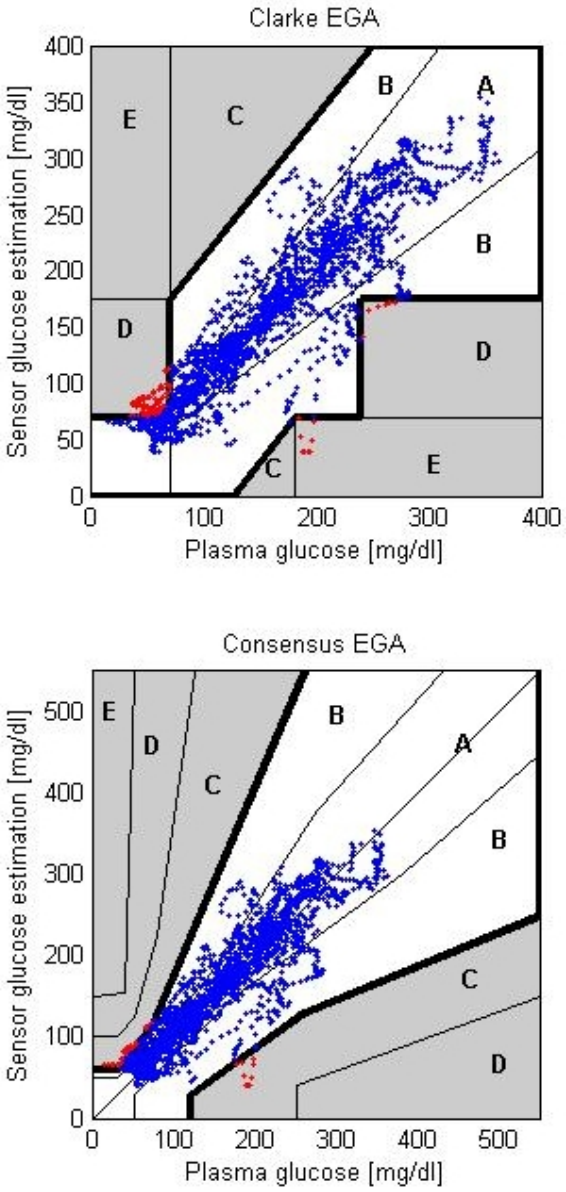

Figure 14. Classification of complete data set following Clarke EGA (top) and Consensus EGA (bottom). Data points located in therapeutically dangerous regions C+D+E are marked in red.

3.3.3 Continuous Glucose Error Grid Analysis

The Continuous-Glucose-EGA (CG-EGA) [33] was developed as a method of evaluating the accuracy of continuous glucose-monitoring sensors in terms

of both accurate blood glucose values and accurate detection rate of BG fluctuations. Unlike the original EGA, the CG-EGA examines temporal characteristics of the data, analyzing pairs of reference and sensor readings as a process in time represented by a bidimensional time series and taking into account inherent physiological time lags. The estimates of point and rate precision are then combined in a single accuracy assessment presented for each one of the preset BG ranges.

3.4 Support Vector Machines

The Support Vector Machine (SVM) algorithm is well grounded in statistical learning theory, offering excellent performance qualities especially for complex real-world problems [144], [145], [146]. SVMs are capable of nonlinear classification with nonlinear boundaries between the classes because they are an extension of linear models. By transforming the input, instance space, into a new space using a nonlinear mapping, SVMs use linear models to represent nonlinear class boundaries. The use of kernels implements this transformation, allowing the classification of complex patterns in an abstract linear representation. Following the nonlinear transformation, the decision boundary that separates the instances by classes is learned. This decision boundary is a Maximum Margin Hyperplane (MMH) in the transformed coordinates. Support Vectors are the instances closest to the MMH and thus, a set of support vectors defines the decision boundary for a given set of instances. Only the Support Vectors represent the decision boundary, thus simplifying its representation because all other training instances are disregarded [147].

3.4.1 SVM training

SVM training involves minimizing a combination of training error (empirical risk) and the probability of incorrectly classifying unknown data (structural risk), controlled by a single parameter, corresponding to the σ-value in case of the Gaussian kernel function. The tuning of the kernel function and the resultant feature space is crucially interesting in theoretical and practical terms because it determines the functional form of the support vectors, i. e. the resulting decision boundary [146]. In this contribution the features vector representing the electrical characteristics of the measured signal and the Minimed CGMS Gold estimation algorithm is considered and normalized by its Euclidean norm:

$$X = \left(ISIG, \frac{dISIG}{dt}, VCTR, G_{CGMS} \right) \tag{3-1}$$

Where *ISIG* stands for the sensor current*, dISIG/dt* its derivative with respect to time, VCTR represents the registered voltage and G_{CGMS} denotes the glucose estimation given as output by Minimed CGMS. Finally, to avoid over-parameterization, the projection on the *(ISIG; VCTR)* dimensions is used as input data set. Projections on other 2- feature combinations were also tested with poorer results.

Also 3-features vector *(ISIG; VCTR; dISIG/dt)* showed no relevant improvements with respect to *(ISIG; VCTR).*

The data set is first classified regarding three different criteria (Classification Scheme 1):

- Clarke's EGA with interpolated plasma glucose values is used as gold standard. A "negative" result means that the data point falls in zone A or B (safe areas) while a "positive" result implies that it falls in zones C, D or E, where the error in the monitor measure leads to a wrong treatment of the patient. Data classification is shown in Figure 14 (top). From the whole data set 6% are positives. Figure 15 shows the classification of the whole data set in the *VCTR-ISIG* space. As it can be observed, both positive and negative data points are not linearly separable. However, some grouping is observed. Thus, SVM is an ideal candidate to solve the complex problem of separating the classes through a nonlinear transformation into a higher order dimension where then, finally, the classes shall be separable.

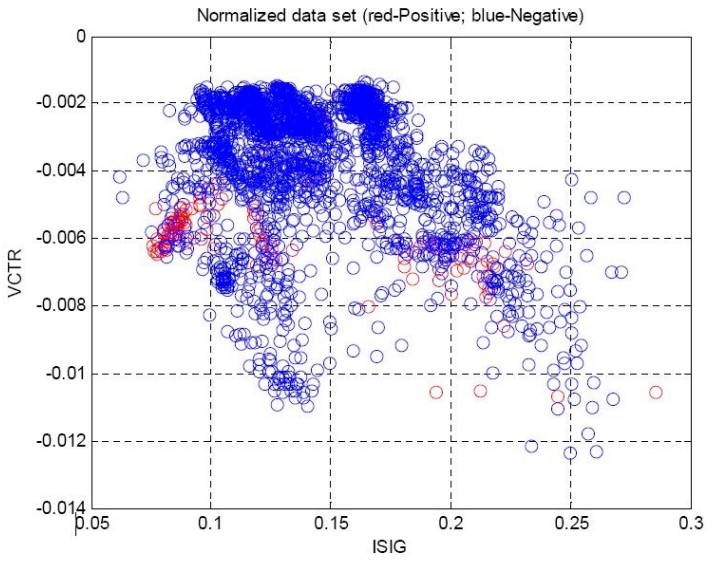

Figure 15. Projected normalized data set. Positive class (red) corresponds to C+D+E zones and Negative (blue) to A+B zones in the Clarke's grid.

- In this case, Consensus EGA with interpolated plasma glucose values is regarded as the gold standard. Similarly to the former case 1, ”negative” means data point falling in zone A or B while ”positive” implies zones C, D or E. In Figure 14 (bottom) the classification result is shown. Also in this case, the number of positive data points is small, i.e. 3%.

- Following the definition of the CG-EGA, erroneous readings are taken as ”positive” and both accurate readings and benign errors as ”negative” class. Again, using this classification scheme the number of positive data is small (5%).

Due to the fact with the prior classification schemes in all three cases positives are scarce, all experiments were driven in parallel considering the following classification scheme (Classification Scheme 2):

- Clarke’s EGA: A is negative vs. B+C+D+E positive

- Consensus EGA: A is negative vs. B+C+D+E positive

- Continuous Glucose-EGA: Errors and benign errors are positive vs. accurate negative

In Table 3 the overall percentages of positives and negatives corresponding to classification schemes 1 and 2 are presented. Classification results showed that although the input data sets differ substantially, the SVM is able to achieve similar performance. Due to this fact and for sake of simplicity, only experimental results from classification scheme 1 will be exposed here.

Classification scheme	1		2	
	positive	negative	positive	negative
Clarke EGA	6%	94%	21.39%	78.61%
Consensus EGA	3%	97%	19.25%	80.75%
CG- EGA	5%	95%	20.32%	79.68%

Table 3. Data distribution for classification schemes 1 and 2

3.4.2 Assessment of classifier performance

SVM classifier is trained using the above mentioned data set, classifier parameters are optimized and validation is performed. Kernel parameters in the SVM training process, along with feature selection, will significantly impact classification accuracy. Experiments are designed and carried out to find the best SVM kernel parameters to enhance prediction capabilities. Validation is performed using two complimentary methods:

1. k-fold Cross-validation:

Cross-validation is a technique for assessing how the results of a statistical analysis will generalize to an independent data set. It is mainly used in settings where the goal is prediction as it is a means to predict the model fit to a hypothetical validation set. One round of cross-validation involves partitioning a sample of data into complementary subsets, performing the analysis on the training set and validating the analysis on the other subset, i.e., the test set. To reduce variability in the overall assessment of generalizability, multiple rounds of cross-validation are performed using different partitions, and the validation results are averaged over the rounds.

2. Permutation:

Especially in cases where the model significance is questionable, as could be argued in the present case, a permutation test [148] adds crucial information which can be decisive for the existence of the model. The method is based on a repetitive and random reordering of the entries and the response variable. The elements in the original response variable are reordered randomly creating scrambled response variable vectors. These new response variables should have no or very limited association with the predictor variables. Then, the scrambled response vectors are modeled using the intact predictor data and results are evaluated.

3.5 Experimental Results

In the present work, for all the combinations of the three error grid analysis presented in section 3.3 and the two different classification categories defined in section 3.4, the σ-value of the Gaussian SVM is adjusted iteratively using Bioinformatics Toolbox in Matlab^{TM} release 2006b. After the training process, testing of the trained SVM consists of counting the number of detection errors in the positive/negative prediction provided by the trained SVM. For performance assessment, those results are evaluated using Receiver Operation Characteristics (ROC) which plots the true positives rate (TPR) in front of the false positives rate (FPR), i.e., sensitivity in front of 1-specificity.

Results for classification scheme 1 are presented in Figure 16. As it can be observed, detection quality saturates to its best value around specificity of 0.9

and sensitivity of 0.8 corresponding to 92% detection rate for Clarke and Consensus EGA. While in the case of using CG-EGA the saturation point presents a slightly poorer detection quality (detection rate of 91%). It is inferred that this decrease in overall detection quality is due to the more complicated structure of the data when using the dynamic grid. Probably, increasing number of training data points (and spreading their statistical distribution) would result in detection results similar to those of the Clarke and Consensus EGAs.

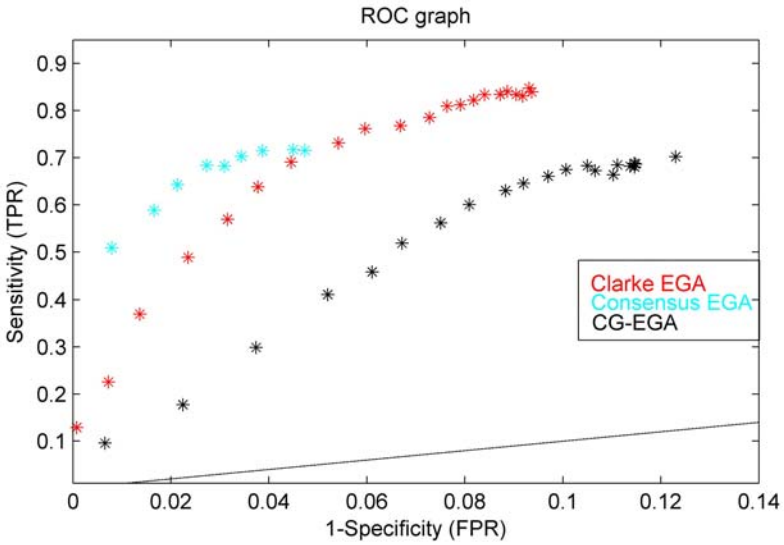

Figure 16. Receiver Operating Characteristics for classification categories Clarke and Consensus EGA: A+B = FALSE and C+D+E = TRUE, CGEGA: white + gray = FALSE and black = TRUE, σ-value: 0.001 - 0.4.

Experiments have also been repeated with gradually increased σ-values (from 0.001 to 0.4. As σ-value increases, also computation time for training increases considerably such for σ=0.3 is double as for σ=0.1. Classification results have shown that, indeed, with increasing σ-value also detection quality

increases, with a heavy nonlinear relationship as it can be observed from Fig.4. Through iteratively adjusting σ- value, a compromise between detection rate and computation time has been obtained for the three EGAs with both classification schemes.

Table 4 shows the average classification results for all three classification schemes and the corresponding optimal σ-value.

EGA	Scheme	σ	Sensitivity	Specificity	Correct rate
Clarke	1	0.335	83%	95%	91%
	2	0.301	82%	93%	90%
Consensus	1	0.362	71%	92%	90%
	2	0.334	70%	93%	89%
CG	1	0.347	70%	88%	89%
	2	0.315	71%	87%	87%

Table 4. Average classification results

1. Validation

As it is indicated in the previous sections, validation is performed using 10 x 10-fold cross validation and results are presented via ROC-graphs. In this work, we present an additional validation technique based on data permutation. Resulting data from 25 permutations per classification issue with additional 10 x 10-fold cross validation are presented in Figure 17 It can be observed that detection quality (both sensitivity and specificity) drops dramatically when permuting input data. As a consequence, it can be claimed that in fact with

presented techniques, the learning machines are able to learn from the presented data and thus, that there is some structure contained in the data.

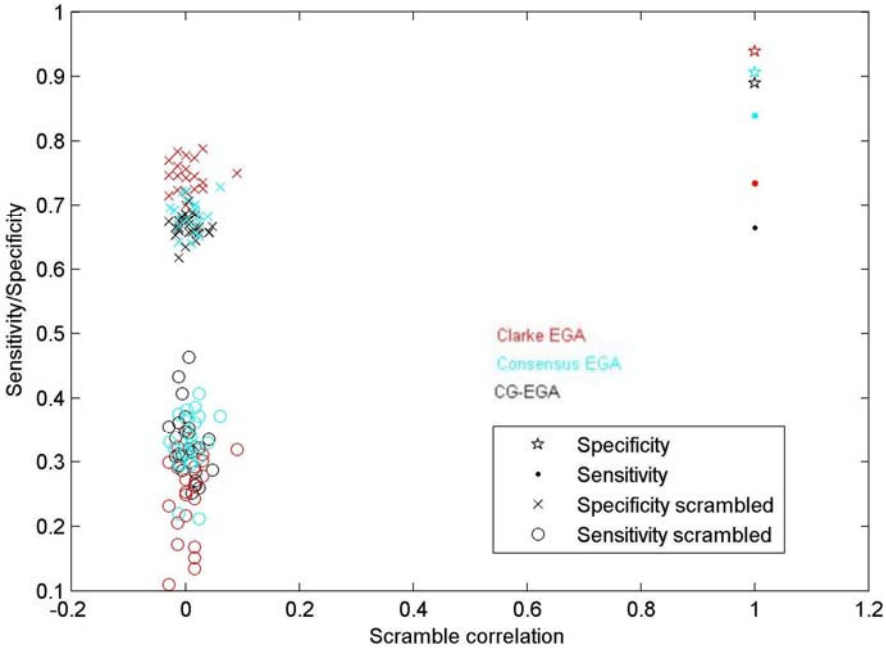

Figure 17. Sensitivity and specificity for Clarke, Consensus and CG EGA with optimal σ in all cases. Classification categories are A+B vs. C+D+E and white + gray vs. black. Input data are permuted 25 times. Results are compared to classification with no scrambling in the data. Similar results are obtained when using classification scheme 2.

2. Individual patient analysis

To see to what extent the error detection influences global clinical performance, an analysis in terms of patient's glucose profiles and not as individual samples is necessary. It may be considered that a good performance is obtained if the system is able to detect the time intervals where the profile shouldn't be trusted because of incorrect measurements inducing, e.g., hypoglycemic episodes to be missed.

In this section we analyze the overall classification results on the temporal sequence of recorded data patient by patient. We compare Clarke EGA, Consensus EGA and CG-EGA in some patient cases.

Figure 18 shows the results for two patients (i.e. patient nr. 11 and nr. 12) with classification scheme 1 and all three considered EGAs where hypoglycemic episodes appeared. True and false positives are presented and the benefits of the proposed work can be clearly inferred. For patient nr. 11 it can be observed that there are two hypoglycemic episodes (around minute 1000 and 1175) that are not measured by the monitor. These two episodes are correctly detected by Clarke and CG-EGA classifiers (Figure 18 top and bottom, blue circles). In contrast, when using Consensus EGA the first hypoglycemic episode is missed. On the other hand, Clarke and CG EGA classifiers show some false positives (around minute 1260) while Consensus EGA classifier does not present false positives for patient nr. 11.

It may be observed in Figure 6 that for patient nr. 12, hypoglycemia remains unnoticed by the monitor from minute 925 (approximately) onwards. This fact is correctly detected by the Clarke, Consensus and CG classifiers (denoted by the blue circles). Some false negatives appear (red circles) for Clarke and CG-EGA. For Consensus EGA the number of false positives increases considerably. However, this does not interfere in the general conclusions drawn out from the graph.

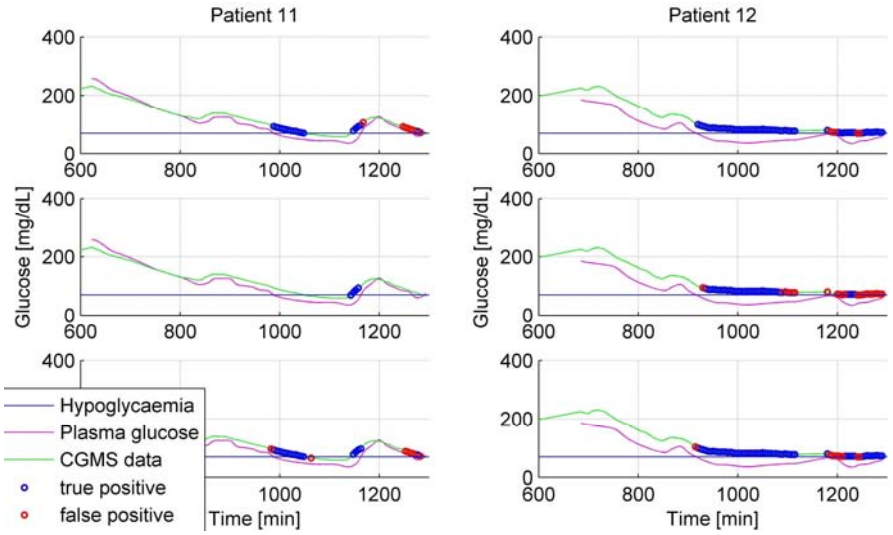

Figure 18. Classification results for patients nr. 11 and nr. 12. The figure features Clarke EGA classifier (top), Consensus EGA classifier (middle) and CG-EGA classifier (bottom). The magenta line represents the gold standard and the green line the CGMS measurements. Inside the latter, blue and red circles indicate true and false positives respectively.

The former analysis is performed for the rest of patients where hypoglycemia episodes remained undetected by CGMS. In cases Clarke and CG-EGA the classifiers are able to detect these episodes from the electrical signal and CGMS glucose estimations. Some hypoglycemic episodes where missed when using Consensus EGA classifier. Although a significant number of misclassifications appeared in some cases, this does not have a significant impact on the analysis of the profiles except some overestimation of the duration of the episodes.

3.6 Conclusions And Future Works

In this work, the detection of therapeutically wrong measurements of Medtronic's Minimed CGMS is addressed by means of Support Vector Machines. Patients were monitored using CGMS and simultaneously blood

samples were taken in a clinical study. Plasma glucose measurements were interpolated for time synchronization with CGMS data, obtaining a total of 2281 samples.

Gaussian SVM classifiers making use of monitor's electrical signal and glucose estimation were tuned. Clarke EGA, Consensus EGA and CG-EGA were used to define the classes. Moreover, two different classification schemes for all of the three EGAs were used. All in all 6 different classification problems have been studied, adapting the σ-value of the Gaussian kernel function systematically. With optimal σ-values validation is performed: 10-fold cross-validation for 10 times permutation. The classification results are similar for all 6 classification problems: average Specificity and Sensitivity result in 92.74% and 75.49%, respectively. The average Correct Rate is 91.67%. Additionally, the permutation technique shows that both Sensitivity and Specificity drop dramatically when scrambling the input data, thus we can conclude that the classifiers indeed have been able to learn the data structure. The best classification results are obtained for the Clarke's Error Grid Analysis with a 90% of correct rate.

An overall good performance is obtained in spite of the somewhat low sensitivity. The classifiers are able to detect the time intervals where the monitor's glucose profile shouldn't be trusted because of wrong measurements. This is illustrated with the detection of hypoglycemic episodes missed by the CGMS.

From this analysis it is concluded that detection of therapeutically wrong measurements given by the continuous glucose monitor Minimed CGMS is feasible through the use of SVM classifiers. For all patients, missed hypoglycemic states were detected, as well as other therapeutically wrong measurements. The presence of False Positives did not alter the conclusions drawn out from the analysis of time profiles. This tool can thus support the clinician in the interpretation of continuous glucose monitor readings.

Chapter 4

Wireless neural signal monitoring

4.1 Problem definition

Studies conducted during the last decade have demonstrated the improvements that neural signal decoding will bring to health care, especially for patients suffering from paralysis [23], blindness [17] or deafness [149]. Recent work indicates that there is a vast universe of possible applications [150], especially considering brain-machine interfaces (BMIs), devoted to create interfaces between the human brain and artificial devices [18], [151], [152], [153]. Scientists from a wide range of disciplines are working on technologies that allow patients to use brain activity signals to control mechanical or electronic devices that allow the patients to restore lost sensory-motor functions [149], [151]-[154], [17], [23]. There are still fundamental questions to be solved in the neurobiology field, however first results of brain-actuated technologies, such as neuro-prostheses or neuro-robots, lead to optimistic expectations.

These promising clinical applications of implantable neuronal sensing devices have shown the utmost **necessity of wireless communication systems that allow real-time monitoring of neural signals**. In fact, the implementation of a wireless transmission method for such systems brings considerable advance especially for in-vivo recordings as the subject wearing the measurement device would then be freely moving around and neural recordings from normal life-style activities would be possible. Wireless implanted neural electrodes that have been characterized and tested in-vivo are reported in [157], [21], [158].

When it comes to the communication systems involved in these BMIs there is still much work to be done. The neural signal, the fundamental information source, hides significant conceptual complexity and thus, its recordings shall be made available to as many researchers as possible [159]. That is why world-wide transmission systems are so important particularly in this area. On the other hand, a fundamental requirement for any communication system aimed towards the development of clinical applications of BMIs, is to be wireless in order to allow patients to wander around during neural recording and monitoring. Moreover, aspects like low power consumption (especially considering implantable devices, not only because of the body proximity but also to extent battery life) and small interference with already existing systems shall be not neglected.

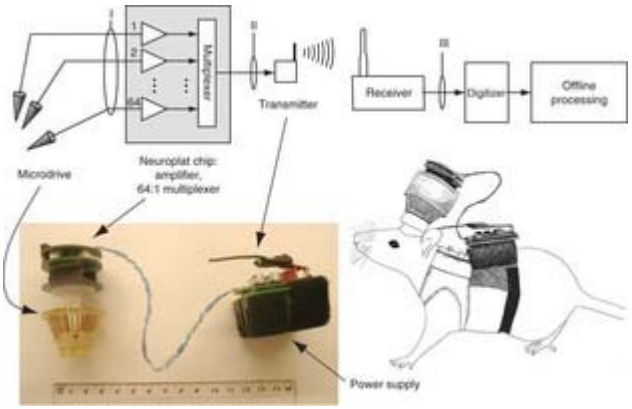

Figure 19. Wireless multi-channel system for recording neural signals from rats developed in [158].

The design of a wireless transmission system for this particular application shall meet several requirements involving source compression of the high data rate neural recording, communication with a standard device as bridge between body area and remote server, and high fidelity of the received signal to ensure effective brain activity monitoring. Neural signals recorded either from in-vitro cultures or from in-vivo subjects, present a high data rate information source. Due to the limited bandwidth of wireless transmission system, compression becomes mandatory. As we will see in the next sections, compression through spike detection becomes extremely attractive when aiming at real-time applications and individual neuron spike pattern analysis.

Neural signal information is mainly carried in the neuron's spiking patterns. That is why, in scientific and clinical applications, it becomes important to identify neural action potentials or spikes from the voltage waveform of each sensing electrode. Figure 20 shows an example of a neural signal recorded

using a microelectrode in the top subplot and the separated firing pattern on the bottom subplot.

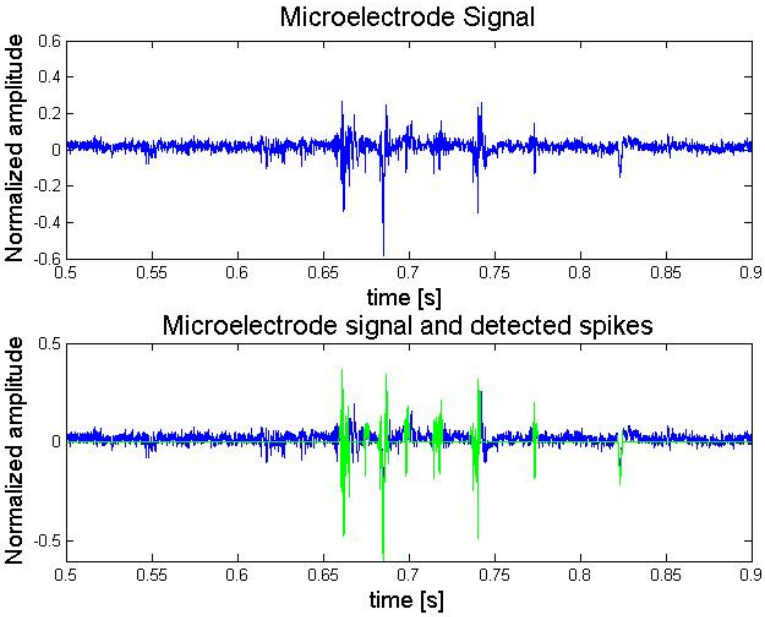

Figure 20. Recorded microelectrode signal (top) and detected spiking pattern (bottom).

Action potential waveforms recorded with extracellular cortical electrodes present amplitudes ranging from tens to hundreds of microvolts peak to peak; pulse widths are typically 1 - 1.5 ms. The noise floor, which includes biological noise from far field neurons and electrical noise from the amplifier circuit, is around 20μVrms; Signal to Noise Ratios (SNRs) usually range from 0 to 12dB, although ratios as high as 20dB are occasionally encountered. Published figures for the signal frequency content vary, ranging from 100 to 400Hz for the low end range and 3 kHz to 10 kHz for the high end range [19]. Published sampling rates also vary, ranging from 15 kHz up to 50 kHz [20]. In general, higher sampling rates produce higher fidelity signals but also produce more

data, requiring faster and higher-power systems to process them, which may become a handicap in a wireless system with limited bandwidth. Analog to digital converter (ADC) resolution should be 10 - 12 bits to provide 60 - 72 dB of dynamic range.

In general, the required transmission bandwidth (BW) can be obtained as $BW = f_s \cdot n_{bits} \cdot N_{ch}$, where f_s is the sampling frequency in samples per second, n_{bits} the number of bits per sample and N_{ch} the number of channels to be transmitted. According to that, transmission of one single channel with a medium sampling rate the required bandwidth is of 180 kbps. When it comes to simultaneous transmission of several channels (up-to-date in-vivo and in-vitro micro-electrode array recording systems provide up to 128 simultaneous channels [160]), including source compressing algorithms in the communication system becomes a must, especially when wireless transmission with limited bandwidth availability is aimed at. Neural signal compression should allow recovering of the neuron's spiking patterns and that is why compression techniques involve detection and separation of individual firing patterns from the underlying neuronal noise. The spiking activity among the recorded channels might differ substantially, and therefore, as widely discussed in literature [161]; spike detection yields the most suitable compression algorithm.

Given the importance of spike detection, it is interesting to be able to quantitatively assess the quality of any implemented detector [20], [179].

However quality assessment requires knowledge of the ground truth, i.e., decisions taken by the algorithm on the presence of spikes must be compared with the real presence of spikes in the signal. Recordings from micro-electrode arrays do not allow intra-cellular recording which means that the ground truth is not known. For the present work, in order to overcome this problem, we select two different types of source signals:

1. First, a set of in-vitro neural activity recordings kindly provided by Multichannel Systems was used. Recordings were obtained using a 64-electrode array (60 recording electrodes and 4 electrodes for stimulation) and signals where sampled at 25 KHz. Figure 21 shows the Multi Channel Systems Multi-Electrode Array (MEA). One channel of the recording was selected and spikes were manually detected by several experts. Manual detections were used as the ground truth for detection algorithms evaluation.

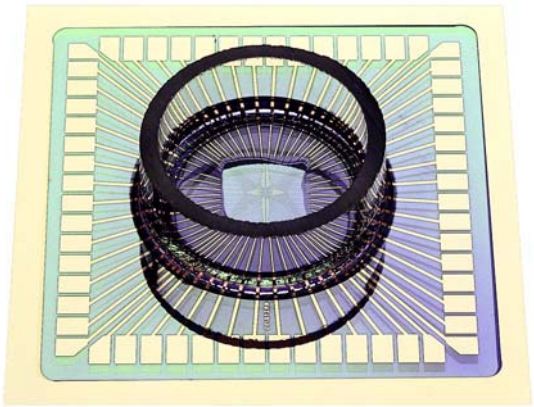

Figure 21. 64-channel Multi-Electrode Array (MEA) from Multi Channel Systems (www.multichannelsystems.com) widely used in neuronal signal recordings.

2. Second, we use a set of synthetic signals from a statistical model resembling real signals, where the spike positions are known and can be used for evaluation of spike detection algorithms.

The set of artificial signals contains 10 different signals resulting from adding an artificially generated neuronal noise with a principal neuron spike train. We started with in-vivo recordings from rat cerebellum's striatum cells, publicly available at [177]. From these recordings we isolated 50 action potentials and an additional one was selected and repeated periodically with a frequency of 50 Hz to construct the principal neuron spike train of 10 s duration. To generate a realistic underlying noise, we assumed that each neuron fires according to a homogeneous Poisson process. The Poisson model is valid if one assumes that each neuronal spike constitutes an independent random variable, which is not totally true but it yields to an approximation that suffices for the generation of additive noise, where the importance is not on the exact spiking times but on the fact that the resulting noise resembles the real neuronal noise present in micro-electrode recordings. The number of noise neurons taken for noise generation is an approximation based on the assumptions that: only neurons within 140μm of the electrode are detectable and that the density of the motor cortex is 30.000 neurons/mm as stated in [17]. A scheme of the procedure is shown in Figure 22. First, the firing rate for each neuron is obtained randomly in the range [50, 90] Hz, then, a firing pattern for each neuron is obtained using the Poisson process model, and finally, the resulting noise is the sum of the individual firing patterns. The principal neuron spike train is added to the

adequately attenuated noise to obtain 10 different signals with SNRs in the range [1, 4.6] dB.

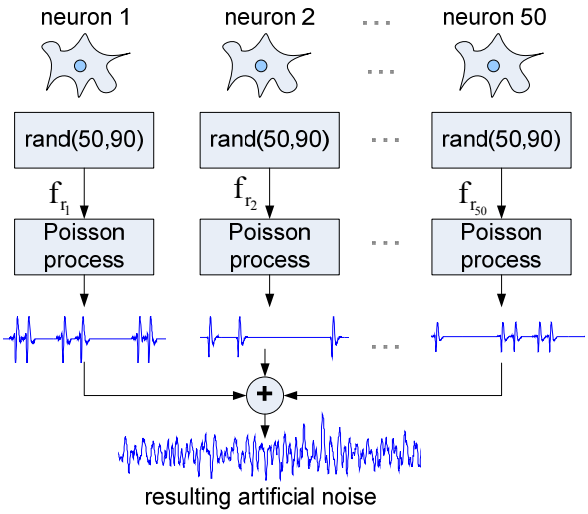

Figure 22. Artificial noise generation process.

4.2 Real time spike detection

As we have seen in previous paragraphs, spike processing techniques and, in particular, spike detection and classification are fundamental in analyzing and interpreting both in-vivo and in-vitro recordings of neural activit . Spike detection is, in fact, a fundamental technique for separating neurons' firing patterns from the captured microelectrodes' signals [155], [156].

Basic spike detection algorithms apply threshold-based detection to identify spikes and, although simple thresholding is attractive for real-time implementations because of its computational simplicity, it is thought to be sensitive to noise and requires user input to set effective threshold levels, as it is exposed in [4]. In neuronal recordings, Signal to Noise Ratios (SNR) vary

with electrode geometry, size and position with respect to the target neuron [5]. That is why it is necessary to individually set the threshold to the appropriate value and automatic and adaptive threshold setting becomes useful.

We have evaluated the adaptive threshold technique with 2 types of pre-processing. First, by applying the absolute value operator, Simple Threshold detector (STH) and second by a Nonlinear-Energy-Operator (NEO), which pre-processes input signal s[n] with the energy operator in (4-1), emphasizing signal energy concentrations.

$$\Psi\left(s[n]\right) = s^2[n] - s[n-1] \times s[n+1] \tag{4-1}$$

Where n is the sample number.

After pre-processing, spikes are detected comparing the pre-processed signal with an adaptive threshold. Real-time adaptation is done by obtaining a noise-envelope estimate via a frame-based noise-envelope tracking method and, then, setting the threshold ($th[k]$) to a certain level which is relative to the estimated noise envelope ($\hat{n}[k]$), where k is the frame number.

$$th[k] = A \cdot \hat{\mathrm{n}}[k] \tag{4-2}$$

The process for noise-envelope estimation is preformed in 50 ms-long frames. Frame processing reduces computational cost since estimation performed only once per frame. The steps for each processing frame are:

1. Calculate the maximum absolute value of the signal amplitude ($|s[k]|_{\max}$).

2. Compare it with the previous noise-envelope estimation: ($|\hat{n}[k-1]|$).

3. If the maximum is bigger than A times the previous noise envelope, assume that there is a spike present in the frame do not update noise estimation.

   Otherwise, update the noise estimate according to:

$$\begin{cases} |s[k]|_{\max} \geq |\hat{n}[k-1]|, & \hat{n}[k] = \alpha_{up} |s[k]|_{\max} + (1-\alpha_{up}) \cdot |\hat{n}[k-1]| \\ |s[k]|_{\max} < |\hat{n}[k-1]|, & \hat{n}[k] = \alpha_{dw} \times |s[k]|_{\max} + (1-\alpha_{dw}) \cdot |\hat{n}[k-1]| \end{cases} \quad (4\text{-}3)$$

Time constants α_{up} and α_{dw} have been experimentally adjusted to $\alpha_{up} = 0.02$ and $\alpha_{dw} = 0.5$.

4.3 Real time spike sorting

Typically, Micro-Electrode Arrays (MEAs) are situated such that for each one of them, there is a number of surrounding neural cells [164]. Therefore, each single electrode records signals originating from several neural cells, thus, obtaining multi-spike trains for each MEA electrode. The exact waveform captured for each neuron depends on the neural cell itself and the geometry of the extracellular space as described in [179]. Moreover, the waveform characteristics of the captured signal are constant over time for each neuron and that can be used to identify the corresponding neuron in a single electrode recording, that is, to classify the detected multi-spike train.

In Figure 23 (top) the detections and spiking frequency obtained for a typical multi-spike train are depicted. Considering that this multi-spike train includes

contributions of three different neural cells, detection and spiking frequency (depicted in Figure 23 (bottom)) are computed for each of the individual neurons, thus implying prior classification. From Figure 23 it becomes apparent that classification is a must when dealing with multi-spike trains. As we have seen, for each MEA electrode recording, the individual contributions of the surrounding neural cells can be distinguished using signal processing algorithms that take advantage of the similar wave form characteristics of the spikes originated by one neural cell. This implies that prior to classification a detection process shall be performed. That is the reason why compression through detection allows neural signal post-processing with similar quality parameters as those yielded for the original recorded signal. However, simultaneous firing of two or more neural cells surrounding one MEA electrode can cause overlapping of the associated wave forms deforming the resulting signal and thus, increasing the difficulty of the spike sorting task.

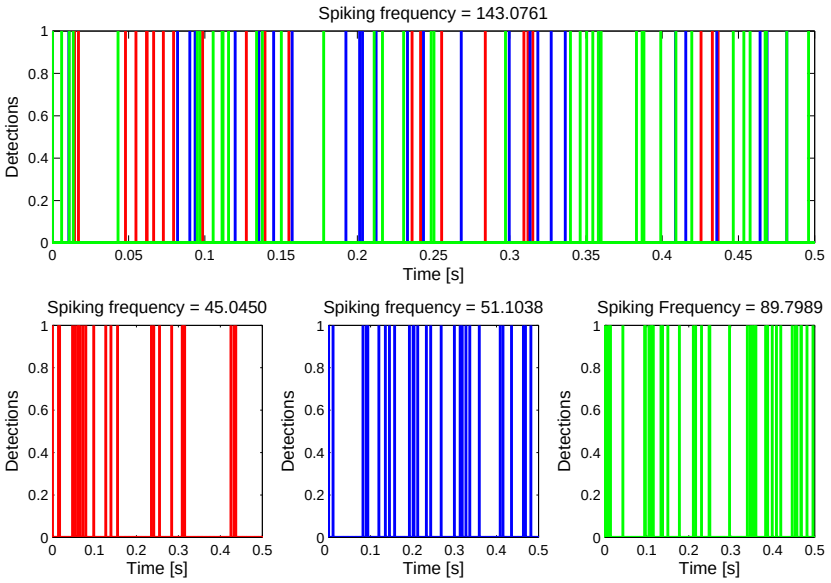

Figure 23. The need of spike sorting in multi-spike trains: Overall spiking pattern differs substantially from individual neural spiking patterns, also spiking frequency are not similar.

Any automatic classification process is based on two consecutive steps:

1. Extraction of the most relevant signal characteristics.
2. Based on the extracted characteristics, determination of the classes and the membership of each of the signals to the classes.

When it comes to the multi-spike train sorting problem, several algorithms for characteristic's extraction are suitable [164], [164]. Here, Principal Components Analysis (PCA) was selected for its demonstrated excellent performance [182]. PCA consists in, for each of the spike sets; a set of sorted vectors that forms an orthogonal base capable of representing the spikes' subspace is obtained. These base vectors indicate the directions of maximum data variation and each spike can be represented as a scaled sum of them.

Base vectors are sorted with respect to their relative contribution in representing the set of analyzed signals. Instead of using the whole set of base vectors to represent the spikes, the complexity can be decreased by selecting a subset constituted by the N base vectors with higher scores and represent the spikes by their projection on the selected base vectors. The N projections or N Principal Components are then used as characteristics in the sorting process.

Once the characteristics (N base vectors or Principal Components) have been extracted, the class membership algorithm k-means is applied to the multi-spike train. This algorithm basically consists in associating to each spike the class with the closest weight centre using the Euclidean distance. The weight centre of the associated class is recalculated after the inclusion of each sorted spike.

4.4 Neural signal compression

As discussed in the previous sections, neural signals recorded either from in-vitro cultures or from in-vivo subjects present a high data rate information source per unit electrode or channel. Moreover, up-to-date in-vivo and in-vitro microelectrode array recordings involve over a hundred of simultaneous channels ([153]). Therefore, when it comes to the simultaneous wireless transmission, inclusion of source compressing algorithms in the communication system becomes a must.

As we have also seen, neural signals contain trains of action potentials or spikes that form particular spiking patterns. For this thesis the interest is in the spiking patters extracted from the trains of action potentials or spikes. The relationship between action potential and local field potentials (LFP) is not well understood and still under investigation ([165], [172]). During the intervals of the signal without spikes, the content of the signal is considered to be exclusively noise for the spiking pattern computation. Therefore regarding spike pattern analysis, it is possible to compress neural signals by coding the impulse trains leaving the noise-only parts away. For doing this, it is necessary to: first detect the occurrence of the spikes, and then code the time, the channel (in the case of a multi-channel recording system) and the spike waveform. In this way, it is feasible to compress and multiplex an arbitrary number of channels into one single stream of data.

In the present thesis, I have considered the Multi Channel Systems MEA case described at the beginning of this chapter, where the recording system has 60 recording electrodes, with the sampling frequency being 25 kHz and the sampling precision 12 bits. The system is then producing a 12 × 25 × 60 = 18000 kbps raw data stream.

The compression algorithm applied works in a frame-based manner. It takes input data in frames containing 1250 samples, i.e., 50ms. For each frame-based step, the algorithm performs spike detection at each channel using the NEO algorithm described in section 4.2 and, when a spike is detected, the time, channel, and the waveform of the spike are coded and sent to the output.

In some cases, coding of all the channels using this scheme may not give sufficient compression and it may result in an excessive amount of data to be fit in the available bandwidth. In such situation, the alternative is to leave out spike waveforms and send timing and channel information only for each occurring spike. As a consequence, total reconstruction of the signal is not possible; nevertheless, considering that individual neurons repeat the spiking waveform over time, previously recorded waveforms can be used and placed in the time of the current spikes, thus obtaining a reconstructed signal. Moreover, timing patterns of the neural signals are of capital importance in neural signal decoding and those patterns can still be obtained when using the described compression scheme.

On the other hand, in multiunit recordings additional difficulties appear. Given that each electrode captures the activity of several neighboring neurons, transmitting only the spiking times and not the waveforms does not provide sufficient information at the receiver side to apply spike sorting techniques. Because of that, spike sorting needs to be performed before transmission, with the subsequent rise in processing complexity. In the end, the choice in the compression scheme becomes a trade-off between processing complexity and bandwidth requirements.

Figure 24 shows both coding structures. Each coded spike results in 78 or 3 output samples to be transmitted, for coding schemes a and b respectively: one sample for the channel number, two for the timestamp and 75 samples corresponding to the spike waveform when scheme a is used.

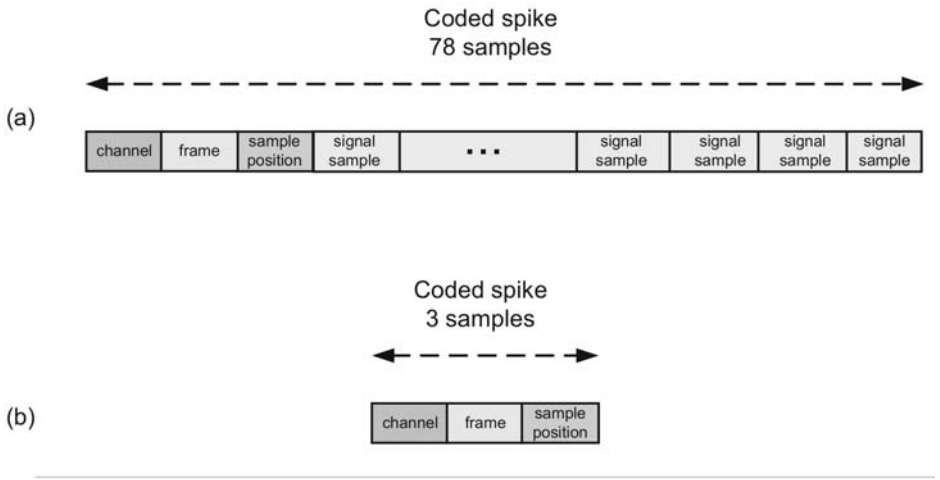

Figure 24. Spike coding schemes.

4.5 Resource Management - Adaptive compression

Signal and information management of high-density neural recording arrays poses many challenges including:

- Data volume: 60-electrode array sampled at 25 kHz with a resolution of 12 bits/sample yields 18Mbps bit rate.
- Variable signal quality: Variability across elements of the array due to temporal and spatial nonstationarity.
- External interferences.
- Reduced energy resources leading to reduced transmission power and therefore to reduced bandwidth.

In this scenario, a wireless point to point transmission system that accomplishes the requirements of this specific application, such as reduced

energy consumption and miniaturization, deals with several restrictions. We are particularly interested in the bandwidth management provided by the ad-hoc designed transmission system. It is clear that it shall be oversized in relation to the actual required bandwidth, which is by nature variable with time offering short-time high-value peaks [172]. However, in order to maintain implantable characteristics, the bandwidth restriction must be tuned to its lower limit coming to a trade-off between guaranteed available bandwidth and power consumption.

From these considerations we can conclude that bandwidth provided by an ad-hoc designed wireless transmission system is not constant over time. Therefore, it becomes mandatory to manage the available transmission bandwidth in order to allow the real time transmission of the most significant information from the neural recording system.

Although near-future technology, such as Ultra Wide Band (UWB), would considerably reduce the need of compression, nowadays in-vitro and in-vivo applications demand effective compression schemes. Approaches based on Principal Components Analysis (PCA) [158] and Wavelet transformation [156] are powerful compression schemes for neural signal application that allow accurate reconstruction of the waveforms with little to no sacrifice in fidelity. However, they present the major drawback of elevated process load that makes them inappropriate for implantable systems with extremely reduced energy resources. On the other extreme, drastically reducing process load one could just down-sample the neural signal to near Nyquist limit. However, in this

case the price to pay is the inaccuracy of the reconstructed neural signal and thus its impracticality for further analysis, such as spike classification or spike frequency assessment.

Here, the author proposes a real time Signal Compression (SC) stage together with a Resource Management (RM) stage that offers a trade-off between process load and neural signal fidelity in the wireless transmission scheme.

The SC stage is based on spike detection [20] yielding an acceptable compromise between signal accuracy and process load. Although quite popular in literature (see [20] and references therein), we have included a novel noise-tracking algorithm for adaptive threshold setting that outperforms the published basic algorithms. The RM stage implements a stepped reduction in the transmitted data rate as the channel bandwidth decreases, enforcing its simplicity for sake of process load saving.

A scheme of the designed system is shown in Figure 25. The inputs to the system are the channels of neural signals on one hand and the instantaneous wireless transmission bandwidth on the other. The system adaptively calculates the neural activity and evaluates the compression scheme to be used in each channel. Neural activity is calculated using spike detection. Once individual channel activity has been obtained, the RM algorithm consisting of an Adaptive Round-Robin with Priorities (ARRP) is applied. Channel priorities are static and have to be set before the algorithm starts. On the receiving side, channels are demultiplexed and signals reconstructed.

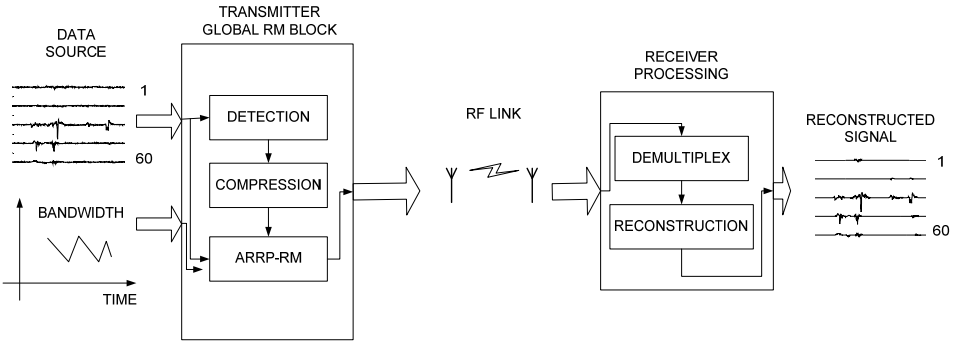

Figure 25. System scheme including RM at the transmitter side and signal reconstruction at the receiver.

Resource management processing is performed in a frame-based manner. Frame step advance is 50ms and the overlap segment between frames equals the spike length of 3ms. The overlapping allows adequate processing of spikes that may fall between consecutive frames. Figure 26 shows a scheme of the frame processing for one channel. The resulting algorithm delay equals the frame length since the output is available after the complete frame has been processed. Therefore, the frame length has been chosen so that the delay is tolerable for neural signal telemetry applications.

For each 50ms-frame, the algorithm works in the following way:

1. Available bandwidth is compared to the bandwidth required for sending the 60-channel raw signal, i.e., 18000 kbps.

2. If the available bandwidth is enough, mode 0 is chosen meaning that the signals from the 60 channels are multiplexed and sent to the output.

3. If not then the detection-compression-resource management block is activated.

    a. Detection is performed and spikes per frame are counted for each channel.

    b. At this point, each channel is processed depending on its priority defined in the priority matrix and 5 modes of operation with increasing compression rate are evaluated sequentially. The first mode that uses less bandwidth than available is selected and data compressed according to it. RM modes are listed in Table 5 and Figure 27 shows the priority matrix chosen for our experiments. Position in the matrix corresponds to electrode position in the multielectrode planar array used for signal recording. Electrode channels are numbered from top to bottom and from left to right. We have set 4 channels with the highest priority and the rest of the electrodes alternate priorities 2 and 3.

4. The selected RM mode is also coded at each frame, thus making decoding and reconstruction possible at the receiver.

	MODE 0	MODE 1	MODE 2	MODE 3	MODE 4
P1	raw signal	raw signal	raw signal	raw signal	ch + time
P2	raw signal	ch + time + wave	ch + time	ch + time	ch + time
P3	raw signal	ch + time + wave	ch + time	not sent	ch + time

Table 5 **Resource Management modes. ch + time + wave and ch + time mean compression schemes a) and b) respectively.**

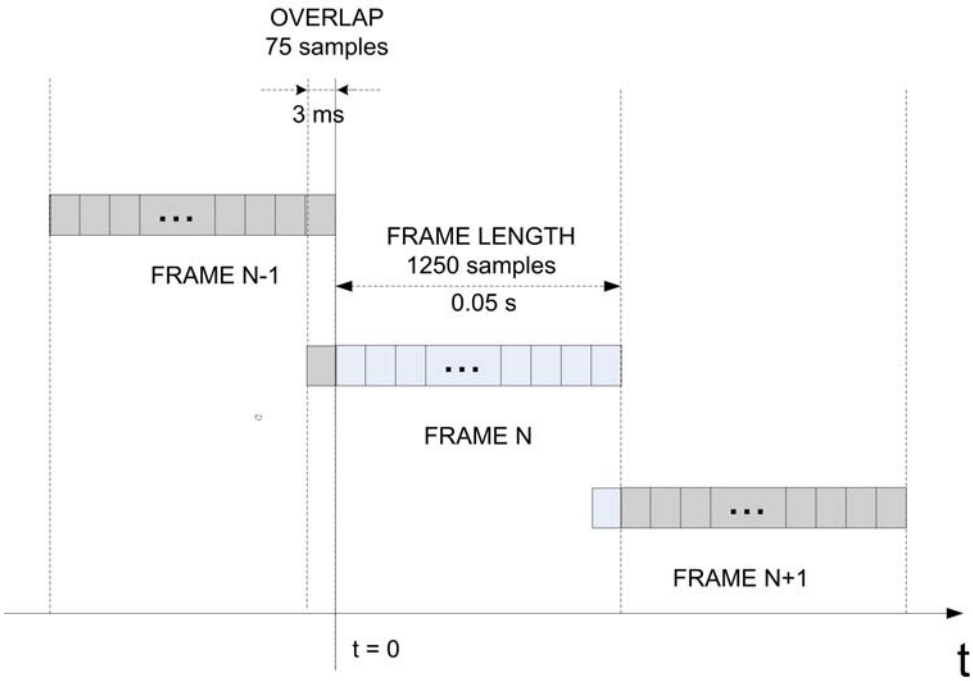

Figure 26. Frame processing scheme.

	2	3	2	3	2	3	
2	3	2	3	2	3	2	3
2	1	3	2	3	2	1	2
2	3	2	3	2	3	2	3
2	2	3	2	3	2	3	2
2	1	2	3	2	3	1	3
2	2	3	2	3	2	3	2
	3	2	3	2	3	2	

Figure 27. Channel priority matrix.

4.6 Decoding and signal reconstruction

The spike coding algorithm described in section 3 is not fully reversible. Although it provides excellent detection performance, missing or spurious spikes may occur. Nevertheless, it takes advantage of the neural signal characteristics thus allowing signal post-processing with similar quality as without compression [156].

At the decoding side, for each received frame, the decoding algorithm provides the crucial information extracted from the frame header as the input for the reconstruction algorithm (see Figure 24). In each frame, the reconstruction algorithm first reads the compression mode and then, according to it, the following samples are extracted as multiplexed raw channels, spike waveforms or spike time-stamps:

a. If one channel has been sent unaltered, it is just demultiplexed.

b. On the contrary, if spike coding has been used, it situates the spike samples on the corresponding channel and time scale.

c. If only the time-stamp is used for spike-coding, a one-sample impulse is used in place of the spike waveform.

Figure 28 shows segments of 0.1 second duration of the reconstructed signal compared to the original signal for 5 of the 60 channels. Reconstructed signal contains the same spikes as in the original while noise-only segments are absent.

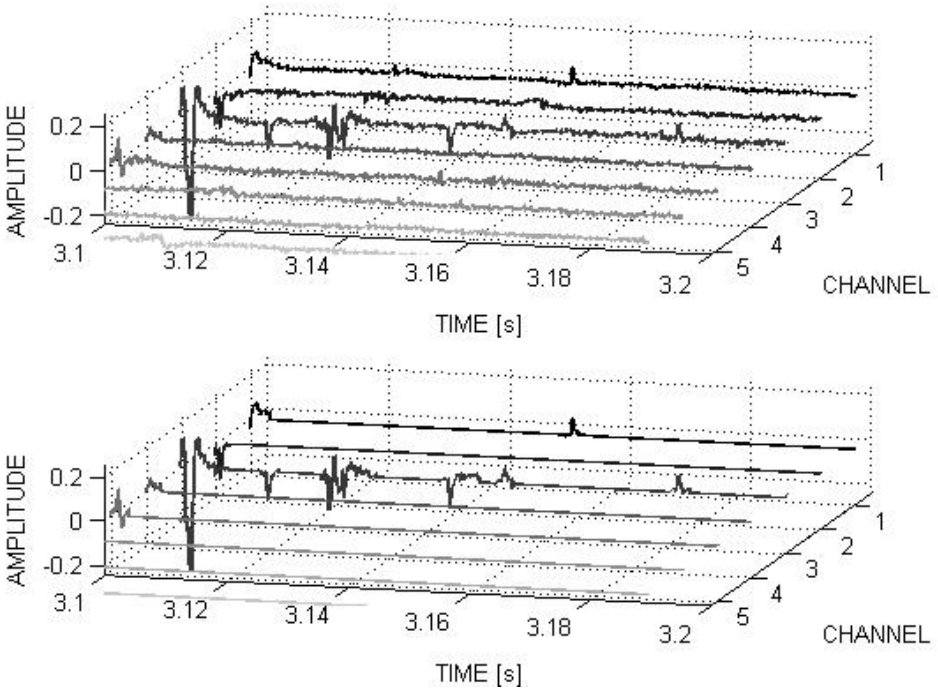

Figure 28. Segment of the original (top) and reconstructed (bottom) control signal corresponding to the first 5 channels.

4.7 Implementation of a wireless neural signal monitoring system

As a demonstration of the compression techniques applied, a prototype for the whole compression-transmission-reconstruction system has been implemented using Bluetooth and third generation mobile communication (3G). These last are particularly interesting wireless transmission methods for neural telemetry systems as they are available on conventional mobile phones and other portable devices [179], [14].

Wireless communication from the neural implant to the external receiver is not covered here; however other works as [169] study the design of reliable

wireless links in the presence of lossy tissue with frequency dependent dielectric properties. It verifies that, in the 0.1 to 6 GHz range, the optimal frequency for power transfer from a cm-size to an implanted mm-size coil in a human skull lies in the 100s of MHz range and exhibits a rather broad optimum. Maximum link gain is about -27dB. The investigation of variability and uncertainty in tissue thickness and dielectric parameters showed that, around the optimal frequency, the variability of tissue thickness and of the dielectric properties and produce a 5 dB difference in power transfer which can severely affect the overall operation of an implanted device, it will be necessary to take this variation into account while designing future wireless neural interfaces. Other works as [170] use infrared communication to overcome the implant to external link. Any of these solutions could be used in conjunction with our system and we will only discuss here the rest of it.

The neural signals are recorded by micro-electrode arrays and then, real-time compressed and transmitted over a Bluetooth link to a mobile phone. This mobile device immediately, without intermediate storage, re-transmits the signals over 3G to a remote server where data processing and analysis is performed. Reconstruction of the coded neural signal provides the input to high performance spike classification algorithm allowing the tracking of individual neuron spiking patterns. Figure 29 represents the overall transmission scheme. The information source is a personal computer (PC), where neural data recorded by the Multi Channel Systems MEA are stored. This PC establishes via a Bluetooth-Dongle a wireless communication link with a mobile terminal.

The stored data are compressed and transmitted over the Bluetooth link from the information source to the mobile device that receives them and, without intermediate storing, re-transmits them via a 3G link to a remote server PC, where the data are definitely stored, reconstructed and post-processed.

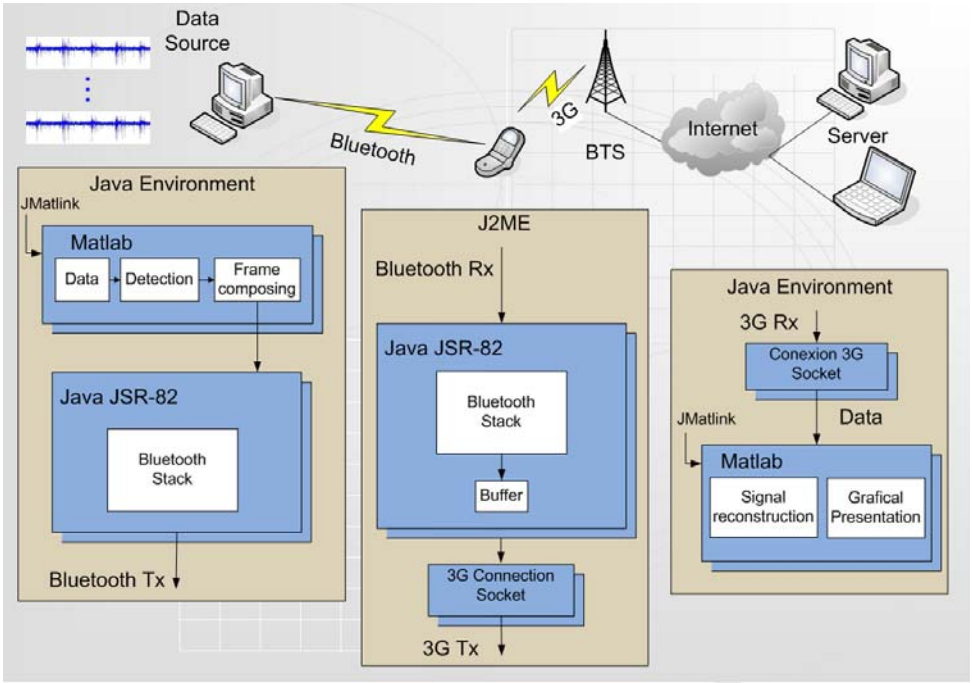

Figure 29. Wireless Bluetooth-3G transmission.

Bluetooth is a flexible and capable technology for providing short-range radio communications between devices in an ad-hoc manner using the 2.4 GHz band. It is well suited as a low power radio transceiver (transmitter and receiver) operating at up to 1 Mbps [73]. Two types of channels are used in Bluetooth systems: SCO and ACL. SCO are Synchronous Connection Oriented links with fixed 64 kbps data rate used exclusively for voice traffic; while ACL are Asynchronous Connection-Less links. As shown above in Section 2, streaming of multi-channel or even single channel neural signals demands

such a bandwidth which can not be offered by SCO links. The Bluetooth connection type capable of flexible and higher bandwidths is the Asynchronous Connection-Less link [158], [167]. Figure 30 shows the core Bluetooth protocol layers.

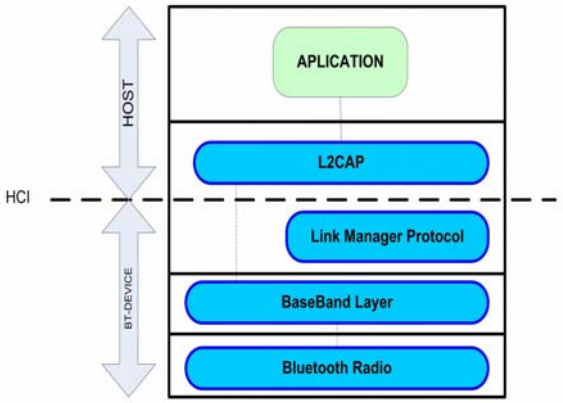

Figure 30. Core Bluetooth Architecture.

The baseband layer enables the physical RF link between Bluetooth units making a connection. Link Manager Protocol (LMP) is responsible for link set-up between Bluetooth devices and managing security aspects such as authentication and encryption. L2CAP adapts upper layer protocols to the baseband. It multiplexes between the various logical connections made by the upper layers. Audio data typically is routed directly to and from the baseband and does not go through L2CAP.

Given that our communication scheme includes a client application implemented on the information source and the server application running on a mobile phone, it is reasonable to choose a Bluetooth programming technology that is provided in nowadays mobile devices. That is why we have decided to

use the standard Bluetooth Java programming API JSR-82 currently supported in a wide range of mobile devices from different manufacturers [176]. JSR-82 API allows us to establish an L2CAP point-to-point connection between client and server devices through which the neural signals are transmitted. JSR-82 supports Bluetooth standard v1.1 which is therefore the version used in our experiments.

In order to have control over the Bluetooth transmission we have programmed the client and server applications implementing the communication. In this scheme, first, an L2CAP connection is established between the master and the slave. Once communication is established, the client application running on the slave starts sending data over the connection to the master's server application. The data packet size used in the connection can be selected at compilation time and a 2 Mbytes neuronal signal of the type described at the beginning of this chapter is used as data source. The transmitter monitors the channel quality by inspecting throughput.

As the mobile device receives the neural data from the information source, they are retransmitted immediately to the remote server over the 3G network. Once the mobile phone is registered in the network, a profile containing all necessary parameters for the 3G transmission, such as access point etc., is established. The TCP, Transmission Control Protocol, is used for the data transmission. It offers a point-to-point connection-oriented reliable link recovering a huge variety of errors dynamically and adaptively. In order to use the TCP, the transmitter (in this particular case the mobile phone) and the

receiver (equivalent to the remote server in our application) shall create the terminal points of the connection, called sockets. A socket is defined by a transmission protocol (TCP is this case), an IP address and a port number. In our experiments the mobile phone is programmed to be the client. It requests the opening of a TCP-socket to the server that is waiting for inquiries.

The application running on the mobile phone implementing both, the Bluetooth and 3G transmission is programmed in J2METM (due to the limited device resources). Also, the server application is programmed using Java™.

In Figure 29, it can be observed that both the application running on the information source PC and the remote server application incorporate the JMATLink software package. This package allows the integration of MATLAB™ applications with Java™ applications.

Especially for data pre- and post-processing as well as for real-time data representation this package offers huge advantages. The data compression algorithms described in Section 4.4 are implemented in MATLAB™ and launched by JMATLink. For the evaluation of the transmission, real-time graphical data representation is required on the server, also implemented in MATLAB™ and launched by JMATLink.

Due to the fact that the Bluetooth L2CAP connection is a secure channel, retransmissions assure the correct arrival of each single packet and until the acknowledgment of the former packet does not confirm its correct reception a new packet is not transmitted. For this reason, measuring transmission

throughput is equivalent to measuring reception throughput. Moreover, this ensures the real-time transmission as long as the data stream generation velocity does not surpass the channel throughput.

4.8 Results and discussion

4.8.1 Spike detection results

Both STH and NEO detectors have been used to detect spikes in the set of real and artificial signals. Figure 31 shows spike detections given by STH detector with automatic noise-envelope tracking. One can observe that threshold adaptation to the appropriate level above the underlying noise occurs in about 0.5 seconds and that it is not affected by the spiking activity. Comparison among the four tested channels shows the algorithm ability to adapt to different SNR conditions (Figure 31 (a) to (d)). One can observe that threshold adaptation to the appropriate level above the underlying noise occurs in about 0.5 seconds and that it is not affected by the spiking activity.

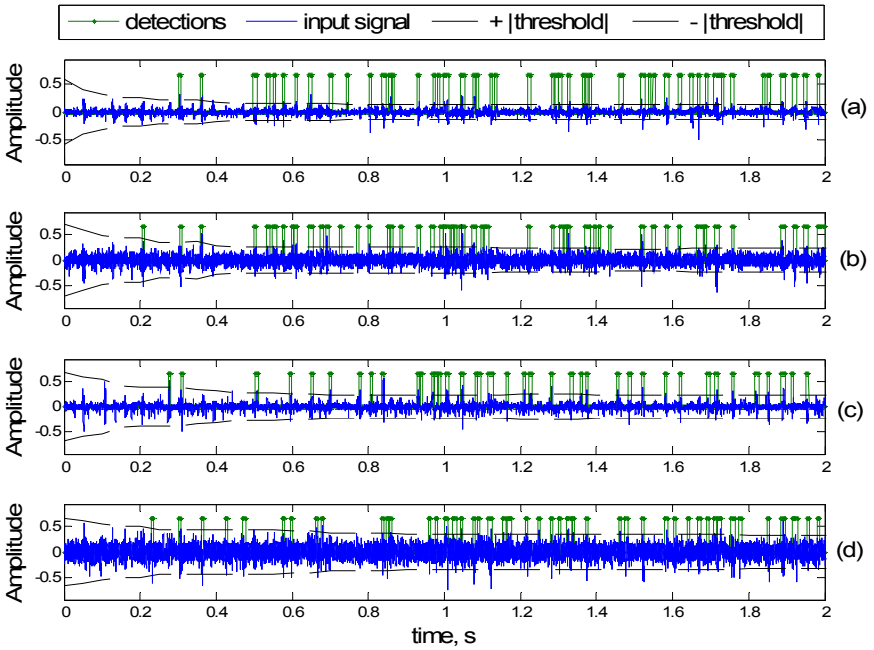

Figure 31. Automatic neural-signal noise-envelope tracking for different real recording channels with different signal to noise ratios.

In order to compare STH's and NEO's performance, the Receiver Operating Curves (ROCs) have been plotted from the spike detection results. Figure 32 shows ROC families obtained for STH (top) and NEO (bottom) when applied to the artificial signals set. It also includes resulting probabilities of detection and false alarm for the different SNRs obtained using the adaptive threshold method. Here one can see that the adaptation mechanism sets the detection working point according to the input SNR. Arrows in Figure 32 indicate the moving direction of the working point with changing SNR if a fix threshold is used with the consequent performance degradation.

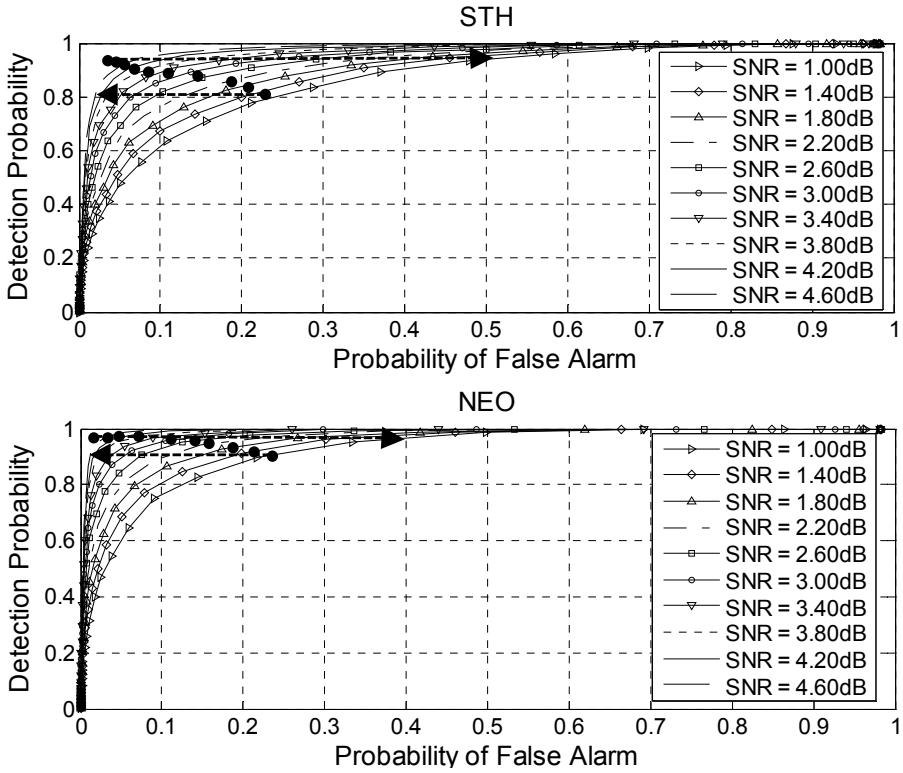

Figure 32. Family of ROC curves obtained for the set of 10 artificial signals with SNRs ranging from 1 to 4.6 dB. Top: STH detector, bottom: NEO detector. Thick dots on of the curves correspond to the detection and false alarm probabilities obtained using adaptive threshold. Arrows indicate working point moving direction if a fix threshold is used for the rest of SNR conditions.

Similarly, Figure 33 plots ROCs corresponding to the real signal and shows that NEO curve is closer to the ideal detection curve, which is the step function. Area-under-curve figure for NEO is 0.9473 against 0.9258 for STH.

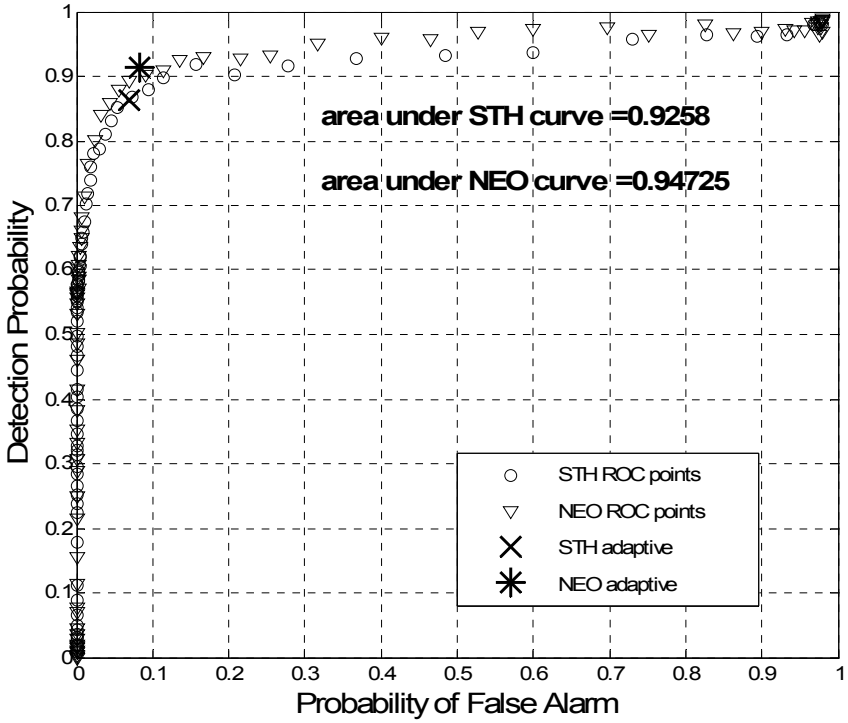

Figure 33. ROC curves obtained using real data for STH (circles) and NEO (triangles). The use of adaptive threshold for STH or NEO results in only one working point on the ROC curve represented as a cross and an asterisk for STH and NEO, respectively.

From the results we conclude that a new method for adaptive threshold spike detection has been applied that successfully adapts to different input SNRs. It can be used for both STH and NEO spike detectors improving detection and eliminating the need for manual threshold setting. Additionally, spike detection quality for STH and NEO has been assessed. Although previous publications (Obeid and Wolf [6]) show that STH detection is comparable to NEO when the input signal is previously high-pass filtered; here we show that, when no pre-filtering is applied, NEO brings a significant improvement to spike detection results.

4.8.2 Spike sorting results

In order to assess performance quality of the implemented classification algorithm it has been applied to both, the artificially generated signals and the real recordings from Multi Channel Systems.

Similarly to the process described in section 4.1, artificial signals containing two trains of spikes randomly superposed were generated and in fact, the artificial multi-spike train classification were used to interactively tune several parameters of the classification process such as Principal Component score, clustering distance etc. Once the optimized parameters are obtained, the classification algorithm is applied to the real signal recordings from Multi Channel Systems described also in section 4.1.

Figure 34. to Figure 37 show graphically the developed classification process applied to one channel of real recordings. In Figure 34 the superposition, aligned to the minimum, of the detected spikes is shown. These spikes represent the input set for the PCA. As a result of the PCA, a sorted list of base vectors is computed.

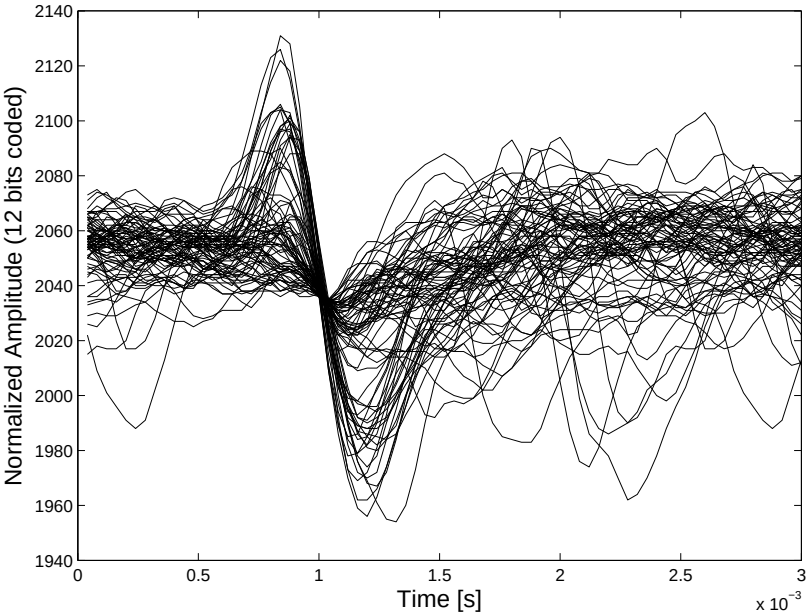

Figure 34. Superposition of the detected spikes of one channel. Alignment is performed to the minimum value.

The computed scores of the Principal Components of the complete input spike set that form the sorted list are shown in Figure 35 (top). The three higher scored Principal Components collect more than 81% of the overall scores, thus yielding a high-fidelity representation of the complete input set when truncating at a 3-dimensional representation. Precisely these three most relevant signals are depicted in Figure 35 (bottom). They form an orthogonal vector base that will be used for the whole input set space.

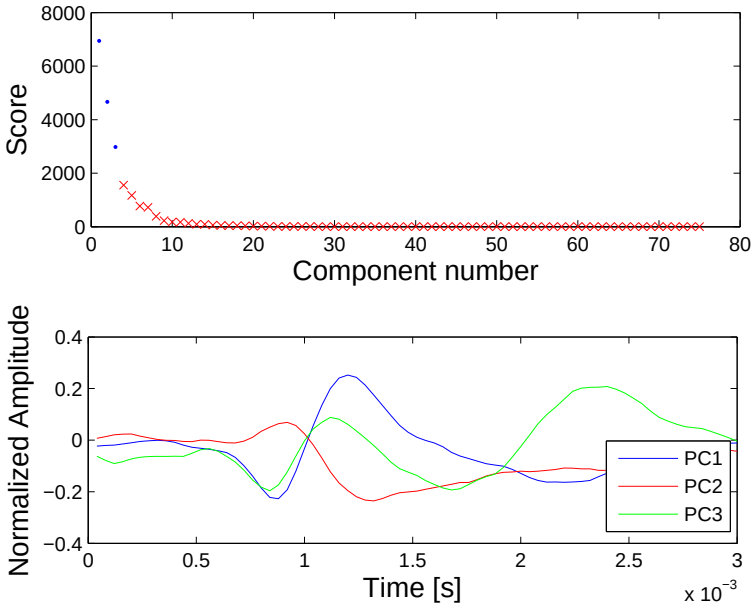

Figure 35. Scores of Principal Components of the input spike set (top) and three most relevant Principal Components (bottom).

From this 3-dimensional representation the k-means clustering algorithm is applied to establish the membership of each spike to one determined class. Figure 36 (top) shows the 3-dimensional representation of the complete spike input set separating color-wise the 3 different classes. For sake of clarity, the 2-dimensional projection on the two first Principal Components is also shown in Figure 36 (bottom).

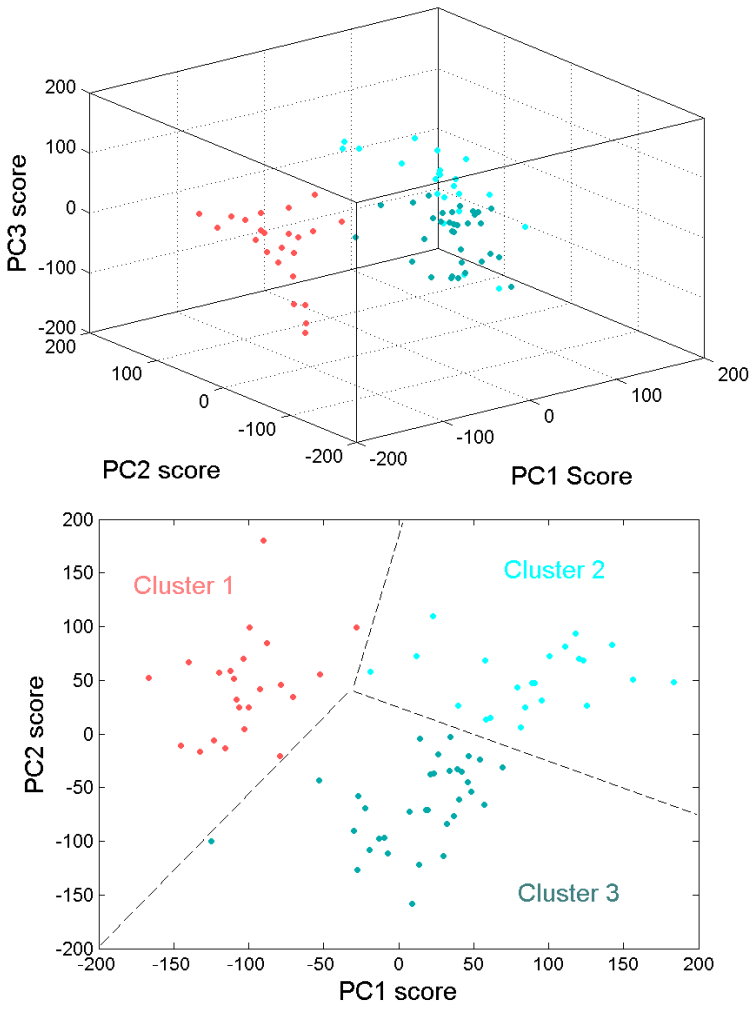

Figure 36. Dimensional representation of the input spike set (top) and 2-dimensional projection (bottom).

The overall result of the classification is summarized in Figure 37 (top) that shows the input spike set separated color-wise depending on its class membership. As it can be observed from Figure 37 (bottom), the spikes belonging to one class show similar wave forms.

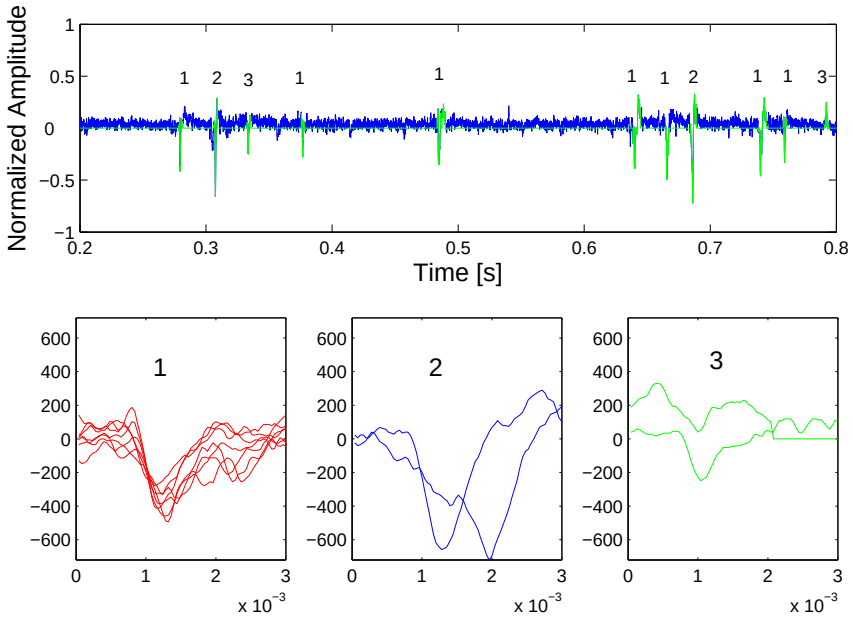

Figure 37. Classified input spike set (top) and spikes belonging to class 1-3 (bottom).

The classification performance for the set of artificial multi-spike trains yields to 92% of correctly classified spikes.

For the real data recorded by Multi Channel Systems, the classification performance shall be assessed through evaluation of experts, similarly to the assessment of the detection quality described in section 4.2.

4.8.3 Compression and transmission results

We have conducted several experiments using the input neural signals described in section 4.1, control recording and NMDA recording (Figure 38), in conjunction with dynamic transmission bandwidths. In order to consider real-life conditions experimentally measured instant Bluetooth data rates are used as

input signal. Additionally, an experimental increasing bandwidth is computed as input signal which allows design facility of a fixed-bandwidth point-to-point transmission system:

- Experimental Bluetooth v1.1 data rates.
- Experimental Bluetooth v2.0 EDR data rates.
- Increasing bandwidth from 1Mbps to 20Mbps in 1Mbps steps.

System performance has been evaluated using the set of configurations given by the combination of the input signals and input bandwidths. While running the model several parameters were stored which allowed subsequent performance analysis. Figure 39 and Figure 40 show the results. Both figures contain similar information but corresponding to Control and NMDA experiments respectively. The top subplots show neural activity per channel and total neural activity. The following pairs of subplots show available bandwidth compared with the resulting occupied bandwidth corresponding with the selected RM operation mode, and the selected operation mode, respectively.

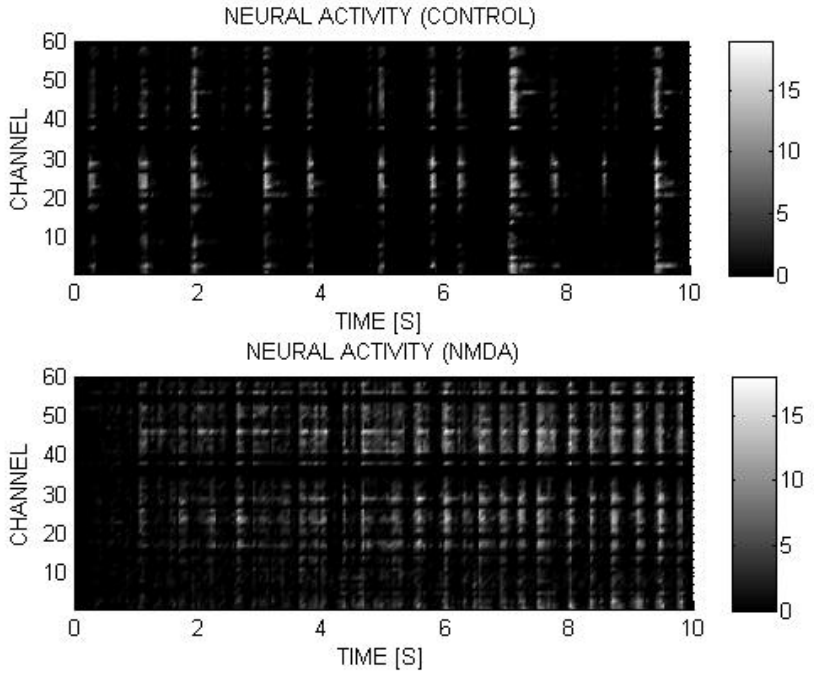

Figure 38. Neural activity (brightness indicates activity in number of spikes per second). Top: control experiment before drug application. Bottom: experiment after application of NMDA.

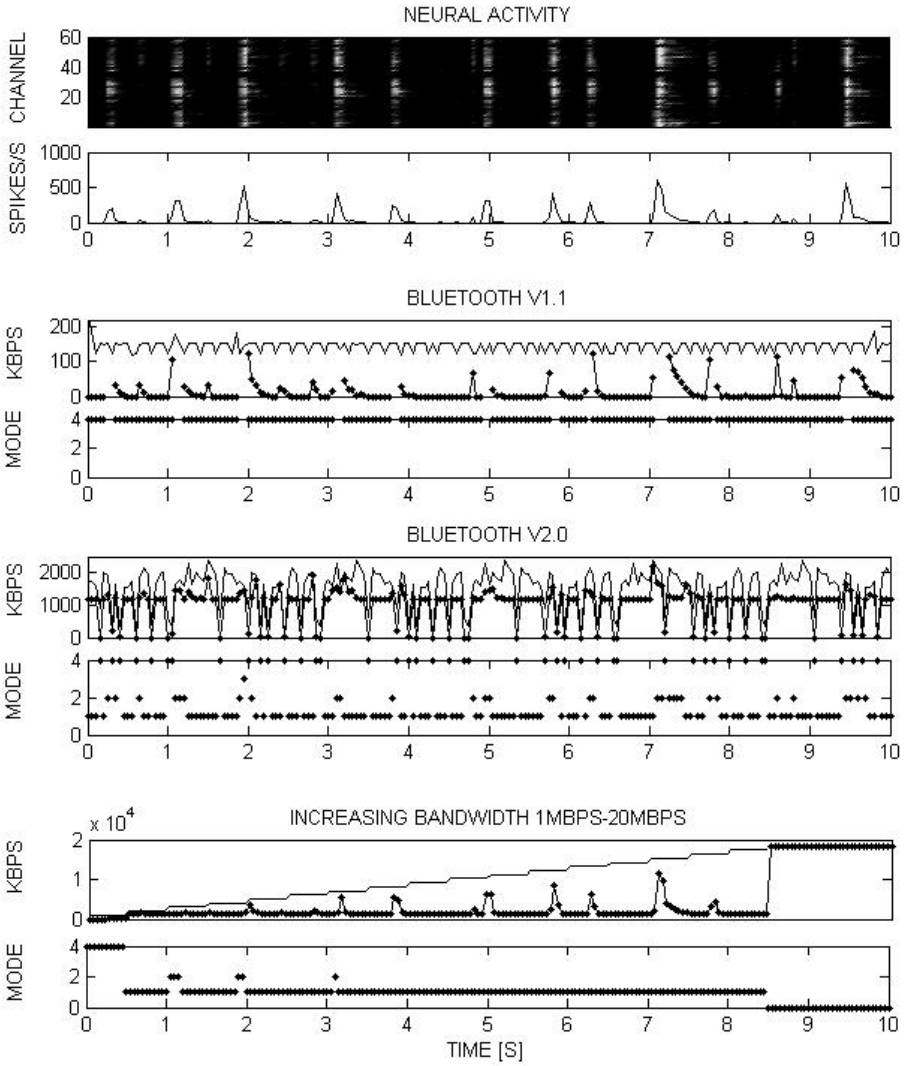

Figure 39. Resource Management results for control signals. Transmission bandwidth corresponding to Bluetooth v1.1. Bluetooth v2.0 EDR and increasing from 1Mbps to 20 Mbps. Full line: Available Bandwidth, Dotted line: Occupied Bandwidth.

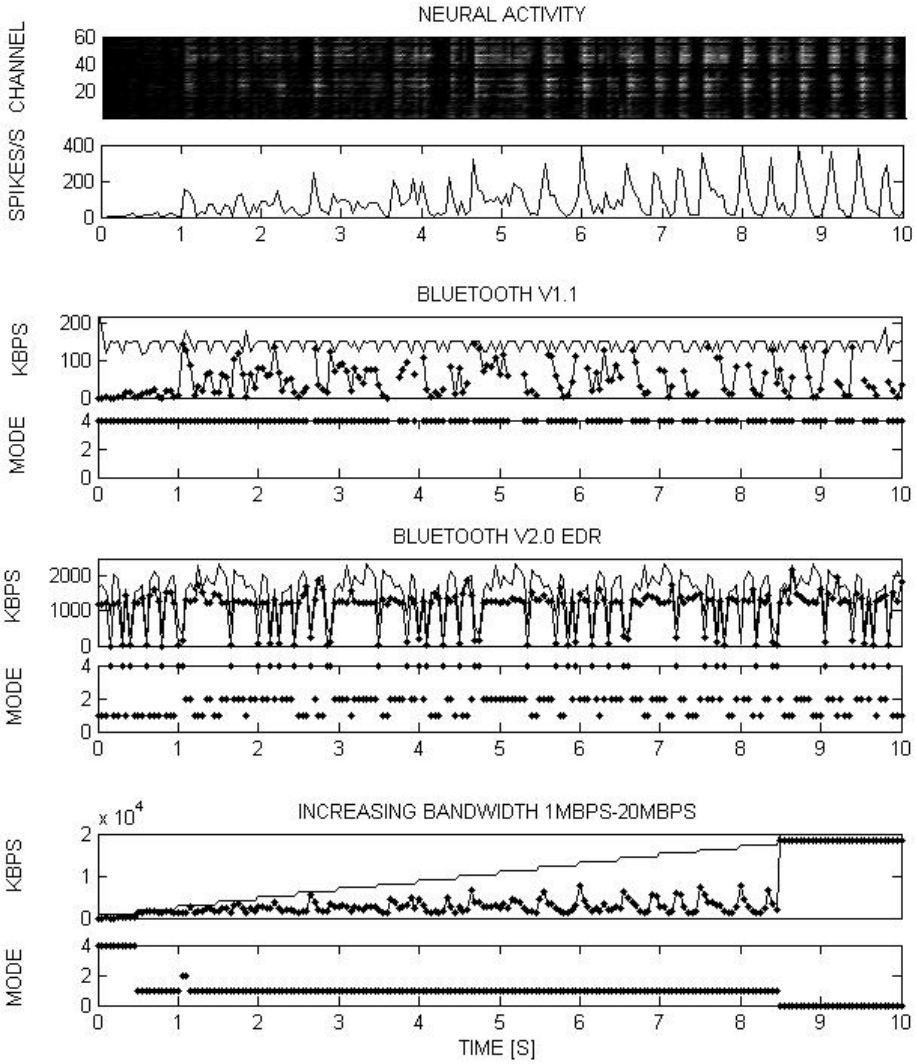

Figure 40. Resource Management results for NMDA signals. Transmission bandwidth corresponding to Bluetooth v1.1. Bluetooth v2.0 EDR and increasing from 1Mbps to 20 Mbps. Full line: Available Bandwidth, Dotted line: Occupied Bandwidth.

From the figures, one can observe that, in general, the adequate mode is selected at each time so that the occupied bandwidth does never surpass the available bandwidth. However, in the case of Bluetooth v1.1, there are some high-activity frames in which signals can not be fitted into the available

bandwidth with any of the resource management modes given that Bluetooth v1.1's bandwidth is too low. That fact is presented in the figure as gaps in the occupied bandwidth representation and in the selected mode. In such case, the alternative is to just send the number of channels that fit and leave the rest unsent. This result proves that Bluetooth v1.1 is not suitable for simultaneous real-time transmission of 60 neural signals. On the contrary, the use of Bluetooth v2.0 EDR in conjunction with the ARRP-RM algorithm makes that objective possible.

When looking at the results corresponding to the experiment in which the bandwidth provided by the wireless link is slowly increasing from 1Mbps to 20Mbps, both for control and NMDA neural activity, in the first frames, the bandwidth is only enough for RM mode 4, so spike coding is used in every channel and only channel number and timestamp is sent for each spike. As the bandwidth increases RM modes 1 and 2 are used and the raw signals of the 4 channels with higher priority are sent while the rest of the channels are compressed using spike coding. In this period one can observe how occupied bandwidth follows the dynamics of the spiking activity. As expected, an available bandwidth of 18 Mbps is above the level required for transmitting raw signals from all the channels and therefore RM mode 0 is chosen. However, some over sizing shall be included for unexpected interferences with other systems.

In order to summarize the results, Figure 41 shows the resulting percentage of the available bandwidth that is occupied as the input neural activity

increases. Different lines in the graphic represent different transmission bandwidths. For the 3 curves corresponding to bandwidths of 2048, 4096 and 8192 kbps, one can observe that the occupied bandwidth increases with the neural activity. Obviously the occupied bandwidth can not surpass the available transmission bandwidth and, therefore, when the occupied bandwidth approaches 100%, the algorithm automatically changes the compression scheme and this results in a downwards jump in the graph. After the jump, the percentage of occupied bandwidth continues to rise towards 100%. In the cases of 1024 and 16384 kbps, the graphic does not show a jump. The reason is that, for the represented spiking activity range, the occupied bandwidth does not reach 100%, and, therefore, the same compression scheme is used across the whole range.

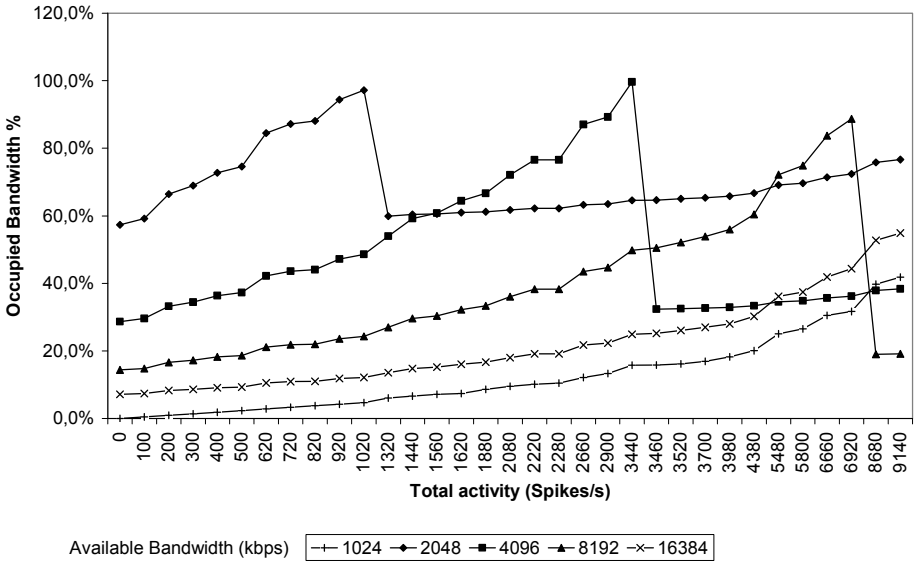

Figure 41. Resulting percentage of occupied bandwidth against the spiking activity of the cellular culture. Different available bandwidths are presented.

In summary, a compression and resource management algorithm to be used in the wireless transmission of neural signals has been designed and tested. The frame-based algorithm is capable of adapting signal compression of the 60 channels at the input according to the neural activity present, the priority set to each channel and the bandwidth available at each processing frame. As a result, signals are compressed and multiplexed in a single transmission frame.

The reconstruction algorithm at the receiving side is able to demultiplex and decode signals to reconstruct the spiking patterns. Ideally, signals from each channel should contain original spikes so that sorting algorithms can be used to isolate individual neuron's activity. That is eventually not possible when the bandwidth is too low, then the strategy is to send spike timestamps only. Spike sorting at the transmitting end should be done to overcome the problem.

In the presented ARRP-RM algorithm, channel priorities can be configured at compilation time and can be based on observed channel activity or on correlation among channels. Precisely this characteristic makes the developed algorithm highly useful for nowadays in-vitro and in-vivo applications: For example, only one out of two highly correlated channels will be assigned with the highest priority whereas the other will be given the lowest. In case of bandwidth restrictions, the latter will not be sent given that the information it carries is somehow redundant. In another application example, the proposed algorithm can be used in the neural recording stage of a Brain Machine Interface (BMI) so that the channels containing signals from highly-tuned cells will be given the highest priority. The signals captured form them will always be

sent to the receiver whereas less significant cells will only be monitored in high bandwidth availability conditions.

4.8.4 Bluetooth-3G transmission results.

The system described in section 4.7 is evaluated for its application to the real-time transmission of neural signals captured by implanted micro-electrode array sensors. Average compression rate of 75% of the neural signal is achieved through detection using nonlinear energy operator pre-processing and automatic threshold adaptation. The transmission rate is limited by the Bluetooth and 3G links, depending on the transmission packet size. Due to the limited resources of the mobile phone, the maximum transmission unit is also bounded, thus achieving a maximum transmission rate of 323.1 Kbps. With this transmission rate, it is not possible to transmit more than one neural signal in real-time over the Bluetooth link without compression. With the developed compression algorithm the system performance is enhanced allowing real-time transmission of 4 neural signals considering average spiking activity and taking into account that no buffering is performed.

In Figure 42, the transmission mean throughput in relation to the defined packet size is represented. The mean throughput is calculated as the number of transmitted bits divided by the overall time required for transmission in nanoseconds. It can be observed that the mean throughput increases with the packet size. For a packet sizes smaller than 1000 bytes the throughput is below 180 kbps. Due to the fact that the required minimum transmission data

rate for neural signals, as described in section 2 is 180 kbps, only packet sizes greater than 1000 bytes provide real-time transmission of one neural signal. For these packet sizes (> 1000 bytes) as the packet size increases, saturation in the mean throughput is observed. The obtained maximum mean throughput value is below 230 kbps.

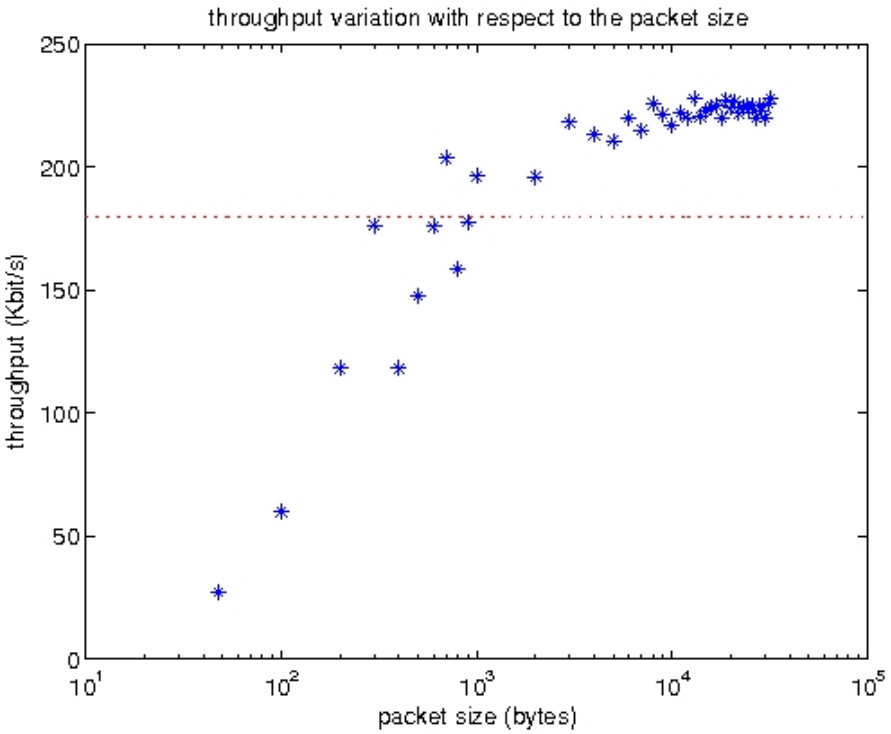

Figure 42. Measured mean throughput with respect to the transmission packet size.

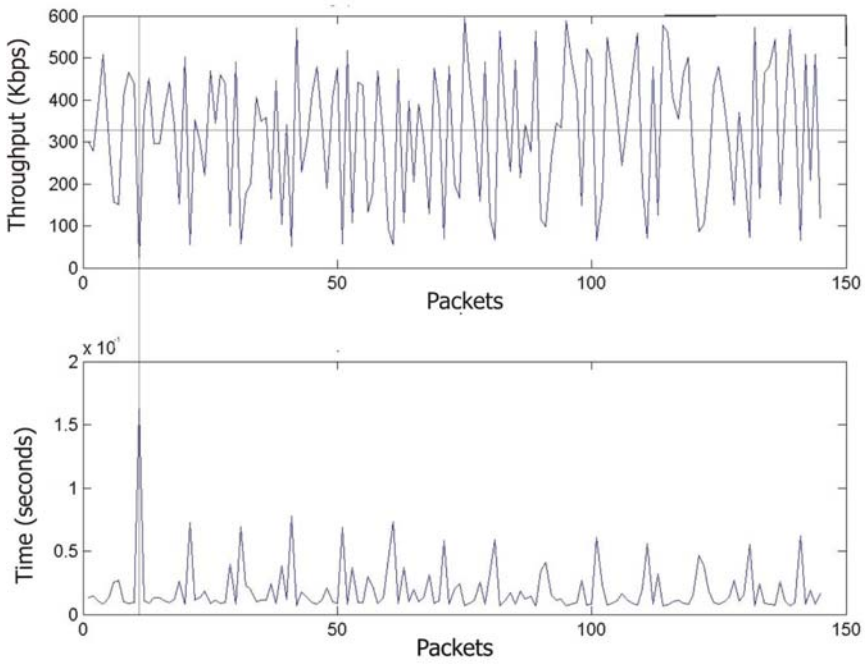

Figure 43. Measured throughput and packet transmission time for packet size 512 bytes with EDR.

Fortunately, the measured throughput values are improved by using Bluetooth v.2. EDR (Enhanced Data Rate). With this standard, data rates up to 3 Mbps are achieved. Due to the limited processing and storage capabilities of the mobile phone, the maximum packet size for the Bluetooth transmission is 512 bytes. In Figure 43 (top) the real-time evolution of the transmission throughput for a packet size of 512 bytes is represented. It can be observed that peak values of up to 695.6 kbps appear while the minimum value is 24.61 kbps. The mean throughput obtained for a 512-bytes-packet size is of 323.1 kbps for the experiment shown. Figure 43 (bottom) shows the corresponding time profile. It can be observed, that throughput peak values in Figure 43 (top) correspond to time minimum values as appears in packet nr. 8. The mean

packet transmission time is calculated to be 12.67ms. The obtained throughput allows the real-time transmission of one neural signal channel (180 kbps required for each channel). Therefore, adequate data compression before transmission is mandatory.

Analyzing the real-time throughput evolution, it is observed that less than 20% of the measured throughput values fall below the range of the mean value. Therefore, an adequate mean throughput value guaranties the channel capacity for over the 20% of the time.

The developed compression algorithm described in section 4.4 is able to reduce the required data transmission rate on average to 75% depending on the spiking activity of the particular culture. Therefore, with the transmission rate limited to 323.1 kbps and taking advantage of the compression algorithm, on average, it is possible to transmit in real-time 4 neural signals (considering 25Khz sampling and 12 bits resolution).

As a conclusion, the system has shown the feasibility of a wireless transmission system. however, considering the high data rates generated by implantable neural sensors, Bluetooth does not provide enough capacity in practice. Future applications will probably start to exploit technologies able to provide higher data rates as Ultra Wideband (UWB) [181], [175], [174]. UWB presents several characteristics that make it very attractive for this particular application:

- considerable high transmission rates of over 100 Mbps

- extremely low power consumption
- no interference with other wireless technologies due to its spread transmission spectrum (short pulse transmission)

There are some additional considerations to be regarded. UWB allows only short distance communications with these high transmission rates, which is perfectly assumable for body area networks but raises the need of a bridge between the close body field and remote stations.

Chapter 5

On-Body UWB Channel modeling

5.1 Introduction

The recent advent of wireless data acquisition systems will facilitate fully implantable BMI systems obviating the need for transcutaneous wires and offering a high grade of mobility to the patients [159]. Incorporating spike detection will allow the BMI to transmit only the action potential waveforms and spiking times instead of the sparse, raw signal in its entirety, thus reducing significatively the extremely high transmission rates [210]. However, for neural signal analysis, making the entire raw signal available in real-time will offer enormous possibilities to explore neural signal characteristics, such as evaluating spike detection and classification in real-time, or performing real-time parameter adaptation for more efficient algorithms. Most commercially available wireless transmission systems do not offer the sufficient data rates to transmit the raw neural signal captured from multi-electrode recording systems [211], [7], [180]. In addition, a wireless transmission system designed for BMI

applications shall also fulfill extremely severe low-power requirements, not only because of near-body radiation considerations but also to extend battery life.

In this context, Ultra Wideband (UWB) is the best candidate because it provides outstanding high data transmission rate together with extremely low power consumption [180]. Nonetheless, it has to be taken into account that UWB, as any other wireless transmission system will have to deal with data losses due to possible interferences with other systems, reflections, dispersion, multipath components or signal fading.

As described above, a high-data rate on-body wireless transmission system would enormously benefit the development of neural signal monitoring systems for both research and therapeutic applications. It would make it possible for researchers to study neural codes in freely-moving subjects and the therapeutic community to design better devices without the need for uncomfortable cables. That is the motivation behind the presented study of the on-body UWB propagation. The objective is to characterize the channel and assess the limitations for future transceiver design.

In this chapter, first, general channel modeling and specific UWB stochastic modeling are introduced, then, the need for on-body UWB channel modeling is exposed. Following that, the on-body UWB measuring campaign is described and the results and conclusions are devised. Finally an evaluation on the effects of UWB transmission on neural signal characteristics is presented.

5.1.1 BAN-UWB channel stochastic modeling

As channel one understands the set of propagation effects occurring between transmitter and receiver in a communication link, such as ordinary free space loss, multipath, diffraction, refraction, and scattering, as well as general background noise. These effects have an influence on the transmission resulting in an effective link capacity for information transmission, as is described in the Shannon's law, see eq. (5-1), where C is the link capacity, B is the channel bandwidth, S is the signal power and N is the noise power.

$$C=B\cdot\log_2\left(1+\frac{S}{N}\right) \tag{5-1}$$

The specific propagation effects that must be accounted for depend on the characteristics of the system, i.e., the frequency of operation, the symbol rate, the modulation, coding, antenna types and heights, the environment rates of movement, and other geometrical factors (e.g., distances between antennas and distances to reflective surfaces). For low-data-rate systems, multipath transmission can often be represented as flat fading, i.e., as a time-varying attenuation that affects the amplitudes but not the shapes of received signal pulses. For higher data-rate systems, however, multipath causes distortion of pulses and inter-symbol interference; these effects can be crucial in determining waveform parameters and receiver characteristics, including equalization, rake reception, error control coding and interleaving, and the use of spread spectrum techniques. The objective in channel modeling is to

characterize all the set of propagation effects in order to predict the behavior of the channel when used in a communication link.

Channel models can be grouped in deterministic and stochastic models. Deterministic models precisely describe the behavior of the channel but they require an equally precise description of the propagation environment, which becomes unrealizable for complex scenarios as it is the on-body propagation. On the other hand, stochastic empirical models use simplified descriptions of the scenario and produce statistically accurate results. For this thesis, the aim is to obtain a stochastic channel model and to extract its characterization parameters.

We start with some definitions, first, if we define $h(t,\tau)$ as the random time-varying channel impulse response at the moment in time t for delay τ, then $E\left\{h^*(t,\tau_1)\cdot h(t,\tau_1+\tau)\right\} = P(\tau)$ is the Power Delay Profile (PDP) of the channel. The discrete model for the PDP assumes that it is a discrete sum of individual contributions at different delay times of the form:

$$P(\tau) = \sum_{K=1}^{N} a_k \cdot \delta(\tau - \tau_k) \tag{5-2}$$

Coherence time is the approximate time window over which the channel appears static. It is a measure of how fast the transmission environment changes over time. In fact, when the coherence time is shorter than the length of the transmitted symbol, the channel is said to be **fast-fading**, on the contrary, when coherence time is larger than the length of the transmitted

symbol, the channel is said to be **slow-fading**. In other words, fast fading occurs when the channel changing rate is faster than the symbol transmission rate and slow fading in the opposite case.

Coherence bandwidth is the approximate range of frequencies over which the channel appears static. The cause of frequency incoherence is multipath propagation. A channel is **frequency-selective** when its coherence bandwidth is smaller than the bandwidth of the transmitted signal and it is said to have **frequency-flat fading** otherwise.

The **delay spread** is the time delay between the arrival of the first received signal component (Line Of Sight (LOS) or multipath) and the last received signal component associated with a single transmitted pulse. If the delay spread is small compared to the inverse of the signal bandwidth, then there is little time spreading in the received signal. However, when the delay spread is relatively large, there is significant time spreading of the received signal which can lead to substantial signal distortion.

5.1.2 The need for on-body UWB channel modeling

Wireless Body Area Networks (WBANs) are wireless communication networks where either transmitter, receiver or both are placed on the human body. Nowadays, with the raising number of applications in health monitoring and telemedicine, characterization of the channel behavior involving the human body is becoming increasingly important. Body-worn devices must be permanently available and, at the same time, operate at a low transmission

power, not only because of the body proximity but also in order to extend battery life. In such scenario, Ultra Wideband (UWB) technology appears as an appropriate solution for wireless communication, providing considerable transmission rates at a relatively low power consumption cost. It is therefore of interest to obtain a realistic model of the on-body UWB channel model to be used in the design of the communication devices for new health monitoring, telemedicine and sports applications.

5.1.3 Head-to-body UWB channel model

In the literature, several measurements and models of the UWB channel for indoor and outdoor propagation can be found [183], [184], [185] and [187]. Some studies try to model the effects of the human body as it interferes with a wireless network by interposing a person between two antennas [188]. Others [189], [190] consist on measurement campaigns where only the transmitter antenna is placed on the body. Additionally, studies performed by Alomany et al. [191] place both antennas on the body, but the focus lies in finding out which kind of antennas are best fitted to be used in WBAN channel estimation. In [192] measures are done in a hospital room but not in an anechoic chamber. The results of [181] demonstrate the propagation mechanisms on the head, like diffraction or absorption, but without an exhaustive analysis of the propagation channel. In [193], the authors use a human model and the finite-difference time domain (FDTD) method. Finally, characterization of the channel with transmitter and receiver antennas along the torso is performed in [196],

[197]. Despite all the above studies, it has been found that there are few works taking into account the human head.

In this thesis, the analyzed channel is defined by transmitter placed on the head and the receiver placed in several parts along the torso, arms or legs. The objective is to study the behavior of the UWB channel surrounding the body for the specific application described in Chapter 4: the transmission of signals recorded from the head to a device such as a mobile phone or a PDA that the person is carrying or also from the transmitter on the head to other devices located along the body. In future medical applications those devices would be either monitoring or active devices.

Stochastic channel models are based on experimental channel measures taken at a number n instants of time using either a VNA or a channel sounder. From the obtained measures channel statistics are derived. Section 5.2 describes the set of measuring campaigns carried out in this work to obtain the realizations for the channel model. Using the traditional Saleh–Valenzuela discrete- time approximation for the wideband multipath channel model defined in [183], we made several assumptions and modifications to the model. Previous works, like [184] and [185] among others, also made similar modifications. This model is especially useful in the study of spread spectrum systems and RAKE receivers, as explained in [200].

The channel model is described in [183] as follows:

$$h(t) = \sum_{l=0}^{L-1} \sum_{k=0}^{K-1} \alpha_{k,l} \cdot \delta\left(t - T_l - \tau_{k,l}\right); \quad (5\text{-}3)$$

Where h(t) is the channel impulse response, L is the number of clusters and K is the number of multi path components inside each cluster. $\alpha_{k,l}$ is the small scale amplitude of the k−th ray of the l−th cluster. T_l is the arrival time of the l−th cluster and $\tau_{k,l}$ is the arrival time of the k−th multi path component relative to the l−th cluster. The statistics of the channel for a given t are thus given by the statistics of $\tau_{k,l}$, T_l and $\alpha_{k,l}$. In the next section we describe the set of channel measures that were conducted to obtain the statistics for those parameters.

5.2 BAN-UWB Channel measuring campaigns

Previous studies such as [26] have shown that typical on body channel impulse responses are the result of two additive propagation parts: first the **diffraction components** corresponding to waves on the body surface and a second part corresponding to **reflections** of the environment. Total channel characterization can therefore be divided in the diffraction channel characterization and the reflection channel characterization. In this work, channel measurements are done in an anechoic chamber and are intended to obtain the diffraction model.

5.2.1 Experimental set-up

Measurements are performed in an anechoic chamber. A Vector Network Analyzer (VNA) is used and the complex frequency transfer function of the

channel, S-parameter S_{21}, is recorded for a large set of discrete frequencies in the range from 1 to 12 GHz. Specifically, the particular vector network analyzer is the ZVA40 model from Rhode & Schwarz. This analyzer allows measuring magnitude and phase of a signal from 300 kHz to 50 GHz with up to 150 dB dynamic range. Two antennas are connected to the VNA by means two MFR-57500 cables, a 5m length A94-245 and 9 m length A90-199. These cables are suitable for measured frequency ranges and their attenuation will not affect the measure thanks to the calibration process of the VNA.

The VNA setup is summarized at Table 6, basically transmission power was 10dBm, the sampling frequency (f_s) 24GHz, the measurement frequency range was from 1GHz to 12GHz and with a bandwidth resolution (ΔBW) of 1 KHz and the frequency step (Δf) was 50MHz. As a result, 221 complex samples in frequency domain were obtained for each repetition. The sweep time was 500ms and 100 repetitions were taken for each spatial point.

Location	Anechoic Chamber (ENSTA)
Measurement System	VNA R&S ZVA40
BW, Δf (GHz)	[1 – 12]
Resolution BW (kHz)	1
frequency step, δf (MHz)	50
frequency samples, N	221
Sweep time (ms)	~ 500
Source power (dBm)	10
Cable length	X+ Y
Cables attenuation	A(f1), B(f2), C(f3)

Table 6. Parameter setting for channel measurement in the Anechoic Chamber

The post processing of measured data from the VNA follows the Hermite process, this is, the measurement from the signal parameter $S_{21}(w)$ from the lowest frequency to origin is completed with zeros (zero padding), later, we add the symmetric complex conjugate to obtain the complete signal parameter. After that the real Channel Impulse Response (CIR) is obtained applying Inverse Fourier Transform (IFFT).

Antennas

During the measuring campaign design the choice of the antenna among a set of available antennas was made based on the antenna's performance in the measured band. Figure 44 shows the S_{11} parameter with respect to the frequency for the set of 6 antennas that where compared. Best performance in the 1-12 GHz range was for the Dual-Fed Microstrip Monopole antenna with Dielectric Lens (DFMM-DL) [198] and for the monocone antenna. We have selected the DFMM-DL antenna that been designed and manufactured at the Laboratory of Electronics and Computer Engineering of the ENSTA[2] in Paris.

[2] ENSTA: École Nationale Supérieure de Techniques Avancées (France).

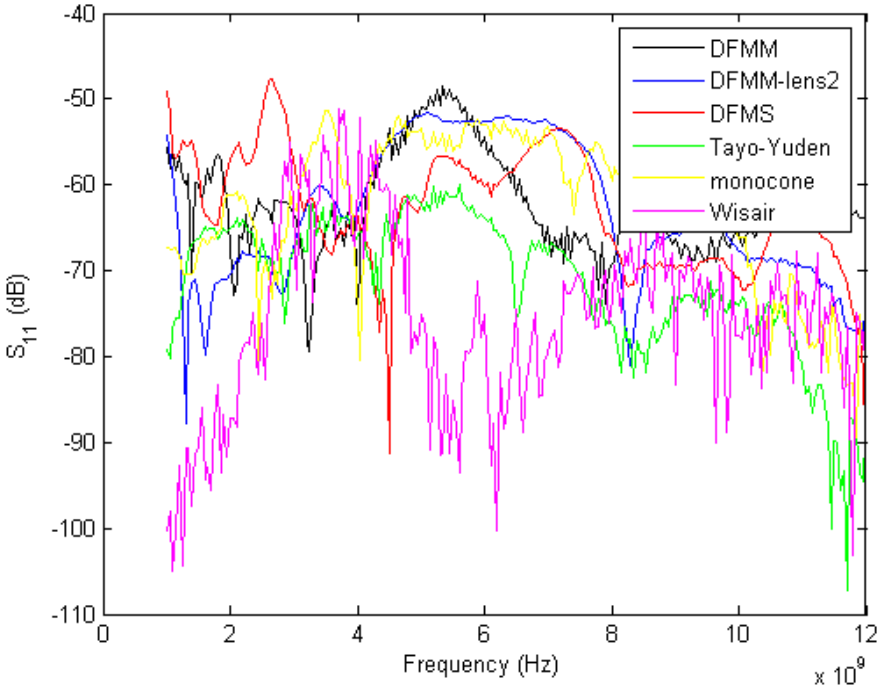

Figure 44. Antenna comparison (S_{11}) in the measured frequency band.

Each measurement was made with (Dual-Fed Microstrip Monopole antenna with Dielectric Lens) DFMM-DL directive antennas [198]. The DFMM-DL antenna is a 33 mm x 20 mm x 11.5 mm UWB semi-directional antenna. It combines a quasi omni-directional radiator with a dielectric lens which focuses the radiation. This type of antenna, when placed on the body directs the radiation opposite to the body, thus avoiding radiation towards the body. That is beneficial since it increases the level of power that is lost by body absorption. The achieved input bandwidth is 3.9-15 GHz. Its main lobe covers a large zone. This should be a good trade-off in order to improve the link-budget margin, i.e. the power attenuation that is allowed without compromising correct

signal reception, while preserving the robustness of the link and the small size of the antenna.

Figure 45. DFMM-DL antenna by the ENSTA.

In order to measure the channel in the scenarios representative for the neural signal monitoring application, a set of transmitter and receiver positions were defined. **Figure 46** shows the complete set of positions. The transmitter is placed on the head at four different locations: top, right side, left side and back of the head. Receiver is according to two different types of applications. First, for applications were the receiver is a hand-held device, receiver antenna is placed at six probable hand-held device locations along the body: in the hand with extended arm, in the hand with half extended arm, in the hand with the arm flexed to the chest, near the ear (talking on the phone), in the front pocket and in the back pocket. Second, assuming the receiver would be a wearable device; locations of the receiving antenna are set along 12 different positions along the front and back of the human body. Measurements between each transmitter and each receiver result in a total of 72 different arrangements corresponding to 72 different propagation channels. Table 7 shows the transmitter and receiver positions together with the corresponding channel number and link distance.

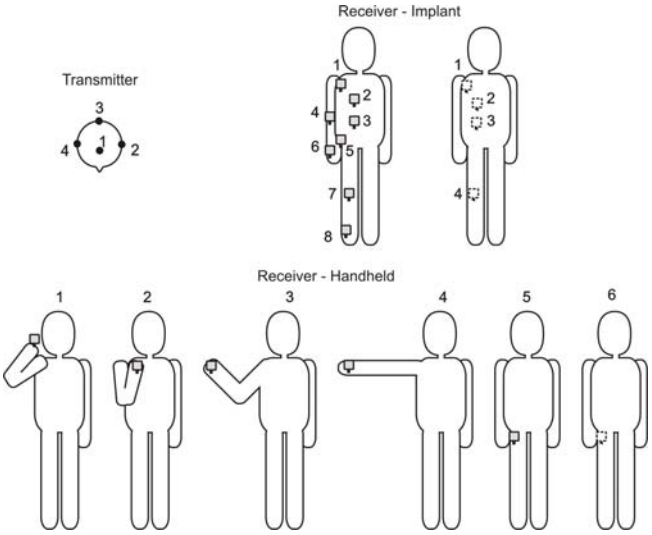

Figure 46. Transmitter and receiver positions.

The whole set of measures was repeated for two subjects, one male and one female in order to analyze subject variability. However measures in the conference room were performed on the female subject only.

		Distance [cm]							
		Female				Male			
		TX1	TX2	TX3	TX4	TX1	TX2	TX3	TX4
Front	1	43	33	34	27	40	33	28	26
	2	59	35	41	28	50	31	33	29
	3	75	56	60	50	63	45	50	43
	4	69	56	54	50	70	60	56	55
	5	80	66	69	62	85	68	65	67
	6	92	83	78	75	96	88	77	80
	7	133	113	111	102	130	124	120	117
	8	174	154	151	146	170	157	154	155
back	b1	44	34	23	35	50	41	25	38
	b2	50	40	38	52	57	48	32	50
	b3	74	56	50	56	79	52	48	61
	b4	128	115	109	118	137	128	110	120
Hand-held	h1	21	28	15	1	23	33	16	3
	h2	32	20	28	21	34	20	29	19
	h3	68	64	60	56	54	65	48	50
	h4	89	86	81	80	84	95	78	80
	h5	97	79	80	78	93	76	80	77
	h6	88	80	70	78	103	90	78	90

Table 7. Link distances.

5.3 BAN-UWB modeling results

5.3.1 Averaged Power Delay Profiles (APDPs)

The power delay profile of the channel is an average power of the channel as a function of an excess delay with respect to the first arrival path which is denoted by the variable τ [194]. APDPs have been calculated by averaging the 100 sweeps taken at each transmitter/receiver combination. This is done in order to reduce noise in the measures.

Figure 47 contains the 3-D Averaged Power Delay Profiles for all the valuated channels. Each figure groups channels with the same transmitter position. Separate subplots are given for male and female subjects. Although no quantitative conclusions can be extracted from the graphs, they are useful in order to have a global view of the measured channels and in order to see the energy concentrations in each case. They may also become convenient to point out at first glance any big differences between the two subjects can be observed.

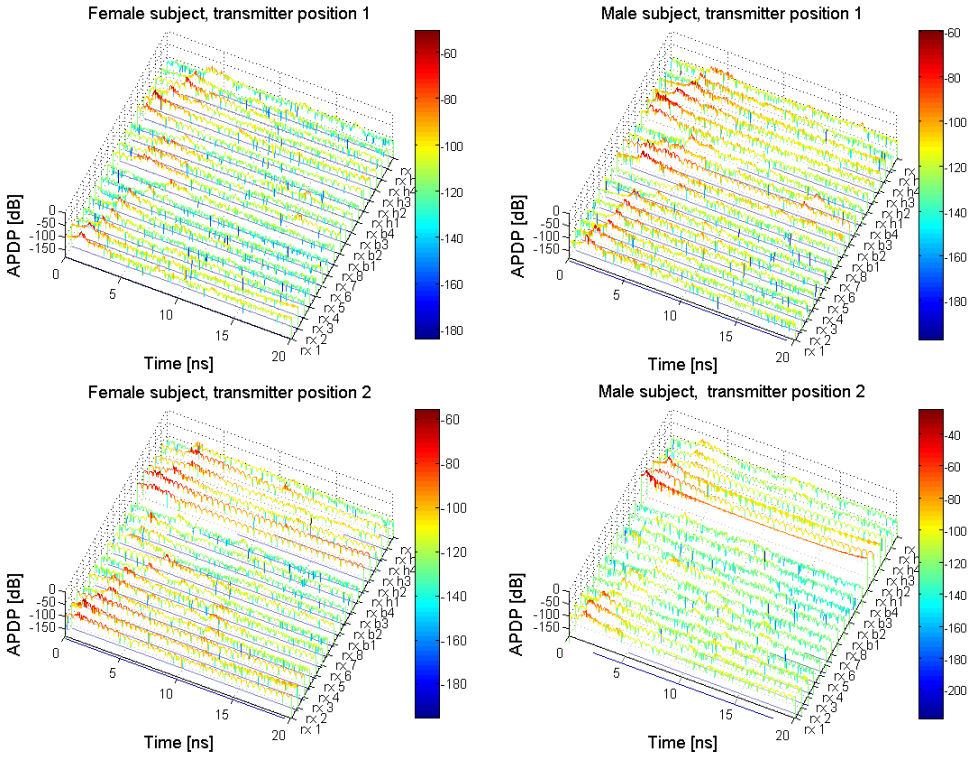

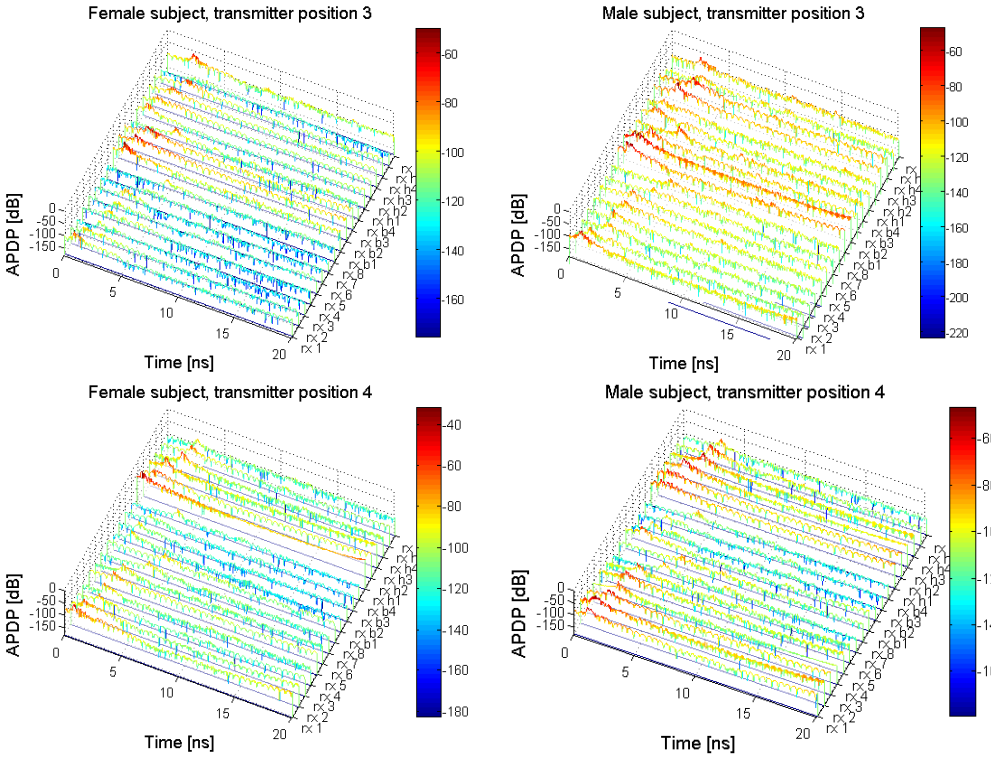

Figure 47. Averaged Power Delay Profiles of the 72 channels grouped by transmitter position and by subject.

5.3.2 Dispersion Parameters

Mean excess Delay (τ_m) and RMS Delay spread (τ_{RMS}) parameters are calculated according to (5-4) and (5-5), respectively [195].

$$\tau_m = \frac{\sum_{l=0}^{L-1}\sum_{k=0}^{K-1}\alpha_{k,l}^2 \cdot \tau}{\sum_{l=0}^{L-1}\sum_{k=0}^{K-1}\alpha_{k,l}^2}; \quad (5\text{-}4)$$

$$\tau_{RMS} = \sqrt{\tau^2 - \left(\tau_m\right)^2} \quad (5\text{-}5)$$

where $\alpha_{k,l}$ is the amplitude of the measured multi path component (MPC).

Bandwidth and Time coherence can be approximately calculated from τ_{RMS} as $B_C = 1/50 \times \tau_{RMS}$ and $T_C = 9/16\pi f_d = 9c/16\pi v f_c$ respectively. Where c is the speed of light, f_d is the Doppler frequency $f_d \simeq \frac{v f_c}{c}$, f_c=5,5GHz is the central frequency and $v \simeq 1,5\ m/s$ is the average human body speed. Average human body speed is taken for coherence time calculation since channel variability measures have not been taken.

Figure 48 shows the relation between the RMS delay spread, the signal bandwidth and whether the channel presents a frequency-selective or flat fading. The figure is extracted from [194].

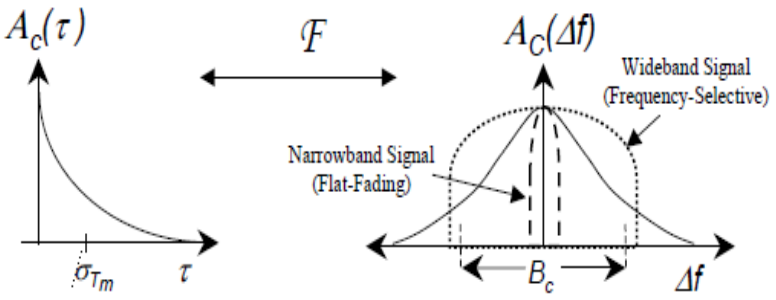

Figure 48. Power Delay Profile (Ac(τ)), RMS delay Spread and Coherence Bandwidth. σTm corresponds to the RMS delay spread (τRMS).

All presented parameters are listed in Table 8 where results are separated in three columns. The first column shows the calculated parameters when all the measures have been taken into account. The second and third columns present the results for transmitter and receiver positions in which there is line-of-sight (LOS) or not (NLOS), respectively.

	ALL	LOS	NLOS
τ_{m} [ns]	1.06	0.65	1.40
τ_{RMS} [ns]	1.81	1.30	2.24
B_C [MHz]	11.05	15.44	8.91
T_C [ns]	9.76	9.76	9.76

Table 8. Calculated channel dispersion parameters

RMS delay spread values are comparable to those obtained in measures along the torso in [181]. Coherence bandwidth of 11.05 MHz implies that for signal bandwidths up to 11MHz, which is not the case in UWB, the channel is flat and thus the signal will experience "flat fading" [194]. For negligible ISI the Symbol rate should be much smaller than the inverse of the RMS delay spread [194], $\mathrm{T_S} \gg \tau_{RMS}$, i.e. $\mathrm{T_S} \gg 10 \cdot \tau_{RMS} = 10 \cdot 1.81 = 18.1\ ns.$ This implies a maximum symbol rate of $1/\mathrm{T_S} = 55.2$ Msymbols/s.

5.3.3 Large scale statistics (Path Loss)

As explained in detail in [194] and other well-known books on the topic, the linear path loss of the channel is the ratio of transmitted power to received power:

$$PL = \frac{P_t}{P_r} \tag{5-6}$$

which we can express also as the difference in dB between the transmitted and received signal power:

$$PL(dB) = 10 \cdot \log_{10}\left(P_t / P_r\right) \tag{5-7}$$

Path loss is caused by dissipation of the power radiated by the transmitter as well as effects of the propagation channel. Path loss models generally assume that path loss is the same at a given transmitter-receiver distance. Shadowing is caused by obstacles between the transmitter and receiver that attenuate signal power through absorption, reflection, scattering, and diffraction. When the attenuation is very strong, the signal is blocked. Variation due to path loss occurs over very large distances (100-1000 meters), whereas variation due to shadowing occurs over distances proportional to the length of the obstructing object (10-100 meters in outdoor environments and less in indoor environments). Since variations due to path loss and shadowing occur over relatively large distances, this variation is sometimes referred to as large-scale propagation effects. Variation due to multipath occurs over very short distances, on the order of the signal wavelength, so these variations are sometimes referred to as small-scale propagation effects.

Obtaining a probabilistic model of the path loss is important in the design of a communications system because if one knows the value of the received power which is needed for a successful communication and the probability for a given path loss between transmitter and receiver, one can obtain the communication range as a function of the transmission power.

We will use an empirical path loss model in dB between the transmitting and the receiving antenna as a function of the distance d. It is based on the Friis

formula in free space [194] and where the random effects of shadowing are modeled as a random process:

$$PL(d) = PL(d_0) + 10 \cdot n \cdot \log_{10}\left({}^{d}\!/\!_{d_0} \right) + S \qquad (5\text{-}8)$$

Where d_0=10cm is the reference distance n is the path-loss exponent and S is a normally distributed variable with zero mean and standard deviation σ representing the Shadowing. Shadowing is the result of the random variations due to blockage from objects in the signal path, which give rise to changing values of the received power at a given distance. Such variations are also caused by changes in reflecting surfaces and scattering objects.

In Figure 49 one can see the result of fitting the measurement points to the above mentioned model. The analysis is performed for the whole measurement set and also for the separated in LOS and NLOS channels. One can observe that is all the cases the polynomial power decay behavior of propagation is almost completely obscured by the superimposed shadowing. On the right side of the figure we observe that the power variations due to shadowing can be realistically modeled as random normally distributed variables with standard deviation of about 12dB for both LOS and NLOS channels is of about 15dB if we consider the whole data set (LOS and NLOS) together.

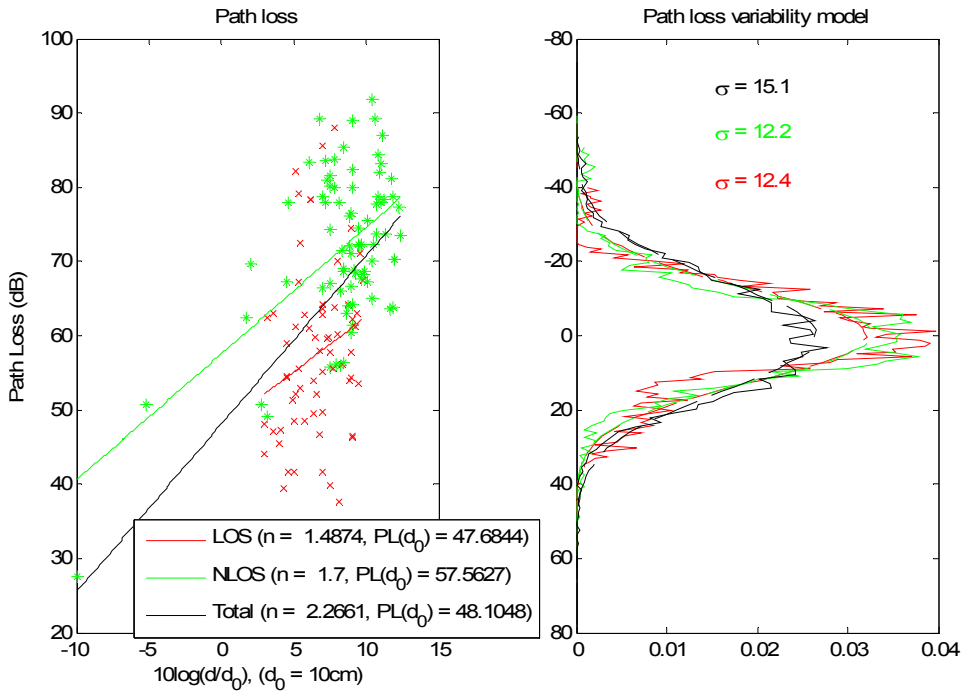

Figure 49. Path loss linear fit (left) and Shadowing model fit.

Comparison of our results with previous IEEE WPAN models [199]

The path loss figures extracted from our measurements in the anechoic chamber have been compared with figures provided by the IEEE WPANs Working Group [199] for the S4 to S5 scenarios: Body surface to body surface CM3 (Scenario S4 & S5) for 3.1-10.6 GHz (see Table 9).

In [199], two different models A and B are presented based on 2 separate measurement campaigns. A and B measures where performed around and along a human torso respectively. Table 10 and Table 11 present the IEEE models A and B together with our measurements' results (right-most column). Model B is based on measures along torso where there is no obstacle between transmitter and receiver, that is why we have compared that model with our

LOS results. Path loss at 10 cm and path loss exponents obtained by us are comparable to those published by the IEEE BAN working group, however our measures present much higher path loss variability at each distance point. This can be due to the effect of the subject's head shadowing, i.e. whether the head presents an obstacle or not in the channel probably affects in the total path loss more than the distance.

Scenario	Channel Description	Frequency Band	Model
S1	Implant to Implant	402-405 MHz	CM1
S2	Implant to Body Surface	402-405 MHz	CM2
S3	Implant to External	402-405 MHz	CM2
S4	Body Surface to Body Surface (LOS)	13.5, 50, 400, 600, 900 MHz 2.4, 3.1-10.6 GHZ	CM3
S5	Body Surface to Body Surface (NLOS)	13.5, 50, 400, 600, 900 MHz 2.4, 3.1-10.6 GHZ	CM3
S6	Body Surface to External (LOS)	900 MHz 2.4, 3.1-10.6 GHZ	CM4
S7	Body Surface to External (NLOS)	900 MHz 2.4, 3.1-10.6 GHZ	CM4

Table 9. IEEE WPANs Working Group on-body scenarios[3].

[3] Table is extracted from [199]

	IEEE Along torso		Our measurements (LOS & NLOS)
	(0mm antenna-body)	(5mm antenna-body)	
PL model	$PL(d)[dB] = P_0[dB] + 10 \cdot n \cdot \log_{10}\left(d/d_0\right)$		
P_0 dB	56.5	44.6	48.1
d_0 m	0.1	0.1	0.1
n	3.1	3.1	2.3
• n: Path loss exponent • P_0: Path loss at the reference distance • d_0: Reference distance			

Table 10. Measured parameters vs. IEEE model 8.2.7. B

	IEEE Around torso	Measured (LOS & NLOS)
PL model	$PL(d)[dB] = a + b \cdot \log_{10}(d) + N$	
a dB	34.1	48.1
b	-31.4	-22.6
σ_n	4.85	15.1
• a and b : Coefficients of linear fitting • d : Tx-Rx distance in mm • N: Normally distributed variable with zero mean and standard deviation σ_n		

Table 11. Measured parameters vs. IEEE model 8.2.7. A.

5.3.4 Small scale statistics

As stated in section 5.1.3, to characterize the channel model we need to determine the statistics for the number of clusters (L) and MPC (K), the amplitude contributions ($\alpha_{k,l}$), the cluster arrival times (T_l) and the MPCs arrival times is the arrival time of the k−th multi path component relative to the corresponding ($\tau_{k,l}$). Here we will obtain the statistics for those variables.

Number of Clusters and MPCs (L, K)

To identify the number of clusters in a particular APDP we use visual inspection as it is done in previous works like [183], [184], [201] and [202], because as far as we know, robust algorithms for cluster identification have not yet been found. Once clusters have been identified, we obtain the average number of clusters $\overline{L}$ by just averaging the count through the whole set of measured APDPs.

In the same way, the average number of MPCs $\mu_{k,l}$ is obtained by averaging the number of MPCs per cluster through all the APDPs.

When fitting the obtained distributions for the number of clusters and for the number of MPCs to a probabilistic distribution, we find that they can both be represented as an exponential distribution of the form:

$$f\left(x\middle|\lambda\right)=\frac{1}{\lambda}e^{-\frac{1}{\lambda}x} \tag{5-9}$$

Or specifically for each of them:

$$\begin{aligned} f\left(x\middle|\overline{L}\right)&=\frac{1}{\overline{L}}e^{-\frac{1}{\overline{L}}x}\\ f\left(x\middle|\mu_{k,l}\right)&=\frac{1}{\mu_{k,l}}e^{-\frac{1}{\mu_{k,l}}x}\end{aligned} \tag{5-10}$$

Figure 50 shows the histogram for the number of clusters while in Figure 51 we observe the exponential fit of the cumulative distribution function for the number of MPCs. **Table 12** presents the resulting fit parameters.

The number of significant MPCs gives an indication of the number of RAKE fingers required to extract most of the channel energy and significantly influences

the performance of many UWB receivers [203]. Given the high number of MPCs, the RAKE receiver will require many fingers if all the scattered energy is to be collected. However a trade-off between complexity of the receiver and transmission power will need to be done.

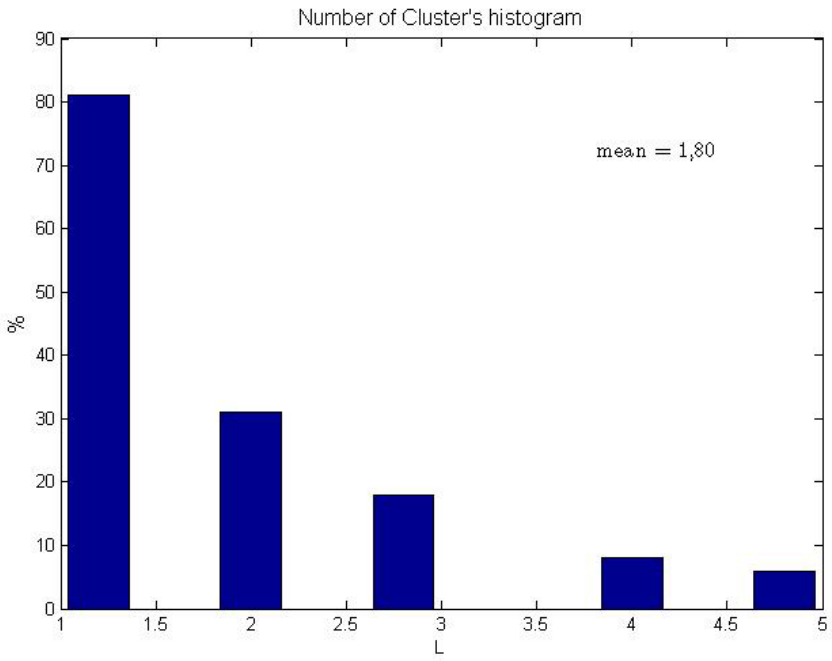

Figure 50. Histogram for the number of clusters.

	ALL	LOS	NLOS
L	1.80	1.20	2.31
μ_{kl}	38.68	40.06	38.07

Table 12. Average values for the number of clusters and MPCs.

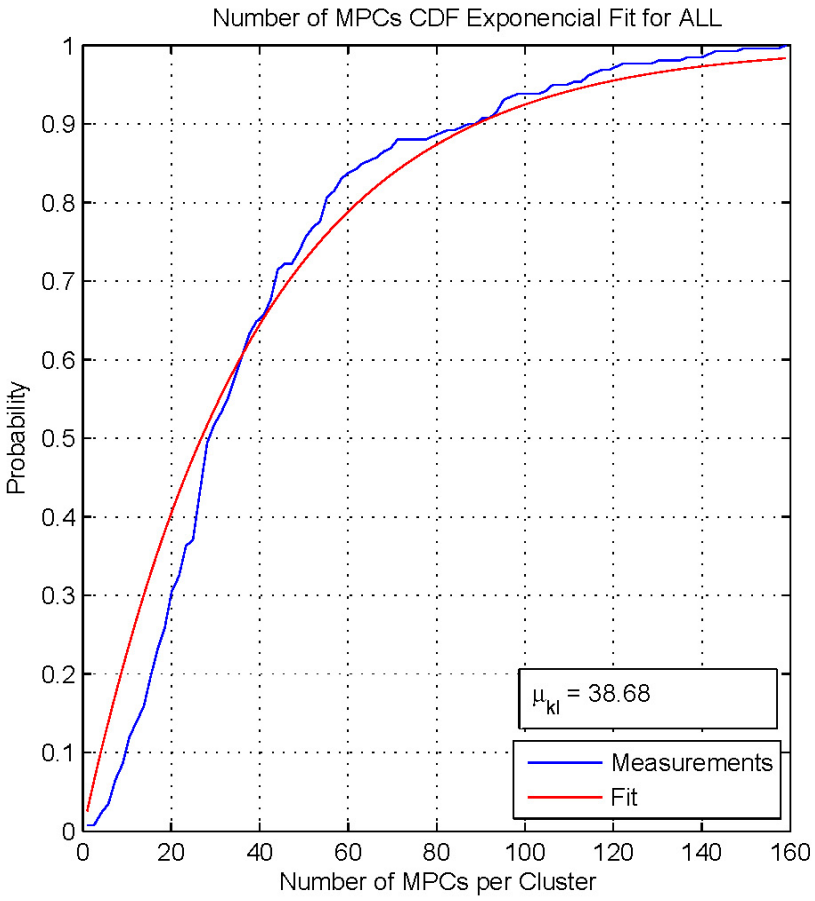

Figure 51. Number of MPCs, Cumulative Distribution

Small Scale Amplitude ($\alpha_{k,l}$)

During the process of model fitting for the amplitude of the MPCs $\alpha_{k,l}$, several candidate distributions like Weibull, Normal, Nakagami and exponential were considered. In Figure 52 the most relevant distributions are compared. Visual inspection shows that the log-normal Cumulative Density Function (CDF) is the curve that best follows the experimental CDF. Moreover when evaluating the fitting errors we find that **log-normal** fitting outperforms both

Weibull and Exponential fits. Root Mean Squared Error for log-normal is 2% while it reaches 5% and 14% for Weibull and Exponential respectively. Fitting parameters and corresponding errors are presented in Table 13.

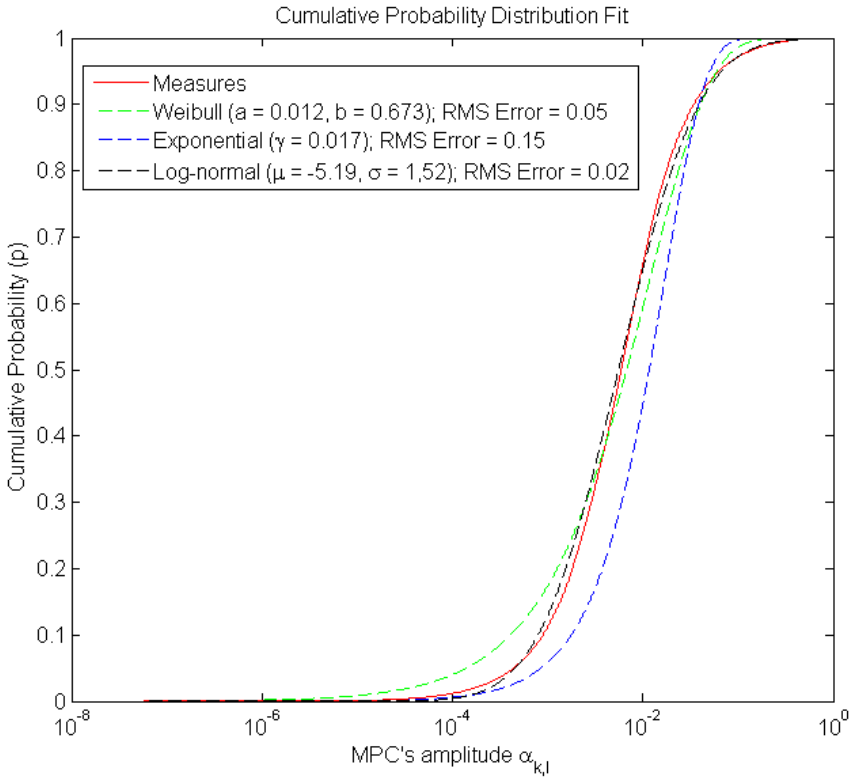

Figure 52. Small Scale Amplitude fit Comparison using candidate distributions: log-normal, Weibull and exponential

	μ	σ	RMS Error
LOS	− 5.52	1.55	2.2 %
NLOS	− 4.90	1.42	2.4 %
ALL	− 5.19	1.52	2.0 %

Table 13. Log normal fit parameters

We therefore derive that normalized small scale amplitudes for all the measurements from APDPs are log normal distributed as (5-11), where x is the small scale amplitude. Distribution parameters μ and σ correspond to the mean and standard deviation of the associated normal distribution.

$$\alpha_{k,l} \simeq L\left\{x\middle|\mu,\sigma\right\} = \frac{1}{x\sigma\sqrt{2\pi}} e^{-\frac{(\ln x-\mu)^2}{2\sigma^2}} \tag{5-11}$$

Previous authors like [26], [204], [205] and [206] confirm the log-normal distribution for the amplitude of the MPCs.

Amplitude Decay Factors

Decay factor for Cluster and MPCs amplitudes follow an exponential distribution which can be described (5-12).

$$\overline{\alpha_{k,l}^2} = \overline{\alpha_{0,0}^2} e^{\left(-\frac{\tau_{0,l}}{\Gamma}\right)} e^{\left(-\frac{\tau_{k,l}}{\gamma}\right)} \tag{5-12}$$

Where $\overline{\alpha_{0,0}^2}$, Γ and γ are the expected mean power of the first multipath component and the cluster and MPC exponential decay factors respectively.

In order to characterize parameters Γ and γ, it becomes necessary to isolate each parameter individually. In the case of Γ, we identify the first multipath component of each cluster and its respective delay. Amplitudes are normalized with respect to the strongest MPC and as Γ is an exponential decay factor the natural logarithm of the measurements is taken and therefore we have a linear equation (5-13).

$$\alpha_{0,l}{}^2 = \alpha_{0,0}{}^2 \cdot e^{-\frac{\tau_{0,l}}{\Gamma}}; \tag{5-13}$$

$$
\begin{aligned}
&\alpha_{0,l}{}^2 = \alpha_{0,0}{}^2 \cdot \mathrm{e}^{-\frac{\tau_{0,l}}{\Gamma}};\\
&10\cdot\log\left(\alpha_{0,l}{}^2\right)=10\cdot\log\left(\alpha_{0,0}{}^2\cdot\mathrm{e}^{-\frac{\tau_{0,l}}{\Gamma}}\right);\\
&20\cdot\log\left(\alpha_{0,l}\right)=10\cdot\log\left(\alpha_{0,0}{}^2\right)+10\cdot\log\left(\mathrm{e}^{-\frac{\tau_{0,l}}{\Gamma}}\right);\\
&20\cdot\log\left(\alpha_{0,l}\right)=20\cdot\log\left(\alpha_{0,0}\right)+10\cdot\log\left(\mathrm{e}^{-\frac{\tau_{0,l}}{\Gamma}}\right);\\
&20\cdot\log\left(\alpha_{0,l}\right)=20\cdot\log\left(\alpha_{0,0}\right)-10\cdot\frac{\tau_{0,l}}{\Gamma}\cdot\log(\mathrm{e});\\
&20\cdot\log\left(\alpha_{0,l}\right)=20\cdot\log\left(\alpha_{0,0}\right)-4{,}97\cdot\frac{\tau_{0,l}}{\Gamma};
\end{aligned}
\tag{5-14}
$$

$$
\mathrm{m}_\Gamma = \frac{-4.97}{\Gamma};\quad \Gamma = \frac{-4.97}{\mathrm{m}_\Gamma} \tag{5-15}
$$

The value of the decay factor Γ is obtained by means of a Least Square Fit process where the fit equation is a linear approximation, so the parameter can be calculated as $\Gamma = -(4.97/\mathrm{m}_\Gamma)$ where m_Γ is the slope of the fit equation.

Results are shown in Figure 44 with the normalized amplitude of the first MPC of each cluster plotted against its delay with respect to the first MPC of the APDP.

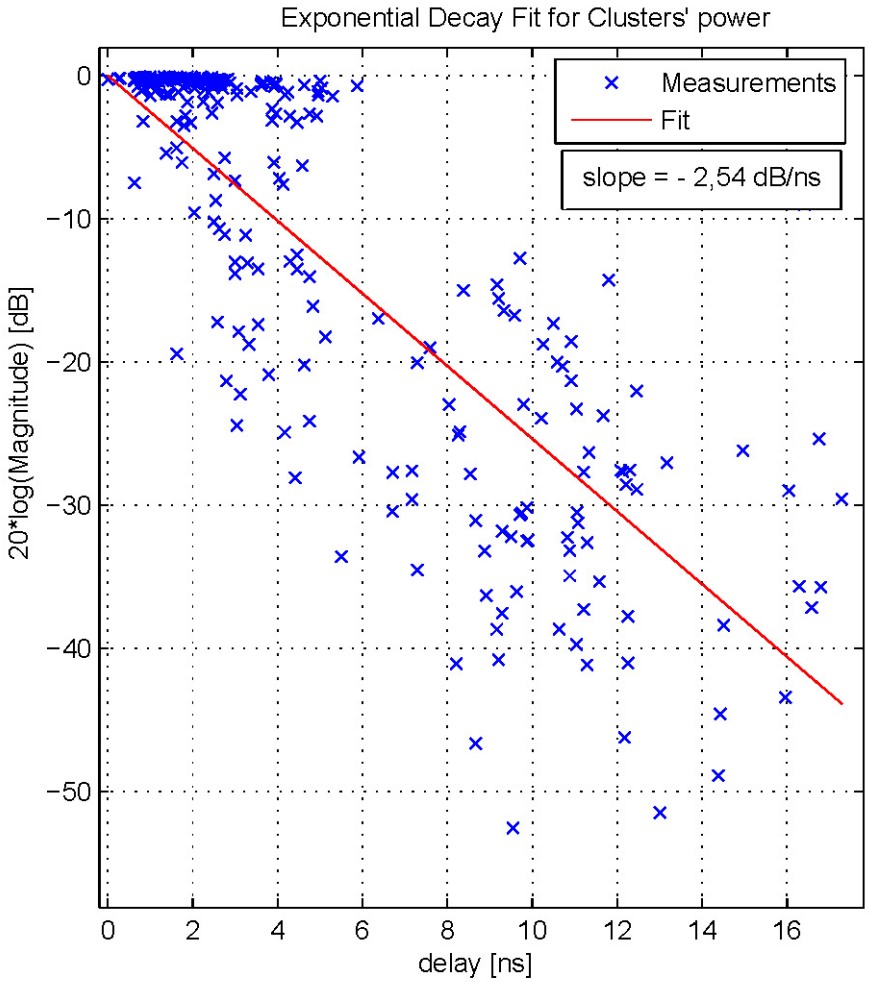

Figure 53. Cluster's Power Decay Factor Fit

We follow a similar procedure to identify the MPC decay factor. In this case, all MPCs inside each cluster are used. Each of the components is normalized and the logarithm taken. Then it is presented against its delay with respect to the beginning of the cluster $\tau_{0,l}$. Following that, MPC decay factor (γ) is calculated using a least square fit algorithm of a linear (5-16).

$$\gamma = m_\gamma x; \quad \gamma = -4.97/m_\gamma \tag{5-16}$$

Table 14 summarizes the resulting parameters for LOS, NLOS and ALL (both LOS and NLOS) scenarios.

	ALL	LOS	NLOS
Γ [ns]	0.39	0.37	0.39
γ [ns]	0.11	0.13	0.10

Table 14. Cluster and MPCS decay factor parameters

Figure 54 presents the fitting results graphically.

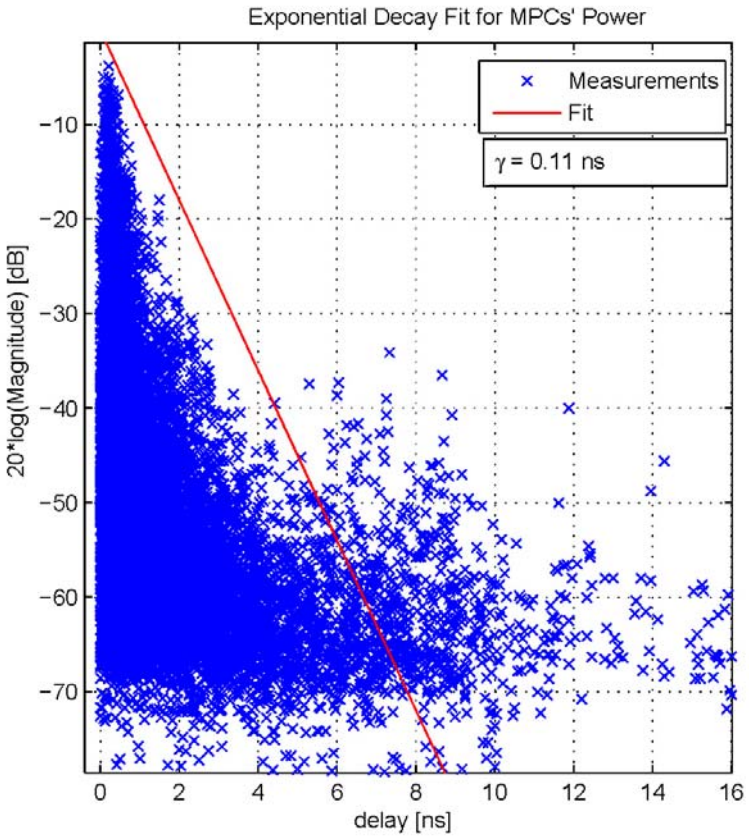

Figure 54. MPC's Power Decay Factor Fit

Clusters and MPCs Inter Arrivals Time's Statistics

As it is stated in previous works as [184], [185] and [200], cluster arrival times follow a Poisson process. Besides, it is also known that if the arrival time follows a Poisson distribution, then the time between two arrivals follows an exponential distribution ([207], [208]). Therefore the inter-arrival time between clusters can be described as and exponential of the form:

$$p\left(T_l \left| T_{l-1}\right.\right) = \Lambda e^{-\Lambda(T_l - T_{l-1})}, \quad l > 0 \tag{5-17}$$

Where $p(T_l|T_{l-1})$ is the conditional probability that a cluster will arrive at time T_l given that the previous one has arrived at time T_{l-1} and $1/\Lambda$ is the mean inter-arrival time between Clusters.

Once defined that the model for the inter-arrival times follows an exponential distribution we will fit the parameter Λ using the Complementary Cumulative Distribution Function ($CCDF_{exp}$, the probability of the variable to be above the level). See eq. (5-19).

$$\begin{aligned} CDF_{\exp} &= p\left(\Delta t \le x\right) = \int_0^x p(\Delta t)\cdot d\Delta t = \int_0^x \Lambda \cdot e^{-\Lambda\Delta t}\cdot d\Delta t \\ CDF_{\exp} &= -e^{-\Lambda\Delta t}\Big|_0^x = -e^{-\Lambda x} - -e^{-\Lambda 0} = -e^{-\Lambda x} + 1 \\ CCDF_{\exp} &= p\left(\Delta t > x\right) = 1 - CDF_{\exp} \end{aligned} \tag{5-18}$$

$$CCDF_{\exp} = e^{-\Lambda x} \tag{5-19}$$

Additionally, in order to ease the fitting process, the $CCDF_{exp}$ is log-scaled so that Λ can be obtained by means of a linear fit as shown in (5-20).

$$\ln(CCDF_{\exp}) \; = \; -\Lambda x \tag{5-20}$$

Figure 55 plots the results of the fitting process and Table 15 presents the fitted parameters for the LOS and NLOS scenarios separately and also for the combination of both (ALL).

	ALL	LOS	NLOS
Λ [ns^{-1}]	0.36	0.39	0.35

Table 15. Cluster inter arrival times

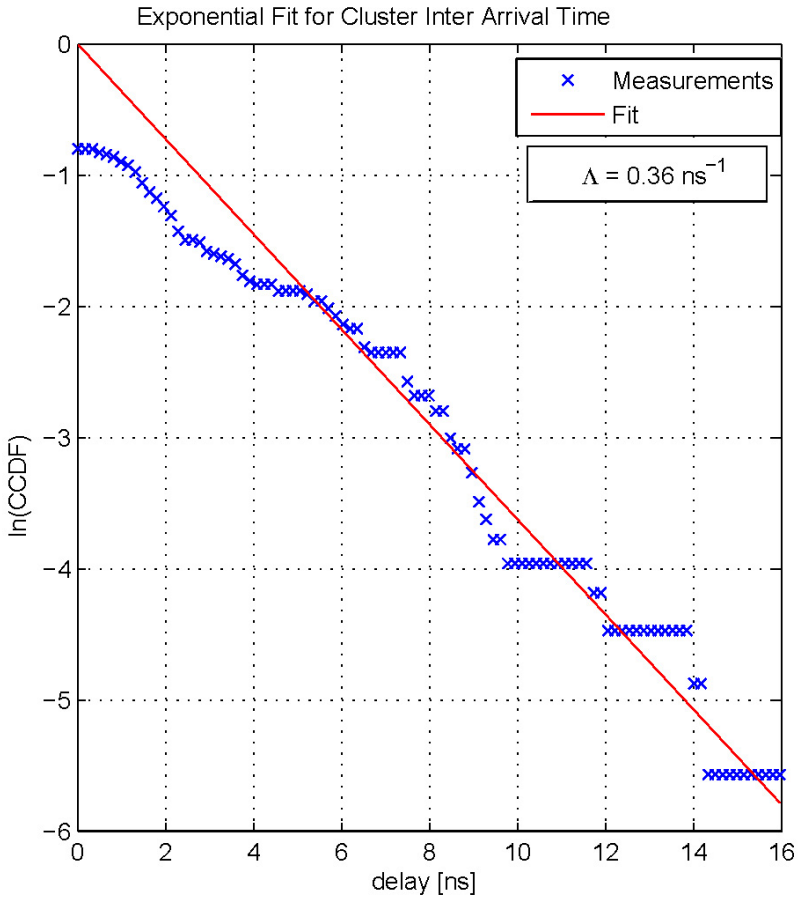

Figure 55. Clusters Inter Arrival Time Fit

The statistical model for MPCs inter-arrival time is deduced in a similar way. Previous works use simple Poisson process to model the arrival time for

MPCs, however in UWB, inter-arrival time does not follows this behavior. Studies like [184] and [200] present an alternative where a Poisson mixture distribution is proposed as in (5-21).

$$p\left(\tau_{k,l}|\tau_{k-1,l}\right)=\beta\lambda_1 e^{-\lambda_1\left(\tau_{k,l}-\tau_{k-1,l}\right)}+\left(1-\beta\right)\lambda_2 e^{-\lambda_2\left(\tau_{k,l}-\tau_{k-1,l}\right)};\quad \forall k>0 \tag{5-21}$$

Where 1/λ1 and 1/λ2 are the inter arrival mean times of two exponential processes inside the same cluster, and β is the mixture parameter.

Fitted parameters are presented in Figure 56 and least square fitting values are shown in Table 16.

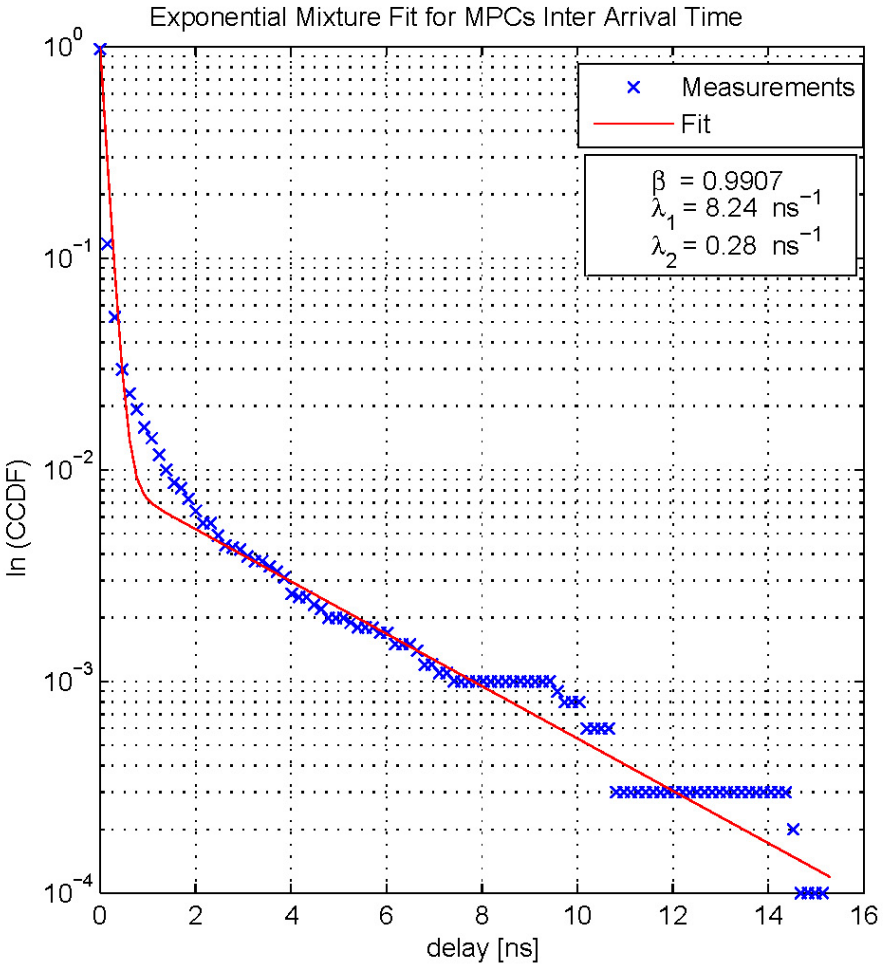

Figure 56. MPCs Inter Arrival Time Fit

	ALL	LOS	NLOS
β	0.9907	0.9910	0.0095
λ_1 [ns^{-1}]	8.24	9.18	0.30
λ_2 [ns^{-1}]	0.28	0.24	7.95

Table 16. MPCs inter arrival times

5.4 Discussion

A statistical BAN channel model is presented for on-body UWB communications. In particular the study is centered in the conditions where the transmitter is placed on the head and the receiver is placed in several parts along the torso, arms or legs. The objective is to study the behavior of the UWB channel surrounding the body.

Dispersion parameters have been calculated and, based on the results, we derive that the coherence bandwidth lies in the range 11-12 GHz, meaning that communication using a signal bandwidth bellow 10 GHz would not experience frequency selectivity, i.e., the channel will be flat-fading [194]. With signal bandwidth B_S = 10 GHz, the symbol time would be T_S = 1/ B_S=0.1 ns. However, on the other hand, if we analyze it in terms of Inter-Symbol Interference (ISI) the channel will not present important ISI as far as the inter-symbol time T_s is bigger than $10\tau_{RMS}$ =18.1ns. This implies a symbol rate of 55 Msymbols/s. Increasing this rate will always man that the ISI effects will need to be softened by using channel equalization techniques.

In the large scale modeling, path loss is modeled as a logarithmic decay with respect to the distance and with a superimposed shadowing effect. The results show that the shadowing effect is so strong that logarithmic behavior is almost hidden by it. These results show higher shadowing (on the order of 15dB power fluctuations) than previous UWB on-body channel models, which that can be explained by the fact that the transmitter is located on the head and it causes stronger diffraction effects in all the measured channels as it presents

an early obstacle to direct transmission. For a communication system this means that the link budget would need to be of about 15dB.

Additionally, in the small-scale field, we show that in the presented scenario, propagation can be described using a modified Saleh–Valenzuela model which presents clusters with Poisson arrival times, a mixed Poisson distribution for MPC arrival times and in which scatterers are sparse. Evidences of cluster overlapping were also observed. The number of clusters and MPCs are exponentially distributed while cluster and MPC's power both present exponential decay with respect to the delay. Inter-arrival time variations are produced because propagated rays have several paths around human body to arrive from transmitter to receiver, diffraction being the dominant process in propagation. Such conditions produce an average of 2-3 clusters in the channel power delay profile, thus the human body behaves as a sparse environment. The surface of the reflecting areas are big (like arms and legs), therefore reflecting rays are propagated and reflected in big scatterers. In this way, arrival paths can have similar delays, thus producing the cluster overlapping observed in our measurements. Body symmetry can be one of the reasons for overlapping clusters since, propagation from head to legs has symmetric reflectors in both sides of the body and therefore two cluster are expected to be produced by the symmetric reflectors. Finally, regarding the small scale amplitude contributions, we conclude that they are log-normally distributed.

This channel model can be used to in realistic on-body UWB channel simulations and help in the design of an UWB communications system to be used in neural signal monitoring systems. For example, the long delay spread can be positive and negative in different senses. It is beneficial because multipath arrivals will undergo fewer amplitude fluctuations (fading) since there will be fewer reflections that cause destructive/constructive interference. But on the negative side, received energy is distributed between a number of clusters. In impulse-based UWB, RAKE receivers would need to be used to capture the energy of several clusters. The fact that the channel is sparse implies that the RAKE receiver will be complex as the number and position of the fingers will need to be calculated to capture the strongest MPCs and thus collecting enough energy for reception, since not every tap carries significant energy. System design falls out of the scope of this work but the proposed channel parameterization will be a starting point of the definition process.

5.5 Performance of an Ultra Wideband wireless system for real-time neural signal monitoring

Taking one step further in the evaluation of UWB for real-time neural signal monitoring, in this section we present the effects of transmission in several scenarios of real neural signals. The purpose of this work is to benchmark the best case performance of UWB for handling spike data, and future work will characterize its performance in moving data from inside to outside of the cranium, scalp or body.

Spike detection quality is selected as the main spiking characteristic of evaluated signals since spike timing information constitutes one of the most relevant neural signal characteristics. That is why transmission effects are evaluated by comparing spiking characteristics between transmitted and received signals presented through corresponding Receiver Operating Characteristics (ROCs) and Area-Under-the-Curve (AUC) for different experimental set-ups.

In order to assess spike detection quality, a set of artificially generated neural signals is constructed from real neural recordings such that the ground truth is known. Data analysis shows how channel Signal-To-Noise-Ratio (SNR) variation affects AUC in different signal SNR cases.

5.5.1 Neural Signal Source and Spike Detection

For the performance evaluation of the wireless transmission system the detected spiking characteristics of the received neural signal are analyzed and presented through corresponding ROCs. As it has widely been discussed in the literature [20], quantitatively assessing spike detection requires knowledge of the ground truth. Recordings from micro-electrode arrays do not allow intra-cellular recording which means that the ground truth is not known. As it is described in Chapter 4, section 4.1.1, in order to overcome this problem we have constructed a set of synthetic signals adding artificially generated neuronal noise with a principal neuron spike train. Signals with different levels of noise, i.e., with different SNRs are used in order to compare the effects of

transmission in varying input SNR conditions. Spike Detection is performed using a thresholding technique as has already been described in section 4.2.

Figure 57 presents the experimental setup that is used to evaluate the performance of the designed wireless UWB transmission system for neural signal monitoring. As described above, the data source is a set of synthetically generated signals from a statistical model resembling real signals. These signals are multiplexed to form one unique bit stream, and then transmitted via the UWB module. On the other end, the UWB module receives the Radio Frequency (RF) and in the next processing stage the BER is calculated considering the transmitted bit stream. The neural signals are then demultiplexed and the spiking quality of the received signals is analyzed in comparison to the original recordings assessing spike detection performance via ROC calculation.

The commercially available product selected to implement the UWB link is the Wisair Development Kit DV9110M, which is based on the WiMedia standard and incorporates two OFDM-UWB transmitter/receiver modules. Each module provides a physical (PHY) and a medium access control (MAC) layer implementation providing Frequency Band Group 1, between 3.168 and 4.752GHz, and an output power of -42dBm/MHz.

Different transmission rate configurations of the UWB module are selected (53.3, 80 and 106.7Mbps) and the wireless link distance is varied between 1, 2 and 3m. As transport protocol the User Datagram Protocol (UDP) is chosen, since, although it does not provide reliability and ordering guaranty, it is fast

and efficient for real-time applications. The experiments are performed in a typical office environment with metallic furniture and cabinets. The signal quality of the received data is analyzed through its spiking characteristics applying the spike detection algorithm described in Section 4.2. For each set-up the experiment is performed 100 times and the resulting mean values are calculated.

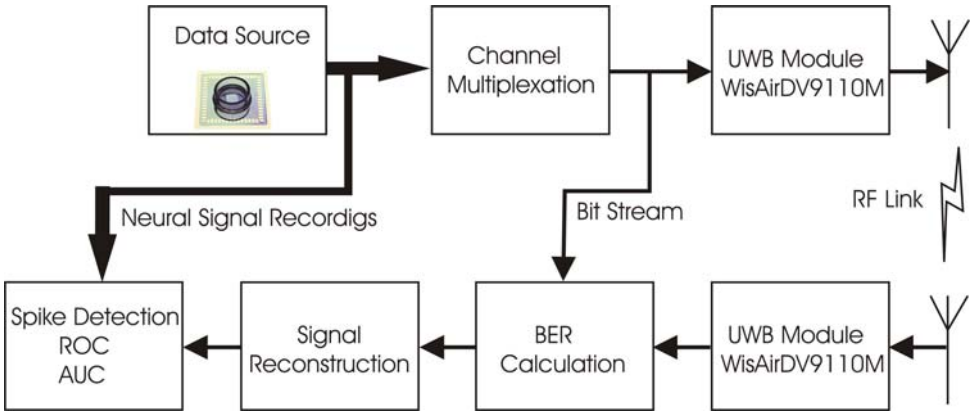

Figure 57. Experimental set-up including data source, UWB link implementing Wimedia standard and signal quality analysis. Data source are a set of synthetically generated signals from a statistical model multiplexed to form one unique bit stream. UWB module DV911M by Wisair receives the RF-signal. BER is calculated and neural signals are reconstructed. Spiking quality of the received signals is analyzed in comparison to the original recordings assessing spike detection performance via ROC calculation.

5.5.2 Results and Discussion

To measure detection quality, ROC curves are used, that show the probability of false alarm versus the probability of detection. The parameter that will be used to compare ROC curves is the Area-Under-the-Curve (AUC), which has value 1 in the case of the ideal detector's ROC, i.e., the area under a step function.

Effect of Channel SNR on Spike Detection

A Matlab™ simulator implementing the UWB Wimedia standard and a wireless indoor channel of 0-4m are used to evaluate the effect of different channel SNRs on spike detection.

Figure 58 explicitly shows channel SNR effects on AUC in various signal SNR cases. Signals with low Signal-To-Noise-Ratios (SNRs) present poor spiking characteristics equivalent to reduced AUC (neural signal with 1dB SNR presents an AUC number of 0.65). Therefore, their spiking characteristics are less affected by varying channel SNR. This can be observed from Figure 58, where for the 1dB signal, the AUC oscillates around 0.5 for low channel SNR and increases up to 0.65 for high channel SNR (AUC variation of less than 30\%), while the spiking characteristics of neural signals with medium and high SNR (4.6dB and 10.6dB in Figure 58 get more deteriorated when channel SNR reduces (from an AUC number of approximately 1 for channel SNR of 15dB reduced to AUC number oscillating around 0.5 for channel SNR smaller than 7dB).

As it can be observed from the figure, the evolution in AUC as the channel SNR improves is not monotonically increasing. The better performance in AUC for signal at SNR = 4.6dB compared to signal at SNR = 10.6dB at medium channel SNR can be an artifact due to the particular data used or due to the Wimedia protocol. The authors are unsure of the true reason of the observed phenomenon.

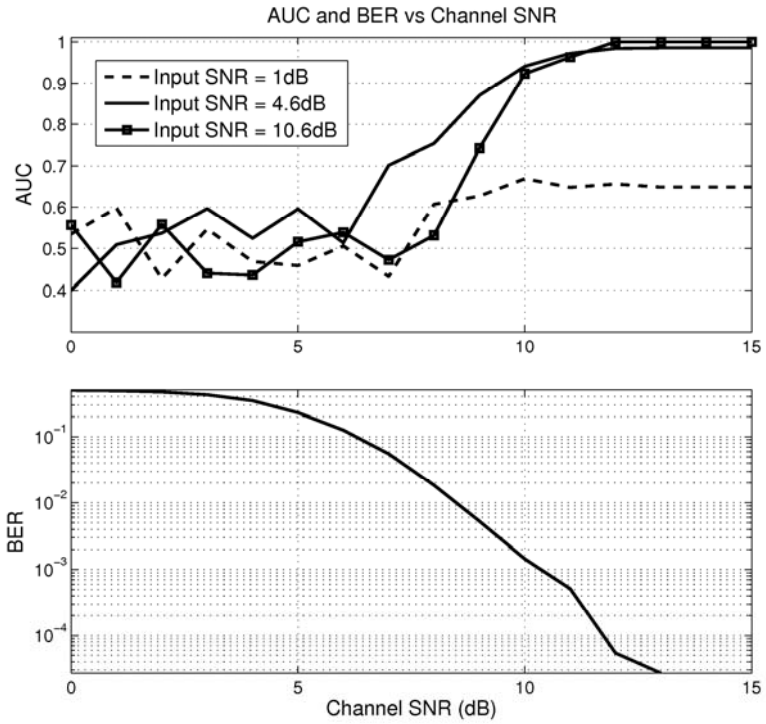

Figure 58. Data show channel quality effects on AUC and how these results are modulated by different signal SNRs. Signals with high SNR get more affected by channel SNR variation than those with reduced SNR. (Bottom) Channel BER versus channel SNR.

Bit Error Rate

Aside from the described computer simulations, in order to evaluate the wireless link communication quality of the experimental set-up described in Figure 57, the Bit Error Rate (BER) is calculated dividing the number of erroneously received bits by the total number of transmitted bits $BER = {}^{erroneous\ bits}/_{total\ bits}$

In Figure 59, the results corresponding to the mean of 100 trials for each configuration (UWB module transmission rate: 53.3 (top), 80 (middle) and 106.7Mbps (bottom); link distance: 1, 2 and 3m) are shown. The mean BER is

plotted versus the actual measured transmission rate. The common characteristic in the three figures and for the three distance cases is that there exists and an inflection point above which the BER increases more rapidly with the transmission rate. That inflection point is situated at about 40% of the configuration rate (23Mbps for the 53.3Mbps case, 32Mbps for the 80Mbps case and 40Mbps for the 106.7Mpbs case). Below the inflection point the BER is below 0.01 for the 1m link, below 0.025 for the 2m link and below 0.07 in the 3m link.

As the actual transmission rate increases also the BER gets higher and when it comes close to the configuration rate, the transmission quality drops dramatically with the BER reaching values of 0.2. Losses from there on are caused by hardware limitations of the UWB module. Furthermore, it can be noticed that the BERs corresponding to 1 and 2m link distances have a similar behavior, but for 3m link distance the BER increases more rapidly at the inflexion point.

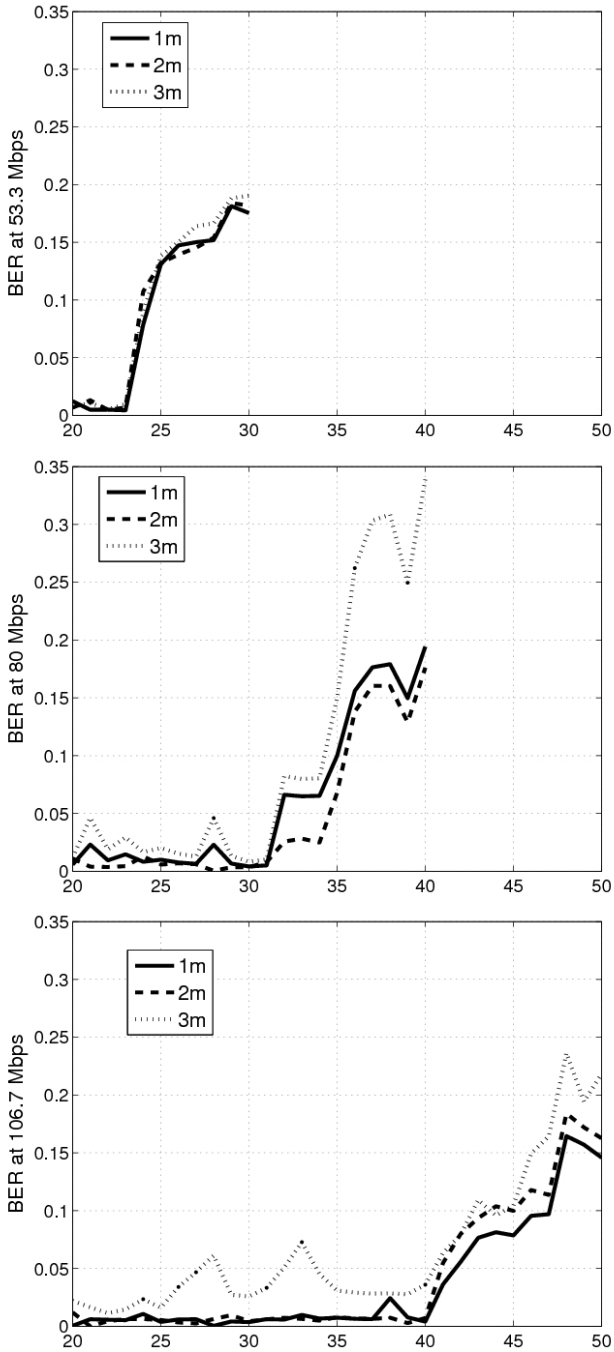

Figure 59. BER for 53.3Mbps (top), 80Mbps (middle) and 106.7Mbps (bottom) at different distances. Evaluation of BER at link layer is considered. Given that Wimedia modes mandatorily support transmission of an acknowledgement, even when UDP is selected, the higher the data rate becomes, the number of retransmissions increases.

Receiver Operating Curves

Evaluation of the transmission quality of the designed system is done through comparison of ROC curves corresponding to transmitted and received signals. This allows studying the degradation of the spiking characteristics of the received signals depending on the BER. The results are compared using the AUC figure.

In Figure 60 an example is shown where the AUC of the transmitted signal is 0.98 while the received signal presents an AUC of 0.95 for a BER of 0.01. As the BER increases, the AUC decreases and the ROC curves show a typical saturation effect that is due to inherent spike losses. In fact, an increasing BER does not modify the received signal such that number of false positives increases but, on the contrary, the number false negatives rises, which is due to data losses introduced by UDP transport protocol. In UDP when the received datagram is erroneous, it is discarded by the receiver.

With no information on the signal contained in the discarded packed, reconstruction is done by replacing the missing segment with a null signal with no spikes and therefore the number of false negatives increases.

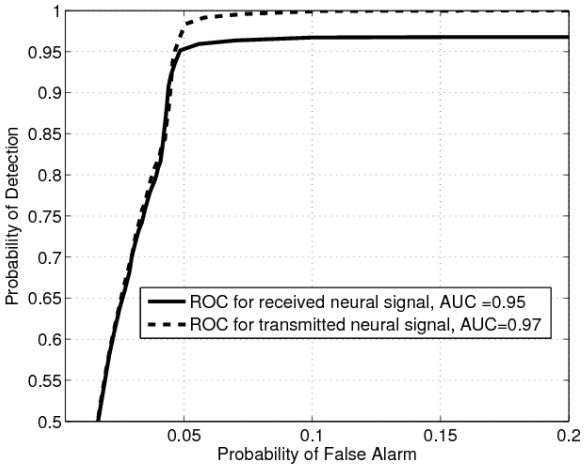

Figure 60. ROC curves for the transmitted and received signal with BER=0.01. NEO detection is used to compute ROC.

Figure 61 shows the AUC depicted against the actual transmission. Signal at SNR = 4.6dB is used in each of the experimental set-ups (UWB module transmission rate: 53.3, 80 and 106.7Mbps; link distance: 1, 2 and 3m). Original calculated AUC for the transmitted signal equals 0.97. Consistently with the results shown in Figure 59, as the BER increases, the detection quality drops. Previous publications state that detectors with acceptable spike detection quality provide a probability of correct detection of around 0.9 with a false positive rate of 5Hz [209]. This corresponds to 0.1 probability of false alarm for an average firing rate of 50Hz. AUC corresponding to such quality in our detector is AUC = 0.95 which means a 5% degradation from the maximum. The results with an AUC below this line do not fulfill the quality requirements and are not suitable for neural signal analysis.

As it can be inferred from Figure 61(top) and Figure 61(middle), for link distances up to 2m, with an UWB module configuration of 106.7Mbps we have

effective transmission rates of up to 40Mbps without dramatic degradation of the signal quality. In these cases, the received signals can be used for further analysis maintaining their fundamental spiking properties.

On the other hand, for link distances higher than 2m (see Figure 61(bottom)), even with the UWB module highest transmission rate configuration, only actual transmission of up to 30Mbps can be achieved without significant spike losses.

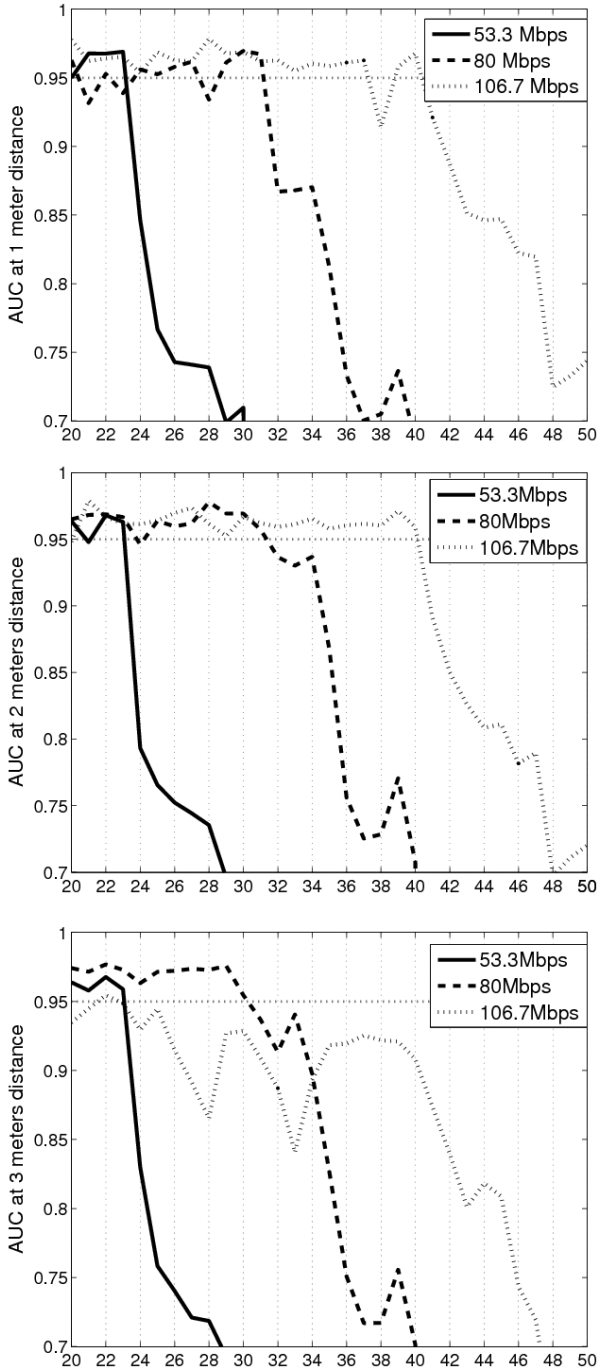

Figure 61. AUC vs. actual transmission rate for all experimental set-ups (signal SNR 4.6dB). Multiplexation of several signal channels yields high signal data rates up to 50 Mbps.

Conclusions and Further Work

In this section, an UWB wireless system for the particular application of real-time neural signal monitoring is evaluated. For performance evaluation the spiking characteristics of the received signals are compared to those of the transmitted signals for different experimental set-ups.

The selected main spiking characteristic of the evaluated signals is the detection quality, an automatic threshold adaptation algorithm to deal with different SNRs. The spike detection results are represented in ROCs and the AUC is calculated as quality indicator. In order to allow correct assessment of the detected spikes, a set of artificially generated neural signals is constructed from real neural recordings such that the ground truth is known.

The experimental set-up involves a commercially available UWB module that is configured for different transmission rates and with several link distances. The spiking quality of the received signals drops as the BER increases, especially as the actual transmission rate comes close to the configuration rate. The received signals exhibit an increase in false negative detection, i.e., spike losses. Increasing BER modifies spiking characteristics of the received signals such that an under-estimation of the spiking frequency is occurs due to spike losses. Acceptable BER values for further signal analysis lie under 0.02. Signals with low SNRs get less affected by reduced channel SNRs than those with higher SNR.

For practical application of real-time neural signal monitoring, UWB seems to offer best transmission conditions in a near-body environment up to 2m. It

allows high-fidelity signal transmission at extremely high data rates with low power consumption.

For the application of UWB in neural signal monitoring the wireless link between the transceiver implanted in the human body and the on-body receiver is composed of two different parts, namely the in-body link and the here considered on-body link. Finally, what is presented here is a proof of concept: The so far collected data represent a benchmark against which future data regarding the degradation of UWB signal through the body can be compared. The results of the present study are an upper bound for in-body communication links. Future work will be devoted to study the BER performance of the in-body link depending on the specific sensor device and considering different tissues, such as nervous cells, cranial bones and dermal tissue.

Chapter 6

Conclusions

As it has been seen during the chapters of this thesis, the main objective for which body centered systems are being developed is to obtain and process biological signals in order to monitor and, in some cases even treat, a physical condition, either a disease or the athletic performance in the case of sports. Since the core of body-centered systems is sensing and processing, signal processing algorithms play a central role in the system's functioning. This thesis is focused on those real-time algorithms that are needed to obtain the relevant information from the sensed signals. In the initial part, the types of sensors and algorithms are reviewed, after that, the thesis deals with two different applications and the related real-time signal processing algorithms are designed and implemented.

The first study case (Chapter 3) is glucose monitoring in diabetes patients, in which learning algorithms for pattern classification are used to the detection of therapeutically wrong measurements of Medtronic's Minimed CGMS. Patients were monitored using CGMS and simultaneously blood samples were taken in a clinical study. Gaussian SVM classifiers are tuned making use of monitor's

electrical signal and glucose estimation. The results show that the classifiers are indeed able to learn the data structure and an overall good detection of wrong measures was obtained in spite of the somewhat low sensitivity of the detector. The classifiers are able to detect the time intervals where the monitor's glucose profile shouldn't be trusted because of wrong measurements. This is illustrated with the detection of hypoglycemic episodes missed by the CGMS.

From the analysis above described, it is concluded that detection of therapeutically wrong measurements given by the continuous glucose monitor Minimed CGMS is feasible through the use of SVM classifiers. For all patients, missed hypoglycemic states were detected, as well as other therapeutically wrong measurements. The presence of False Positives did not alter the conclusions drawn out from the analysis of time profiles. This tool could thus support the clinician in the interpretation of continuous glucose monitor readings. Furthermore, the SVM could be used in the CGMS to generate an alarm for the patient when the CGMS measures could be wrong. In such situations the patient could perform a blood glucose test which would give him the security of a correct measure.

The second application of body centered systems, included in Chapter 4 is neural signal monitoring. Recent medical advances have demonstrated the benefits that such monitoring can bring to medicine and even to other areas as entertainment. That is why nowadays there are many research groups dedicated to develop wireless implantable brain monitors. In this work neural

spike detection, classification and compression algorithms have been implemented and evaluated together with wireless transmission techniques. Such combination will enable in the future the implementation of the wireless brain monitors. A new method for adaptive threshold spike detection has been applied that successfully adapts to different input SNRs eliminating the need for manual threshold setting. For the classification algorithm, a performance of 92% of correctly classified spikes was accomplished. Detection and classifications were used together with a compression and resource management algorithm for efficient wireless transmission of neural signals. The frame-based algorithm is capable of adapting signal compression of the 60 channels at the input according to the neural activity present, the priority set to each channel and the bandwidth available at each processing frame. As a result, signals are compressed and multiplexed in a single transmission frame that adapts to the available bandwidth. The reconstruction algorithm at the receiving side is able to demultiplex and decode signals to reconstruct the spiking patterns. The conjunction of detection, sorting and compression algorithms produce a scheme for neural monitoring system that self-adapts to the signal conditions (adaptive threshold detector) and to the transmission bandwidth. In future research it would be interesting to collaborate with a neural physiology experts in order to evaluate the developed algorithms in a real monitoring environment where signals could be interpreted by experts of neuronal physiology.

Finally, although the main topic of the thesis is signal processing, a chapter has been dedicated to wireless transmission technologies and more precisely to UWB transmission for on-body channels. UWB is selected in this thesis as the most promising transmission technology for body-centered systems because of its characteristics of low-power short-range and high data rates. There are some additional considerations to be regarded. UWB allows only short distance communications with high transmission rates. This is perfectly assumable for body area networks but raises the need of a bridge between the close body field and remote stations. Additionally, UWB can be used for on-body communication, however for implanted neural sensors, as are those described in chapter 4, the signals from neural ensembles still need to be taken out of the skull by means of cables or another wireless technology. Therefore, the wireless link between the transceiver implanted in the human body and the on-body receiver is composed of two different parts, namely the in-body link and the here considered on-body link. This in-body link has not been included in the present thesis but remains a strong handicap for the development of the field. What is presented here is a proof of concept: The so far collected data represent a benchmark against which future data regarding the degradation of UWB signal through the body can be compared. The results of the present study are an upper bound for in-body communication links. In summary, in this work an UWB wireless system for the particular application of real-time neural signal monitoring has been evaluated. For performance evaluation, the spiking characteristics of the received signals are compared to those of the transmitted

signals for different experimental set-ups. Future work will be devoted to study the BER performance of the in-body link depending on the specific sensor device and considering different tissues, such as nervous cells, cranial bones and dermal tissue. The study concluded that for practical application of real-time neural signal monitoring, UWB seems to offer best transmission conditions in a near-body environment up to 2m. It allows high-fidelity signal transmission at extremely high data rates with low power consumption.

Finally, even if body centered systems for medical applications are at the moment a hot topic in biomedical research, for them to become widespread in medical environments, still advances in miniaturization, in implantable materials and in signal processing and transmission will need to be done. The main obstacle is still the high-data rate transmission from implants to monitoring receivers. The conjunction of all these areas of knowledge will eventually produce impressive results in the form of body-centered systems capable of easily monitoring human bio-signals in an easy and comfortable manner. This thesis is a small step towards that objective that is nowadays not very far in the future.

References

Author's published work

Book chapters:

[1] Tarín C. & Traver L. & Martí P. & Cardona N. "Wireless Communication Systems from the Perspective of Implantable Sensor Networks for Neural Signal Monitoring". *Book: Wireless Technology.* Pg. 177-201. Springer US. 2009. ISBN: 978-0-387-71786-9 (Print) 978-0-387-71787-6 (Online).

Scientific publications:

[2] Traver L. & Tarín C. & Martí P. & Cardona N. "Adaptive-threshold neural spike detection by noise-envelope tracking". *Electronics Letters.* (ISSN 0013-5194). 2007, vol. 43 Pg. 1333-1335.

[3] Traver L. & Tarín C. & Martí P. & Cardona N. "Bandwidth Resource Management for Neural Signal Telemetry". *IEEE Transactions On Information Technology In Biomedicine.* (ISSN 1089-7771). 2009, vol. 13. Num. 6. Pg. 1083-1084.

[4] Tarín C. & Traver L. & Cardona N. "Ultra Wideband for Wireless Real-Time Monitoring of Neural Signals". *Medical & Biological Engineering & Computing*. (ISSN 0140-0118), vol. 47. Num. 6. Pg. 649-654. 2009

[5] Tarín C. & Traver L. & Cardona, Narcís. "Wireless Body Area Networks for Telemedicine Applications". *Waves.* (ISSN 1889-8297). Pg. 124-132. 2009

Proceedings:

[6] Traver L. & Tarín C. & Cardona N. "Bluetooth throughput measures for cardiomyocyte extracellular signal telemetry". *3rd International symposium on Wireless Communication Systems (ISWCS 2006)*. September 2006.

[7] Tarín C. & Traver L. & Santamaría J.F. & Martí P. & Cardona N. "Bluetooth-3G wireless transmission system for neural signals telemetry". *Sixth Annual Wireless Telecommunications Symposium (WTS 2007)*. April 2007.

[8] Tarín C. & Martí P. & Traver L. & Cardona N. & Díaz J.A. & Antonino E. "UWB Channel Measurements for Hand-Portable Devices: A Comparative Study". *The 18th Annual IEEE International Symposium on Personal, Indoor and Mobile Radio Communications (PIMRC'07)*. September 2007.

[9] Tarín C. & Traver L. & Martí P. & Cardona N. & Díaz J.A. & Cabedo M. "UWB Channel Measurements for Non-Invasive Wireless Body Area Networks". *3rd IEEE International Conference On Wireless And Mobile Computing, Networking And Communications (WIMOB 2007).* October 2007.

[10] Betancur L. & Cardona N. & Navarro A. & Traver L. "A Statistical Channel Model for On Body Area Networks in Ultra Wide Band Communications". *First IEEE Latin America Conference on Communications (LATINCOM 2009)*.

[11] Betancur L. & Cardona N. & Navarro A. & Traver L. "Modelo estadístico de Canal para Redes de Área Corporal en Canales de Banda Ultra Ancha". *XXIV Simposium Nacional de la Unión Científica Internacional de Radio (URSI 2009).*

[12] Traver L. & Tarín C. & Toledano D. & Roblin C. & Sibille A. & Cardona N. "Head to body UWB-BAN channel measurements". *COST 2100 TD (09)816*, May 2009.

[13] Tarín C. & Traver L. & Bondia J. & Vehi J. "A learning system for error detection in subcutaneous continuous glucose measurement using support vector machines". *IEEE international conference on control applications.* (pp. 1614). 2010.

General References

[14] Ryckaert J. & Desset C. & Fort A. & Badaroglu M. & De Heyn V. & Wambacq P. & Van der Plas G. & Donnay S. & Van Poucke B. & Gyselinckx B. "Ultra-

wide-band transmitter for low-power wireless body area networks: design and evaluation". *IEEE Transactions on Circuits and Systems I*, vol. 52:12, pp. 2515 – 2525. 2005.

[15] Lopez-Casado C. & Tejero-Calado J. & Bernal-Martin A. & Lopez-Gomez M. & Romero-Romero M. & Quesada G. & Lorca J. & Garcia E. "Network architecture for global biomedical monitoring service". *27th Annual International Conference of the Engineering in Medicine and Biology Society.* 2005.

[16] Salamon D. & Bei A. & Grigioni M. & Gianni M. & Liberti M. & D'Inzeo G. & Luca S.D. "Indoor telemedicine in hospital: a PDA-based flexible solution for wireless monitoring and database integration". *27th Annual International Conference of the Engineering in Medicine and Biology Society*. 2005.

[17] Fernández E. & Pelayo F. & Romero S. & Bongard M. & Marín C. & Alfaro A. & Merabet L. "Development of a cortical visual neuroprosthesis for the blind: the relevance of neuroplasticity". *Journal of Neural Engineering,* vol. 2, R1-R12. 2005.

[18] Nicolelis M.A.L. "Actions from thoughts". *Nature*, vol. 409, pp 403–407. 2001.

[19] Obeid I. & Nicolelis M.A.L. & Wolf P.D. "A multichannel telemetry system for single unit neural recording". *The Journal of Neuroscience Methods*, number 133, pp. 33-38. 2004.

[20] Obeid I. & Wolf P.D. "Evaluation of Spike-Detection Algorithms for a Brain-Machine Interface Application". *IEEE Transactions on Biomedical Engineering*, vol. 51, number 6. 2004.

[21] Irazoqui-Pastor P. & Mody I. & Judy J.W. "Transcutaneous RF-powered neural recording device". *Proceedings of the Second Joint EMBS/BMES Conference*, Houston. 2002.

[22] Anderson D.J. & Oweiss K.G. "Capturing Signal Activity and Spatial Distribution of Neurons in a Sub-Millimeter Volume". *Conference Record of the Thirty-Seventh Asilomar Conference on Signals, Systems and Computers*, vol. 1, pp 387-390. 2003.

[23] Hochberg L.R. & Serruya M.D. & Friehs G.M. & Mukand J.A. & Saleh M. & Caplan A.H. & Branner A. & Chen D. & Penn R.D. & Donoghue J.P. "Neuronal ensemble control of prosthetic devices by a human with tetraplegia". *Nature*, vol. 442, pp 164-171. 2006.

[24] Olugbara O. & Adigun M. & Ojo S. & Mudali P. "Utility grid computing and body area network as enabler for ubiquitous rural ehealthcare service provisioning", *9th International Conference on e-Health Networking, Application and Services*, vol. 1, pp. 202–207. 2007.

[25] Monton E. & Hernandez J.F. & Blasco J.M. & Herve T. & Micallef J. & Grech I. & Brincat A. & Traver V. "Body area network for wireless patient monitoring", *IET Communications*, vol. 2, no. 2, pp. 215–222. 2008.

[26] Fort A. & Ryckaert J. & Desset C. & De Doncker P. & Wambacq P. & Van Biesen L. "Ultra-wideband channel model for communication around the human body". *IEEE Journal on Selected Areas in Communications*, vol. 24, no. 4, pp. 927–933. 2006.

[27] Huan-Bang L. & Takizawa K.I. & Bin Zheri & Kohno R. "Body area network and its standardization at IEEE 802.15.MBAN", *16th IST Mobile and Wireless Communications Summit*, vol. 1, pp. 1–5. 2007.

[28] Yoo H.J. & Cho N. "Body channel communication for low energy BSN/BAN", *IEEE Asia Pacific Conference on Circuits and Systems. APCCAS*, vol. 1, pp. 7–11. 2008.

[29] Tayamachi T. & Wang Q. & Wang J. "Transmission characteristic analysis for UWB body area communications," *International Symposium on Electromagnetic Compatibility, EMC,* vol. 1, pp. 75–78. 2007.

[30] Facchinetti A. & Sparacino G. & Cobelli C. "Modeling the error of continuous glucose monitoring sensor data: Critical aspects discussed through simulation studies," *Journal of Diabetes Science and Technology*, vol. 4, no. 1, pp. 4–14. 2010.

[31] Bondia J. & Tarin C. & Garcia-Gabin W. & Esteve E. & Fernández-Real J. & Ricart W. & Vehí J. "Using support vector machines to detect therapeutically

incorrect measurements by the MiniMed CGMS," *Journal of Diabetes Science and Technology*, vol. 2, no. 4, pp. 622– 629. 2008.

[32] Hearst M. "Support vector machines," *IEEE Intelligent Systems,* vol. 13, no. 4, pp. 18–28. 1998.

[33] Kovatchev B.P. & Gonder-Frederick L.A. & Cox D.J. & Clarke W.L. "Evaluating the accuracy of continuous glucose-monitoring sensors: continuous glucose-error grid analysis illustrated by TheraSense Freestyle Navigator data". *Diabetes Care*, vol. 27, no. 8, pp. 1922–1928. 2004.

[34] Suarez K.V. & Silva J.C. & Berthoumieu Y. & Gomis P. & Najim M. "ECG Beat Detection Using a Geometrical Matching Approach". *IEEE Transactions on Biomedical Engineering,* vol. 54, no.4, pp.641-650, April 2007.

[35] De Luca C. J. "Physiology and Mathematics of Myoelectric Signals". *IEEE Transactions on Biomedical Engineering,* vol. BME-26, no.6, pp.313-325, June 1979.

[36] Muller-Putz G.R. & Pfurtscheller G. "Control of an Electrical Prosthesis With an SSVEP-Based BCI", *IEEE Transactions on Biomedical Engineering,* vol. 55, no.1, pp.361-364, Jan. 2008.

[37] Niedermeyer E. & da Silva F.L. "Electroencephalography: Basic Principles, Clinical Applications, and Related Fields". Lippincot Williams & Wilkins. ISBN 0781751268. 2004.

[38] Cataltepe O. & George J. I. "Pediatric Epilepsy Surgery: Preoperative Assessment and Surgical Treatment". Chapter 5 "Invasive Electrophysiologycal monitoring". New York Thieme. ISBN 9781604062540. January 2010.

[39] Hoppe M. & Wennberg R. & Tai P. & Pohlmann-Eden B. Primary. Book Chapter: "EEG in Epilepsy". Book Title: "Textbook of Stereotactic and Functional Neurosurgery". Springer Berlin. ISBN: 978-3-540-69960-6.

[40] Serruya M.D. & Donoghue J.P. Chapter III: "Design Principles of a Neuromotor Prosthetic Device in Neuroprosthetics: Theory and Practice", ed. Kenneth W. Horch, Gurpreet S. Dhillon. Imperial College Press. 2003.

[41] Jacobs J. & Zijlmans M. & Zelmann R. & Olivier A. & Hall J. & Gotman J. & Dubeau F. “Value of electrical stimulation and high frequency oscillations (80–500 Hz) in identifying epileptogenic areas during intracranial EEG recordings”. *Epilepsia*, 51: 573–582. 2010.

[42] Luther N. & Rubens E. & Sethi N. & Kandula P. & Labar D.R. & Harden C. & Perrine K. & Christos P.J. & Iorgulescu J.B. & Lancman G. & Schaul N.S. & Kolesnik D.V. & Nouri S. & Dawson A. & Tsiouris A.J. & Schwartz T.H. “The value of intraoperative electrocorticography in surgical decision making for temporal lobe epilepsy with normal MRI”. *Epilepsia*, 52: 941–948. 2011.

[43] Lin M. & Li B., “A wireless EOG-based human computer interface”. Biomedical Engineering and Informatics (BMEI) 3rd International Conference *on*, vol. 5, oct. 2010, pp. 1794 –1796. 2010.

[44] Guillory K.S. & Askin R.E. & Smith C.F. & McDonnall D. & Hiatt S. & Wilder A.M. “Wireless electrocortigraph (ECoG) recording system”. *Neural Engineering (NER), 5th International IEEE/EMBS Conference*. April 2011.

[45] Viventi J. & Kim D.H. & Vigeland L. & Frechette E.S & Blanco J.A. & Kim Y.S. & Avrin A.E. & Tiruvadi V.R. & Hwang S.W. & Vanleer A.C. & Wulsin D.F. & Davis K. & Gelber C.E. & Palmer L. & Van der Spiegel J. & Wu J. & Xiao J. & Huang Y. & Contreras D. & Rogers J.A. & Litt B. “Flexible, foldable, actively multiplexed, high-density electrode array for mapping brain activity in vivo”. *Nature Neuroscience.* 2011.

[46] Del Gratta C. & Pizzella V. & Tecchio F. & Romani G.L., “Magnetoencephalography—a noninvasive brain imaging method with 1ms time resolution”, *Reports on Progress in Physics*, vol. 64, pp. 1759–1814. 2001.

[47] Valdastri P. & Susilo E. & Förster T. & Strohhöfer C. & Menciassia A. & Dario P. “Wireless implantable electronic platform for blood glucose level monitoring”. *Procedia Chemistry*, proceedings of the Eurosensors XXIII conference, vol. 1, no. 1, pp. 1255 – 1258, 2009.

[48] Lehmann E.D. & Tarín C. & Bondia J. & Teufel E. & Deutsch T. "Incorporating a Generic Model of Subcutaneous Insulin Absorption into the AIDA v4 Diabetes Simulator 3. Early Plasma Insulin Determinations". *Journal of Diabetes Science and Technology*. 3(1): 190–201. January 2009.

[49] Shibata H. & Tsuda Y. & Kawanishi T. & Yamamoto N. & T Okitsu. & Takeuchi S. "Implantable fluorescent hydrogel for continous blood glucose monitoring". *Solid-State Sensors, Actuators and Microsystems Conference, 2009. TRANSDUCERS 2009*. pp. 1453 –1456. June 2009.

[50] Caduff A. & Talary M. S. & Mueller M. & Dewarrat F. & Klisic J. & Donath M. & Heinemann L. & Stahel W. A., "Non-invasive glucose monitoring in patients with type 1 diabetes: A multisensor system combining sensors for dielectric and optical characterisation of skin," *Biosensors and Bioelectronics*, vol. 24, no. 9, pp. 2778 – 2784, 2009.

[51] Oh J. & Cho S. & Oh H. & Ku Y. & Shim B. & Kim M. & Yang Y. & Kim D. & Eum H. & Miller D.R. "The high-quality spectral fingerprint of glucose captured by Raman spectroscopy in non-invasive glucose measurement". *Proc. SPIE 7906*, Volume 7906, pp. 79060G-79060G-8. February 2011.

[52] Tavakoli M. & Turicchia L. & Sarpeshkar R. "An Ultra-Low-Power Pulse Oximeter Implemented With an Energy-Efficient Transimpedance Amplifier". *Biomedical Circuits and Systems, IEEE Transactions on* , vol.4, no.1, pp.27-38, Feb. 2010.

[53] Redlinger R.Jr. & Kelly R. & Nuss D. & Goretsky M. & Kuhn M. & Sullivan K. & Wootton A.E. & Ebel A. & Obermeyer R., "Regional chest wall motion dysfunction in patients with pectus excavatum demonstrated via optoelectronic plethysmography". *Journal of Pediatric Surgery*, vol. 46, no. 6, pp. 1172 – 1176, 2011.

[54] Bellan L. M. & Wu D. & Langer R.S., "Current trends in nanobiosensor technology," *Wiley Interdisciplinary Reviews: Nanomedicine and Nanobiotechnology*, vol. 3, no. 3, pp. 229–246, 2011.

[55] Panescu, D. “Emerging Technologies [wireless communication systems for implantable medical devices]”. *Engineering in Medicine and Biology Magazine, IEEE*, vol.27, no.2, pp.96-101, March-April 2008.

[56] Cannata J. M. & Vilkomerson D. & Chilipka T. & Yang H. & Han S. & Rowe V.L. & Weaver F.A., “A flexible implantable sensor for post-operative monitoring of blood flow.” *Journal of the Acoustical Society of America*, vol. 128, no. 4, pp. 2304–2304, 2010.

[57] Lee J. & Rhew H.-G. & Kipke D. & Flynn M. “A 64 channel programmable closed-loop neurostimulator with 8 channel neural amplifier and logarithmic ADC”. *IEEE Journal of Solid-State Circuits,* vol. 45, no. 9, pp. 1935 –1945. September 2010.

[58] Shnayder V. & Chen B. & Lorincz K. & Thaddeus R. F. & Fulford J. & Welsh M. “Sensor Networks for Medical Care”. *Technical Report TR-08-05, Division of Engineering and Applied Sciences*, Harvard University, 2005.

[59] Shannon C.E. “A mathematical theory of communication”. *Bell System Technical Journal,* vol. 27, pp. 379-423 and 623-656, July and October, 1948.

[60] Feng D.D. “Biomedical Information Technology”. Elsevier. 2007. ISBN: 9780123735836.

[61] Bruce E.N. “Biomedical Signal processing and signal modeling”. Wiley. January 2001. ISBN: 978-0-471-34540-4.

[62] Blahut R.E. “Fast Algorithms for Signal Processing”. Urbana-Champaign. June 2010. ISBN: 9780521190497.

[63] Hayes MH. “Statistical digital signal processing and modeling”. Wiley India. 2009. ISBN: 978-0-471-59431-4

[64] Kuhn H.W. & Tucker A.W. “Nonlinear programming*”. Proceedings of 2nd Berkeley Symposium*. Berkeley: University of California Press. pp. 481–492., 1951.

[65] Karush W. “Minima of Functions of Several Variables with Inequalities as Side Constraints”. M.Sc. Dissertation. Dept. of Mathematics, Univ. of Chicago, Chicago, Illinois, 1939.

[66] Lin Y.-H. & Jan I.-C. & Ko P.C.-I. & Chen Y.-Y. & Wong J.-M. & Jan G.-J. “A wireless PDA-based physiological monitoring system for patient transport ” *IEEE Transactions on Information Technology in Biomedicine*, vol. 8, no. 4, pp. 439–447, Dec 2004.

[67] http://www.iso.org

[68] www.continuaalliance.org

[69] ZigBee Alliance. (http://www.zigbee.org)

[70] http://standards.ieee.org/develop/project/802.15.4.html

[71] Cavalcanti D. & Schmitt R. & Soomro A. “Performance analysis of 802.15.4 and 802.11e for body sensor network applications”. *4th International Workshop on Wearable and Implantable Body Sensor Networks (BSN 2007)*, vol. 13. Springer Berlin Heidelberg, 2007, pp. 9-14.

[72] http://www.ecma-international.org/publications/files/ECMA-ST/ECMA-368.pdf

[73] Bluetooth special interest group: “Specification of the bluetooth system“. http://www.bluetooth.com. 2004

[74] http://standards.ieee.org/getieee802/download/802.11-2007.pdf

[75] IEEE P802.15.6/D01, “Wireless Medium Access Control (MAC) and Physical Layer (PHY) Specifications for Wireless Personal Area Networks (WPANs) used in or around a body”, May 2010.

[76] Zimmerman T.G. “Personal Area Networks (PAN): Near-field intrabody communication”. M.S. thesis, MIT Media Laboratory, 1995.

[77] Hamida E. & D’Errico R. & Denis B. “Topology dynamics and network architecture performance in wireless body sensor networks”. *New Technologies, Mobility and Security (NTMS), 2011 4th IFIP International Conference on*, pp. 1 –6. February 2011.

[78] http://www.echotx.com/

[79] http://www.dexcom.com/products/download-product-information

[80] http://www.medtronic.com

[81] http://www.minimed.com/products/

[82] http://www.s4ms.com/products_glucose.htm

[83] http://www.integrity-app.com/

[84] http://www.freestylenavigator.com/static/cms_workspace/document/FSN-Fact-SheetART18035_REV-A.pdf

[85] http://starlab.es/products/enobio

[86] http://www.neurofocus.com/pdfs/Mynd_NeuroFocus.pdf

[87] http://www.b-alert.com

[88] http://www.brainproducts.com/products_by_apps.php

[89] http://www.neurosky.com/Products/MindWave.aspx

[90] www.medtronic.com/downloadablefiles/197935002.pdf

[91] http://www.brainfingers.com/

[92] http://technosjapan.jp/eng/bio.html

[93] http://www.ibva.co.uk

[94] http://www.btsbioengineering.com

[95] http://www.brainquiry.com/

[96] http://www.braingate.com

[97] http://www.blackrockmicro.com/en/neuroport.html

[98] https://www.rppl.com/products

[99] http://emotiv.com

[100] Campbell A.T. & Choudhury T. & Hu S. & Lu H. & Mukerjee M.K. & Rabbi M. & Raizada R.D.S. “NeuroPhone: Brain-Mobile Phone Interface using a

Wireless EEG Headset". *Proceedings of the second ACM SIGCOMM workshop on Networking, systems, and applications on mobile handhelds.* 2010. ISBN: 978-1-4503-0197-8.

[101] Rothman S.A. & Laughlin J.C. & Seltzer J. & Walia J.S. & Baman R.I. & Siouffi S.Y. & Sangrigoli R.M. & Kowey P.R. "The Diagnosis or Cardiac Arrhythmias: A Prospective Multi-Center Randomized Study Comparing Mobile Cardiac Outpatient Telemetry Versus Standard Loop Event Monitoring". *The Journal of Cardiovascular Electrophysiology*, Vol. 18, No. 3, p 1-7. March 2007.

[102] http://www.medtronic.com/health-consumers/fainting/device/what-is-it/index.htm

[103] http://www.lifesynccorp.com/products/wireless-system.html

[104] http://www.cardiomems.com/CardioMEMS_Physician_Billing_Guide.pdf

[105] http://www.nonin.com/PulseOximetry/Wireless/Avant4000

[106] http://www.cardiacscience.com/cardiology-products/diagnostic-workstation/carecenter-md.php

[107] http://givenimaging.com/en-us/HealthCareProfessionals/Pages/CapsuleEndoscopy.aspx

[108] http://www.olympus-europa.com/endoscopy/2001_5491.htm

[109] http://www.rfamerica.com/sayaka/index.html

[110] http://intromedic.com/en/product/productInfo.asp

[111] http://www.capsule-endoscopy.info

[112] http://www.telemedicsystems.com/index.php?id=9

[113] http://caretrends.net/

[114] http://www.clevemed.com/CrystalMonitor/overview.shtml

[115] http://www.equivital.co.uk/

[116] http://www.gehealthcare.com/euen/patient_monitoring/products/imm-monitoring/index.html

[117] http://www.welchallyn.com/wafor/hospital/connectivity.htm

[118] http://www.proteusbiomed.com/

[119] http://www.toumaz.com/page.php?page=sensium_life_platform

[120] http://fiji.eecs.harvard.edu/CodeBlue

[121] Patel S. & Lorincz K. & Hughes R. & Huggins N. & Growden J. & Standaert D. & Akay M. & Dy J. & Welsh M. & Bonato P. "Monitoring Motor Fluctuations in Patients With Parkinson's Disease Using Wearable Sensors". *IEEE Transactions on Information Technology in Biomedicine*, Volume 13, Number 6 (2009).

[122] www.xbow.com/pdf/Telos_PR.pdf

[123] Polastre J. & Szewczyk R. & Culler D., "Telos: enabling ultra-low power wireless research". *Proceedings of the 4th international symposium on Information processing in sensor networks*, ser. IPSN '05. Piscataway, NJ, USA: IEEE Press, 2005.

[124] http://www.shimmer-research.com/

[125] Crossbow Technology, Inc. MICA2 Series (MPR4x0). http://www.xbow.com/Products/productsdetails.aspx?sid=72.

[126] Crossbow Technology, Inc. MICAz ZigBee Series (MPR2400). http://www.xbow.com/Products/productsdetails.aspx?sid=101.

[127] http://bullseye.xbow.com:81/Products/productdetails.aspx?sid=154

[128] www.dinesgroup.org/projects/images/pdf_files/iris_datasheet.pdf

[129] http://www.memsic.com/products/wireless-sensor-networks/wireless-modules.html

[130] http://platformx.sourceforge.net/

[131] http://staff.www.ltu.se/~jench/mulle.html

[132] http://www.atmel.com/products/microcontrollers/wireless/modules.aspx

[133] http://www.btnode.ethz.ch/

[134] http://www.thisisant.com/

[135] Chen M. & Gonzalez S. & Vasilakos A. & Cao H. & Leung V. C., "Body area networks: A survey". *The Journal Of Special Issues on Mobility of Systems, Users, Data and Computing*., vol. 16, pp. 171–193, April 2011.

[136] http://www.imec.be/ScientificReport/SR2007/html/1384152.html

[137] Ryckaert J. & Van der Plas G. & De Heyn V. & Desset C. & Van Poucke B. & Craninckx J. "A 0.65-to-1.4 nj/burst 3-to-10 Ghz UWB all-digital tx in 90 nm cmos for IEEE 802.15.4a". *IEEE Journal of Solid-State Circuits, vol.* 42, no. 12, pp. 2860 –2869. December 2007.

[138] http://decawave.com/scensor.html

[139] Jovanov E. & Milenkovic A. & Otto C. & de Groen P.C. "A wireless body area network of intelligent motion sensors for computer assisted physical rehabilitation". *Journal of NeuroEngineering and Rehabilitation*, vol. 2:6, March 2005.

[140] International Diabetes Federation, "IDF Diabetes Atlas, 4th edition,"URL: http://www.diabetesatlas.org/downloads, 2009.

[141] Clarke W. & Kovatchev B. "Statistical Tools to Analyze Continuous Glucose Monitor Data". *Diabetes Technology & Therapeutics*, vol. 11, issue s1. 2009

[142] Clarke W.L. & Cox D. & Gonder-Frederick L.A. & Carter W. & Pohl S.L., "Evaluating clinical accuracy of systems for self-monitoring of blood glucose," *Diabetes Care*, vol. 10, pp. 622–628, 1987.

[143] Parkes J.L. & Slatin S.L. & Pardo S. & Ginsberg B.H., "A new consensus error grid to evaluate the clinical significance of inaccuaracies in the measurement of blood glusose," *Diabetes Care*, vol. 23, no. 8, pp. 1143–1148, 2000.

[144] Vapnik V.N. "The Nature of Statistical Learning", 2nd Edition. Springer, 2000.

[145] Steinwart I. & Christmann A. “Support Vector Machines”. Springer, 2008.

[146] Brereton R. & Lloyd G. “Support vector machines for classification and regression,” *Analyst*, vol. 135, pp. 230–267, 2010.

[147] Hastie T. & Tibshirani R. & Friedman J. “The Elements of Statistical Learning: Data Mining, Inference and Prediction”. Springer, 2001.

[148] Lindgren F. & Hansen B. & Karcher W., “Model validation by permutation tests: Applications to variable selection,” *Journal of Chemometrics*, vol. 10, no. 5, pp. 521–532, 1996.

[149] Ryugo D.K. & Kretzmer E.A. & Niparko J.K. “Restoration of Auditory Nerve Synapses in Cats by Cochlear Implants”. *Science*, vol. 310, no. 5753, pp. 1490 – 1492. 2005.

[150] Martinoiaa S. & Sanguinetib V. & Cozzib L. & Berdondinic L. & van Peltd J. & Tomase J. & Le Massonf G. & Davideg F. “Towards an embodied in vitro electrophysiology: the NeuroBIT project”. *Neurocomputing*, vol. 60, no. 58, pp. 1065 – 1072. 2004.

[151] Taylor D.M. & Helms Tillery S.I. & Schwartz A.B. “Direct cortical control of 3D neuroprosthetic devices”. *Science*, vol. 296, pp. 1892 – 1832. 2002.

[152] Lebedev M.A. & Carmena J.M. & O’Doherty J.E. & Zacksenhouse M. & Henriquez C.S. & Principe J.C. & Nicolelis M.A.L. “Cortical Ensemble Adaptation to Represent Velocity of an Artificial Actuator Controlled by a Brain–Machine Interface”. *The Journal of Neuroscience*, vol. 25, no. 19, pp. 4681-4693. 2005.

[153] Lebedev M.A. & Nicolelis M.A.L. “Brain–machine interfaces: past, present and future”, *TRENDS in Neurosciences*, vol.29, No.9, July 2006.

[154] Wessberg J. & Stambaugh C.R. & Kralik J.D. & Beck P.D. & Laubach M. & Chapin J.K. “Real-time prediction of hand trajectory by ensembles of cortical neurons in primates”. *Nature*, vol. 408, no. 6810, pp. 361 – 5. 2000.

[155] Brown E.N. & Kass R.E. & Mitra P.P. “Multiple neural spike train data analysis: state-of-the-art and future challenges”. *Nature neuroscience*, vol. 7, no. 5, pp. 456 – 461. 2004.

[156] Brychta R.J. & Tuntrakool S. & Appalsamy M. & Keller N.R. & Robertson D. & Shiavi R.G. & Diedrich A. “Wavelet Methods for Spike Detection in Mouse Renal Sympathetic Nerve Activity”. *IEEE Transactions on Biomedical Engineering*, vol. 54, Issue 1, pages: 82-93, January 2007.

[157] Akin T. & Najafi K. & Bradley R. “A wireless implantable multichannel digital neural recording system for a micromachined sieve electrode”. *IEEE Journal of Solid State Circuits*, vol. 1, no. 33, pp. 109-118. 1998.

[158] Szuts T.A. & Fadeyev V. & Kachiguine S. & Sher A. & Grivich M.V. & Agrochão M. & Hottowy P. & Dabrowski W. & Lubenov E.V. & Siapas A.G. & Uchida N. & Litke A.M. & Meister M. “A wireless multi-channel neural amplifier for freely moving animals”. *Nature Neuroscience* 14, 263–269, 2011.

[159] Irazoqui-Pastor P. & Mody I. & Judy J.W. “Recording brain activity wirelessly”. *IEEE Engineering in Medicine and Biology Magazine.* Vol. 24, no. 6, pp. 48 - 54. 2005.

[160] Moo Sung Chae & Zhi Yang & Yuce, M.R. & Linh Hoang & Liu, W. "A 128-Channel 6 mW Wireless Neural Recording IC With Spike Feature Extraction and UWB Transmitter". *Neural Systems and Rehabilitation Engineering, IEEE Transactions on* , vol.17, no.4, pp.312-321, Aug. 2009.

[161] Kim K. & Kim S. “Neural spike sorting under nearly 0 dB signal-to-noise ratio using nonlinear energy operator and artificial neural-network classifier”. *IEEE Transactions on Biomedical Engineering*, vol. 47, no. 10, pp. 1406-1411. 2000.

[162] Jing H. & Si J. & Olson B.P. & Jiping H., “Feature detection in motor cortical spikes by principal component analysis”. *IEEE Transactions on Neural systems and Rehabilitation Engineering*, vol.13, Issue 3, pages 256-262, September 2005.

[163] Ju M.C. & Park C.H. & Hong D.K. & Youn K.J. & Cho J.W. "Link management scheme of bluetooth based on channel quality estimation". *Electronics Letters*, vol. 38, issue 15, pp. 789 - 790. 2002.

[164] Letelier J.C. & Weber P.P. "Spike sorting based on discrete wavelet transform coefficients". *Journal of Neuroscience Methods*, vol. 2, no. 101, pp. 93-106. 2000.

[165] Marzullo T.C. & Dudley J.R. & Miller C.R. & Trejo L. & Kipke D.R. "Spikes, Local Field Potentials, and Electrocorticogram Characterization during Motor Learning in Rats for Brain Machine Interface Task". *Proceedings of the 2005 IEEE Engineering in Medicine and Biology 27th Annual Conference*, Shanghai, China, pp. 429-431, September 1-4, 2005.

[166] Mojarradi M. & Binkley D. & Blalock B. & Anderson R. & Ulshoefer N. & Johnson T. "A miniaturized neuroprosthesis suitable for implantation into the brain". *IEEE Transactions on Neural Systems and Rehabilitation Engineering*, vol. 3, no. 11, pp. 38 – 42. 2003.

[167] Morrow R. "Connecting with a bluetooth piconet". *Fall Wireless Symposium/Portable By Design Conference and Exhibition*, Chicago. 2000.

[168] Obeid I. & Nicolelis M.A.L. & Wolf P.D. "A low power multichannel analog front end for portable neural signal recordings". *The Journal of Neuroscience Methods*, no. 133, pp. 27 – 32. 2004.

[169] Mark M. & Bjorninen T. & Chen Y. & Venkatraman S. & Ukkonen L. & Sydanheimo L. & Carmena J. & Rabaey J. "Wireless channel characterization for mm-size neural implants". *Engineering in Medicine and Biology Society (EMBC), 2010 Annual International Conference of the IEEE*, 31, pp. 1565 –1568. September 2010.

[170] Borton D. & Song Y.-K. & Patterson W. & Bull C. & Park S. & Laiwalla F. & Donoghue J. & Nurmikko A. "Wireless, high-bandwidth recordings from non-human primate motor cortex using a scalable 16-ch implantable microsystem". *Engineering in Medicine and Biology Society, 2009. EMBC*

2009. Annual International Conference of the IEEE, pp. 5531 –5534. September 2009.

[171] Olson B.P. & Si J. & Hu J. & He J. "Closed-Loop Cortical Control of Direction Using Support Vector Machines". *IEEE Transactions on Neural systems and Rehabilitation Engineering*, vol. 13, no. 1, pp. 72 – 80. 2005.

[172] Oweiss K.G. "A Systems Approach for Data Compression and Latency Reduction in Cortically Controlled Brain Machine Interfaces", *IEEE Transactions on biomedical Engineering*, vol. 53, Issue 7, pages 1364-77, July 2006.

[173] Perelman Y. & Ginosar R. "An Integrated System for Multichannel Neuronal Recording With Spike/LFP Separation, Integrated A/D Conversion and Threshold Detection*". IEEE Transactions on Biomedical Engineering*, Vol. 54, No. 1, pp. 130-138, January 2007.

[174] Tarín C. & Martí P. & Traver L. & Cardona N. & Díaz J.A. & Antonino E. "UWB Channel Measurements for hand-portable devices: a comparative study". *IEEE International Symposium on Personal, Indoor and Mobile Radio Communications*, Athens, Greece, pp. 1 – 5. 2007.

[175] Tarín C. & Traver L. & Martí P. & Cardona N. & Díaz J.A. & Cabedo M. "UWB Channel measures for hand-portable and wearable devices". *IEEE International Conference on Wireless and Mobile Computing, Networking and Communications*, New York, USA, pp. 1 – 6. 2007.

[176] Tarín C. & Traver L. & Santamaría J.F. & Martí P. & Cardona N. "Bluetooth-3G wireless transmission system for neural signal telemetry". *IEEE Wireless Telecommunications Symposium*, Pomona, California, USA, pp. 1-6. 2007.

[177] Universite Paris Descartes, UFR Biomedicale. http://www.biomedicale.univ-paris5.fr/SpikeOMatic/Data.html. Accessed 10th July 2008.

[178] Wise K.D. & Anderson D.J. & Hetke J.F. & Kipke D.R. & Njafi K. "Wireless implantable microsystems: High-density electronic interfaces to the nervous system". *Proceedings of the IEEE*, vol. 92, no. 1, pp. 76 – 97. 2004.

[179] Wood F. & Black M.J. & Vargas-Irwin C. & Fellows M. & Donogue J.P. “On the Variability of Manual Spike Sorting”. *IEEE Transactions on Biomedical Engineering*, vol. 51, issue 6, pp. 912 – 918. 2004.

[180] Yu S.N. & Cheng J.C. “A wireless physiological signal monitoring system with integrated bluetooth and wifi technologies”. *27th Annual International Conference of the Engineering in Medicine and Biology Society*, Shanghai, China, pp. 2203 – 2206. 2005.

[181] Zasowski T. & Althaus F. & Stäger M. & Wittneben A. & Tröster G. “UWB for noninvasive wireless body area networks: Channel measurements and results”. *IEEE Conference on Ultra Wideband Systems and Technologies*, pp. 1 – 10. 2003.

[182] Zumsteg Z.S. & Kemere C. & O’Driscoll S. & Santhanam G. & Ahmed R.E. & Shenoy K.V. & Meng T.H. “Power Feasibility of Implantable Digital Spike Sorting Circuits for Neural Prosthetic Systems”. *IEEE Transactions on Neural Systems and Rehabilitation Engineering*, vol. 13, no. 3, pp. 272 – 279. 2005.

[183] Saleh A. & Valenzuela R. “A statistical model for indoor multipath propagation”. *IEEE Journal on Selected Areas in Communications*, vol. 5, no. 2, pp. 128–137, February 1987.

[184] Chong C.C. & Yong S. “A generic statistical-based UWB channel model for high-rise apartments”. *IEEE Transactions on Antennas and Propagation*, vol. 53, no. 8, pp. 2389–2399, August. 2005.

[185] Foerster J.R. & Pendergrass M. & Molisch A.F. “A channel model for ultrawideband indoor communication”. IEEE 802.15.3a standardization group, 2003.

[186] Muqaibel A. & Safaai-Jazi A. & Attiya A. & Woerner B. & Riad S. “Path-loss and time dispersion parameters for indoor uwb propagation”. *IEEE transactions on wireless communications*, 2006.

[187] Ott A.T. & Blechy M.D. & Kraemer M. & Eibert T.F. “Enhanced Parameter Determination of an Empirical UWB Channel Model for European Building Standards*”. German microwave conference 2010*.

[188] Irahhauten Z. & Dacuña J. & Janssen G.J. & Nikookar H. “Uwb channel measurements and results for wireless personal area networks applications”. *European Conference on Wireless Technology*, 2005, October 2005.

[189] Welch T.B. & Musselman R.L. & Emessiene B.A. & Gift P.D. & Choudhury D.K. & Cassadine D.N. & Yano S.M., “The effects of the human body on uwb signal propagation in an indoor environment*”. IEEE Journal in selected areas in communications*, December 2002.

[190] Goulianos A.A. & Brown T.W.C. & Stavrou S. "A Novel Path-Loss Model for UWB Off-Body Propagation," *Vehicular Technology Conference, 2008. VTC Spring 2008. IEEE* , vol., no., pp.450-454, 11-14 May 2008.

[191] Alomainy A. & Sani A. & Rahman A. & Santas J.G. & Yang H. "Transient Characteristics of Wearable Antennas and Radio Propagat.ion Channels for Ultrawideband Body-Centric Wireless Communications". *IEEE Transactions on Antennas and Propagation,* vol. 57, no.4, pp.875-884, April 2009.

[192] Takizawa K. & Aoyagi T. & Takada J.I. & Katayama N. & Yekeh K. & Takehiko Y. & Kohno K.R. "Channel models for wireless body area networks," *Engineering in Medicine and Biology Society*, 2008. EMBS 2008. 30th Annual International Conference of the IEEE , vol., no., pp.1549-1552, 20-25 Aug. 2008.

[193] Wang Q. & Tayamachi T. & Kimura I. & Wang J. "An On-Body Channel Model for UWB Body Area Communications for Various Postures" *Antennas and Propagation, IEEE Transactions on* , vol.57, no.4, pp.991-998, April 2009.

[194] Goldsmith A. “Wireless Communications”. Cambridge University Press. ISBN: 9780521837163. September. 2005.

[195] Rappaport T. “Wireless Communications: Principles and Practice”, 1st ed.Prentice Hall, January 1996.

[196] Reusens R. & Joseph W. & Vermeeren G. & Martens L. “On-body measurements and characterization of wireless communication channel for arm and torso of human“. *International Workshop on Wearable and*

Implantable Body Sensor Networks, BSN07, Achen, March 2007, pp. 26-28. 2007.

[197] Fort A. & Keshmiri F. & Crusats G.R. & Craeye C. & Oestges C. "A Body Area Propagation Model Derived From Fundamental Principles: Analytical Analysis and Comparison With Measurements," *Antennas and Propagation, IEEE Transactions on* , vol.58, no.2, pp.503-514, Feb. 2010.

[198] D'Errico R. & Ghannoum H. & Roblin C. & Sibille A. "Small semi directional antenna for UWB terminal applications". *EuCAP 2006*, pages 1–6, November 2006.

[199] IEEE P802.15 Working Group for Wireless Personal Area Networks (WPANs). Channel Model for Body Area Network (BAN) (IEEE P802.15-08-0780-09-0006). April 2009.

[200] Molisch A.F. & Balakrishnan K. & Cassioli D. & Chong C.C. & Emanmi S. & Fort A. & Karedal F. & Kunisch J. & Schantz H. & Schuster U. & Siwiak K. "IEEE 802.15.4a channel model - final report" IEEE P802.15-04/662r0-SG4a.

[201] Cramer J.M. & Scholtz R. & Win M. "Evaluation of an indoor ultrawideband propagation channel". *IEEE Transactions on Antennas and Propagation,* vol. 50, no.5, pp.561-570, May 2002.

[202] Cassioli D. & Durantini A. "A time-domain propagation model of the UWB indoor channel in the FCC-compliant band 3.6 - 6 GHz based on PN-sequence channel measurements". *IEEE 59th Vehicular Technology Conference, VTC 2004-Spring*, vol. 1, no. 1, pp. 213–217, May 2004.

[203] Hall P.S. & Hao Y. "Antennas and propagation for body-centric wireless communications". *First European Conference on Antennas and Propagation, 2006. EuCAP 2006.* Print ISBN: 978-92-9092-937-6. pp. 1-7. Nice, November 2006.

[204] Zasowski T. & Wittneben A. "Performance of UWB receivers with partial CSI using a simple body area network channel model". *IEEE Journal on Selected Areas in Communications*, vol. 27, no. 1, pp. 17– 26, January 2009.

[205] Katayama N. & Takizawa K. & Aoyagi T. & Takada J.I. & Li H.B. & Kohno R. "Channel model on various frequency bands for wearable body area network". *First International Symposium on Applied Sciences on Biomedical and Communication Technologies. ISABEL*, vol. 1, pp. 1–5, Oct. 2008.

[206] Chen Y. & Teo J. & Lai J. & Gunawan E. & Low K.S. & Soh C.B. & Rapajic P. "Cooperative communications in ultra-wideband wireless body area networks: Channel modeling and system diversity analysis". *IEEE Journal on Selected Areas in Communications*, vol. 27, no. 1, pp. 5–16, January 2009.

[207] Hardle W. & Simar S. "Applied multivariate statistical analysis". ISBN-10: 3540030794, ISBN-13: 978-3540030799. *Springer*, September 2003.

[208] Gray R.M. & Davisson L.D. "An Introduction to Statistical Signal Processing". ISBN-10: 0521131820, ISBN-13: 978-0521131827. *Cambridge University Press*, February 2010.

[209] Kim S. & McNames J. "Automatic spike detection based on adaptive template matching for extracellular neural recordings". *Journal of Neuroscience Methods,* vol. 165, Issue 2, pp. 165–174. September 2007.

[210] Chen H.Y. & Wu J.S. & Hyland B. & Lu X.D. & Chen J. "A low noise remotely controllable wireless telemetry system for single-unitrecording in rats navigating in a vertical maze". *Journal of Medical and Biological Engineering and Computing, vol.* 46, pp. 833–839. 2008.

[211] Oweiss K.G. "Latency reduction during telemetry transmission in brain-machine interfaces". *Proceedings of the 2005 IEEE Engineering in Medicine and Biology 27th Annual Conference*. Shanghai, China, September 1-4, 2005.